DEVELOPMENT AND EXPERIMENTAL VALIDATION

OF A PREDICTIVE MODEL FOR A GTA WELD POOL GEOMETRY

by

GEORGE EM KARNIADAKIS

Engineering Diploma in M.E. and N.A.M.E.

NATIONAL TECHNICAL UNIVERSITY OF ATHENS, 1982

Submitted to the Department of
Mechanical Engineering
in Partial Fulfillment of the
Requirements of the Degree of

MASTER OF SCIENCE IN MECHANICAL ENGINEERING

at the

MASSACHUSETTS INSTITUTE OF TECHNOLOGY

June 1984

Signature of Author: _____
Department of Mechanical Engineering

Certified by: _____
Thesis Supervisor

Accepted by: _____
Chairman, Mechanical Engineering Departmental Committee

DEVELOPMENT AND EXPERIMENTAL VALIDATION OF A PREDICTIVE MODEL FOR A GTA WELD POOL GEOMETRY

by

GEORGE EM KARNIADAKIS

Submitted to the Department of Mechanical Engineering

in partial fulfillment of the

requirements for the Degree of Master of Science in

Mechanical Engineering

ABSTRACT

A computationally simple, but physically based model has been developed to predict the geometry of stationary weld puddles. The overall model couples a weld pool model that includes convection of the molten metal to a heat conduction solution for the solid material to obtain a predictive technique for the fusion boundary. Electromagnetic, surface tension and plasma shear forces are considered in determining the flow pattern in the weld pool. Direct comparison of predicted parameters with experimental data show a very good agreement, especially when the (radiative) heat losses from the plate surface are included. Experiments were also taken to determine the arc efficiency, and an empirical formula was found to correlate the heat input to the workpiece to the power dissipated in the electrode. While additional validation of the model is desirable, the basic approach has been shown to be good and the techniques can now be applied to the transient response of stationary puddles and to the full welding situation.

Thesis Supervisor: Dr. William Unkel

Title: Associate Professor of Mechanical Engineering

TABLE OF CONTENTS

TABLE OF CONTENTS (continued)

LIST OF FIGURES

LIST OF FIGURES (continued)

LIST OF FIGURES (continued)

ACKNOWLEDGEMENTS

I would like to acknowledge with gratitude the assistance of my advisor, Professor William Unkel, in giving direction and encouragement to my endeavors.

This work was funded by the Department of Energy, Contract No. DE-AC02-83ER 13084.

CHAPTER ONE

1.1 INTRODUCTION

Welding is a metal joining process that has broad application in a variety of constructions and repair operations. While simple welds can be made by moderately skilled welders, high quality welds require very skilled welders and must pass stringent inspection criteria. Even a small fraction of faulty welds can cause a substantial increase in the overall cost of welded structures. Producing high quality welds consistently is a major goal of welding research.

The work described in this thesis relates to the behaviour of the molten pool, in particular to the thermal (heat transfer) and fluid (stirring) response of the molten metal during the fusion process. This work has been performed in the context of developing an automatic or "smart" welder that controls directly the weld attributes that lead to a high quality weld. Thus, this smart welder requires not only a manipulator to position the torch and controls the weld arc, but also requires a system to determine the proper position, current and other parameters.

This work focuses on Gas Tungsten Arc Welding (GTAW) a welding fusion process widely used for fusing the root butt joints, where exceptionally high quality is essential e.g. stainless steel piping for nuclear engineering applications. Other materials for which GTAW is suitable are : mild steels, low alloy steels, aluminum and aluminum alloys, copper and copper alloys, nickel and nickel alloys. In GTAW an arc is established between a tungsten electrode and the parent metal forming a weld pool. A non-melting electrode is used, usually made of thoriated tungsten, which gives better arc stability

and higher current capacity than ordinary tungsten. The electrode holder (torch) must be either air or water cooled and the power source can be a.c. or d.c. with standard generators, rectifiers or transformers.

Closed-loop control of the welding variables (current, voltage, torch speed, arc length,etc) represents a promising, cost effective approach to improving weld quality and therefore reducing the total cost of producing welded stuctures. The ultimate goal is to place all significant weld variables under direct closed-loop control such that they depend only on the predetermined desired weld characteristics. The desirable weld characteristics are pre-determined from strength and practical considerations for each particular structure. In addition to those charecteristics, closed-loop control requires four components:

(a) An on line technique for sensing each control variable;

(b) A physically based but computationally simple model relating the weld variables to the process inputs;

(c) At least one control variable on the welding device for each weld variable being controlled; and,

(d) A control algorithm that combines the above components to provide independent output variable control.

A functional sketch of a proposed automated control system is shown in Figure 1. The approach uses inner loops nested within the overall "weld quality" control loop. For example, the inner loop would be the torch/power supply with control parameters those of current, arc length and torch speed (for moving torch). The control of the arc is achieved by a transistor controlled power supply, which is in itself controlled by a computer. The outermost loop is the weld quality loop, where the weld pool depth and width are sensed and the control variables are adjusted to keep these parameters close to the desired ones.

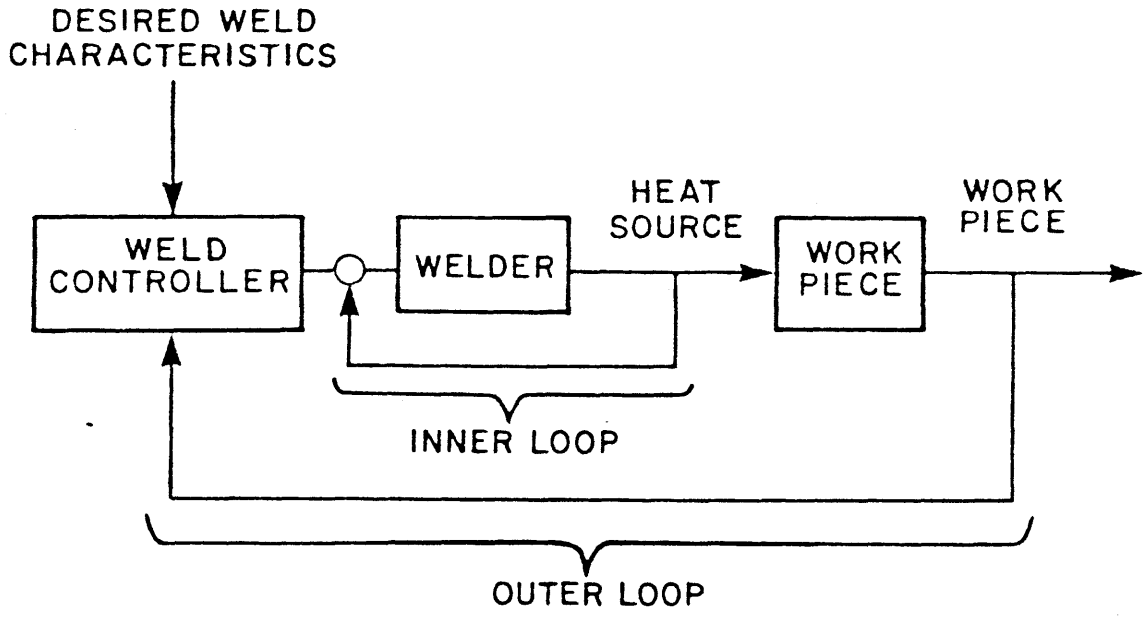

FIGURE 1 Schematic of Overall Control Strategy for Smart Welder.

1.2 PREVIOUS RESEARCH

The importance of predicting the temperature in and around the weld pool has long been recognized and considerable effort given to the task of developing models. The early methods for calculating the geometrical dimensions of the weld pool were based on the assumption that the mode of heat transfer through the plates was pure conduction. By assuming a linear temperature distribution along the thickness of the liquid interlayer (from the boiling point at the surface adjacent to the heat source to the melting point at the fusion boundary) the thickness of the liquid interlayer could be inferred for a certain heat input. The major theoretical contribution on heat flow in welding was made by Rosenthal [1], who applied solutions of the heat conduction equation in two and three dimensions with a moving heat source. This solution in its simplified version as it was given by Wells [2] relates the average fused area width d, with the total heat per unit width q of the plate as follows:

$$q=8\cdot k\cdot \Delta T\cdot (0.2+U\cdot d/(4\cdot \alpha))$$

where k,α are thermal conductivity and diffusivity of the solid respectively, ΔT is the temperature difference between the melting temperature and the surroundings and U is the velocity of the torch relative to the workpiece.

The predicted weld pool size, by the above analysis, has been found to differ by as much as 2-3 times [3] the size measured from experiments. The most probable explanation for this discrepancy is that in this analysis no allowance has been made to account for the enhanced heat transfer in the pool due to motion of the molten metal. One way to include this enhanced heat transfer is to use an effective isotropic or anisotropic conductivity to take care of directionality of heat in the pool or to introduce distributed heat sources or sinks. These techniques, however, have proved to be of very limited

use even to correlate the results. For example, Glickstein [4] found, after an extensive comparison of theoretical with experimental results and by using conductivities in the liquid region two to three times higher than the conductivity of the solid material at high temperatures, that simulation of heat flow in the weld puddle for arc welding cannot be carried out using an exclusively conduction model. Although this conclusion was for a stationary puddle no difference should be expected for moving welds. While several such techniques are used, in some cases, to match the computed fusion boundary to measured contours, these ad hoc techniques are not predictive and can be used only as interpretive tools, but not in new situations under different welding conditions.

Woods and Milner [5] , in 1971, first reported that motion of the molten metal exists in GTAW pools and examined the origin of the stirring forces by partialy mixing dissimilar metals and concluded that stirring forces are not always sufficient to overcome basic incompatibilities in the physical and chemical properties of the weld pool and additives. In parallel, analytical work to study flows induced by electromagnetic forces was initiated by Shercliff [6] in 1970. In this first work a concentrated electric current entering a region of inviscid conducting fluid through an interface was considered and an analytical solution was obtained for the non-linear equation of motion. Sozu [7] and others [8] solved similar problems, but for fluid with finite viscosity and their work has been extended to different geometries and configurations.

These solutions give the general features of free jet type flows for gases, and have been useful in identifying order of magnitude speeds. Unfortunately the flow field in the pool turns out to be much more complex,and other driving forces, besides the electromagnetic force give rise to motion of

the same or opposite direction of the em driven flow. Further, the motion is constrained by a solid boundary and the thermal behaviour induced by convection is important to establish the location of the boundary. The most pronounced effect comes from the surface tension force counteracting the e.m. force so heat is convected from the very hot region, just underneath the arc to the edge of the pool. When surface tension dominates, it tends to produce more shallow puddles. In a very recent paper, Operer et al [9] presented a mathematical model to account for the convection in stationary arc weld pools driven by e.m., surface tension and buoyancy forces, ignoring the effect of the shear stream of the plasma jet. Their results indicate a two cell flow structure and although they treated the flow as laminar their predicted values of velocity results in Reynolds number of about 2000, exceeding by much the critical Reynolds number ,which for this type of flow is expected to be of the order of 600.

To summarize, the effect of directional heat flow in the pool has been found to drastically alter the weld pool geometry. Several ad hoc techniques used so far to compute the fusion boundary gave a very limited use and are no more accurate than the first appeared conduction model by Rosenthal. Most recent numerical models assume the fusion boundary and are therefore incapable of predicting weld pool size.

1.3 SCOPE OF THE PRESENT RESEARCH

Although, the vast majority of the research in GTAW, during the last decade, has been devoted to better understanding the behaviour of the weld pool and how the directional heat flow could possibly influence the weld pool shape, no work has been done to develop a model,which by including all the dominant phenomena occurring in the pool as they are coupled to the arc phenomena and to the heat, which is conducted through the solid material

(plate) could predict the shape and the size of the pool, given the minimum possible information as an input. For automatic welding and control of the weld quality the development of such a model is of great importance, since it minimizes the number of parameters to be measured and ,therefore, minimizes the time needed to make a weld with a prescribed quality.

The purpose of this work is not only to study the directional heat flow in the puddle by inluding all the dominant mechanisms of producing motion in the pool, but also by looking at the arc and the solid material (plate) regions to match the solutions in these three regions since they are all coupled together. From this matching the melting interface can be predicted.

Experiments were conducted to check the validity of the developed model and also to determine the effective heat that goes into the plates from the arc. The comparison of predicted and experimental results is based on measured temperatures at various characteristic locations and on direct comparison of the penetration, for different sizes of mild steel plates. This detailed validation is absent in all previous work.

CHAPTER TWO

THE FULL PROBLEM FOR A GTA WELD PUDDLE

In Figure 2, the full problem with the simplifications adopted in this work is described. The weld pool is normally constituted of approximately equal amounts of material melted from the two plates to be joined and for the stationary welding torch considered here we can assume that axisymmetric conditions are valid. So, instead of the two plates we can use, for simplicity, a single circular plate. The heat and current input are distributed in a gaussian fashion, as shown, with the current leaving symmetrically the workpiece and finally through the copper base going to the ground (Figure 3). The copper plate is relatively large, so the current flows symmetrically out, although the shunt that drives the current out (sink) is located in one side of the plate.

To obtain a steady state condition the workpiece was water cooled at the edge with a rather high cooling flow rate in order to avoid assymetries due to large temperature drop of the cooling water through its passage.

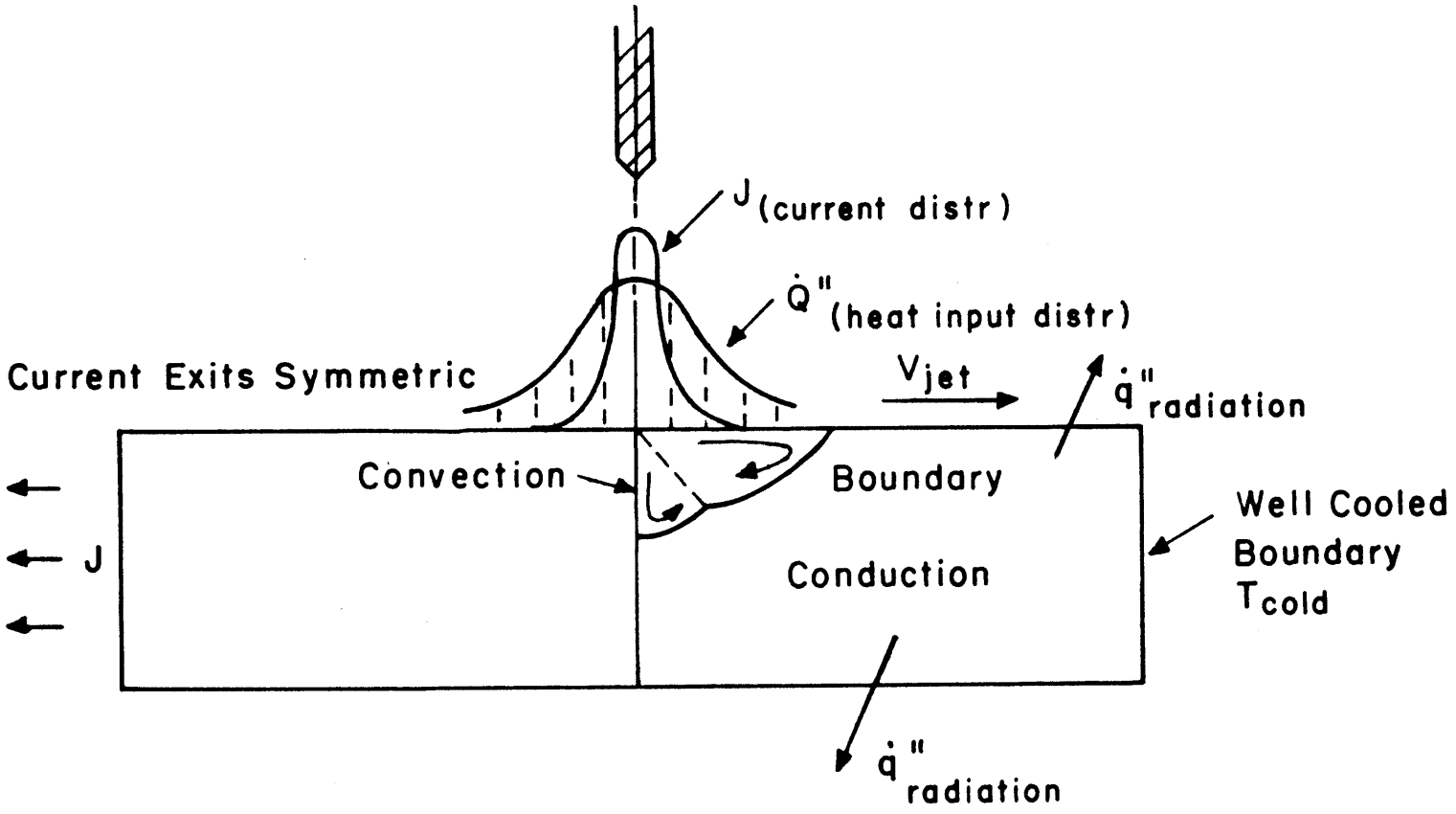

FIGURE 2: The full problem for a GTA weld puddle

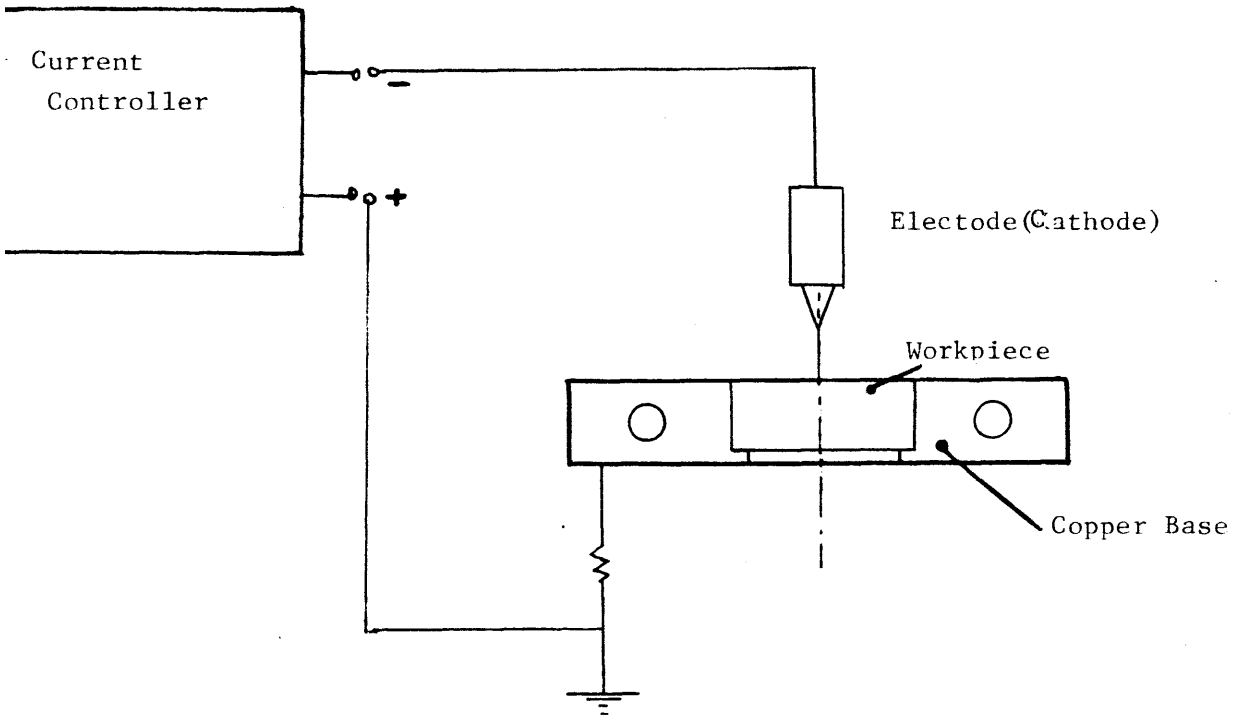

FIGURE 3: The electric circuit

CHAPTER THREE

3.1 EXPERIMENTAL APPARATUS

The experimental station consists of a stationary rig, as shown in Figure 4, designed to allow easy modifications and convenient hook-up.

Mild steel, circular workpieces of three different thickness plates of the same diameter (22 mm), as shown in Figure 5, were silver-soldered into the copper base to reduce the contact resistance. The copper base plate (Figure 6) has an approximately symmetric cooling passage and provides the cooling in order the workpiece to be at steady state for the range of heat inputs from the arc.

A GTAW torch (Airco heliweld h20-c) was used in conjuction with 2/32" diameter 2% thoriated Tungsten electrode surrounded by a 3/8" diameter alumina nozzle, through which argon, the shielding gas, was supplied at a flow rate of about 18 cubic feet per hour.

The welding power supply is a 3-phase rectified supply (AircoCV-450) capable of supplying a maximum current of 450 amperes at 38 Volts, with the current level options of 450 and 300 amperes. A shunt with output of 50 mV at 200 amperes was used to measure the current. The voltage between the tip electrode (cathode) and the workpiece (anode) was also measured.

This power supply was used in combination with a transistorized current controller to control the current passing through the arc. A schematic is shown in Figure 7 and a more detailed description can be found in [10]. An external reference signal from 0 to 10 Volts full scale provided by a Krohn-Hite Model 5200A signal generator was used to specify the output current value from 0 to 300 amperes. The current regulator was designed with the control measurements on the cathode side, since the anode is usually grounded. The cathode (electrode) operates at a negative voltage relative to ground.

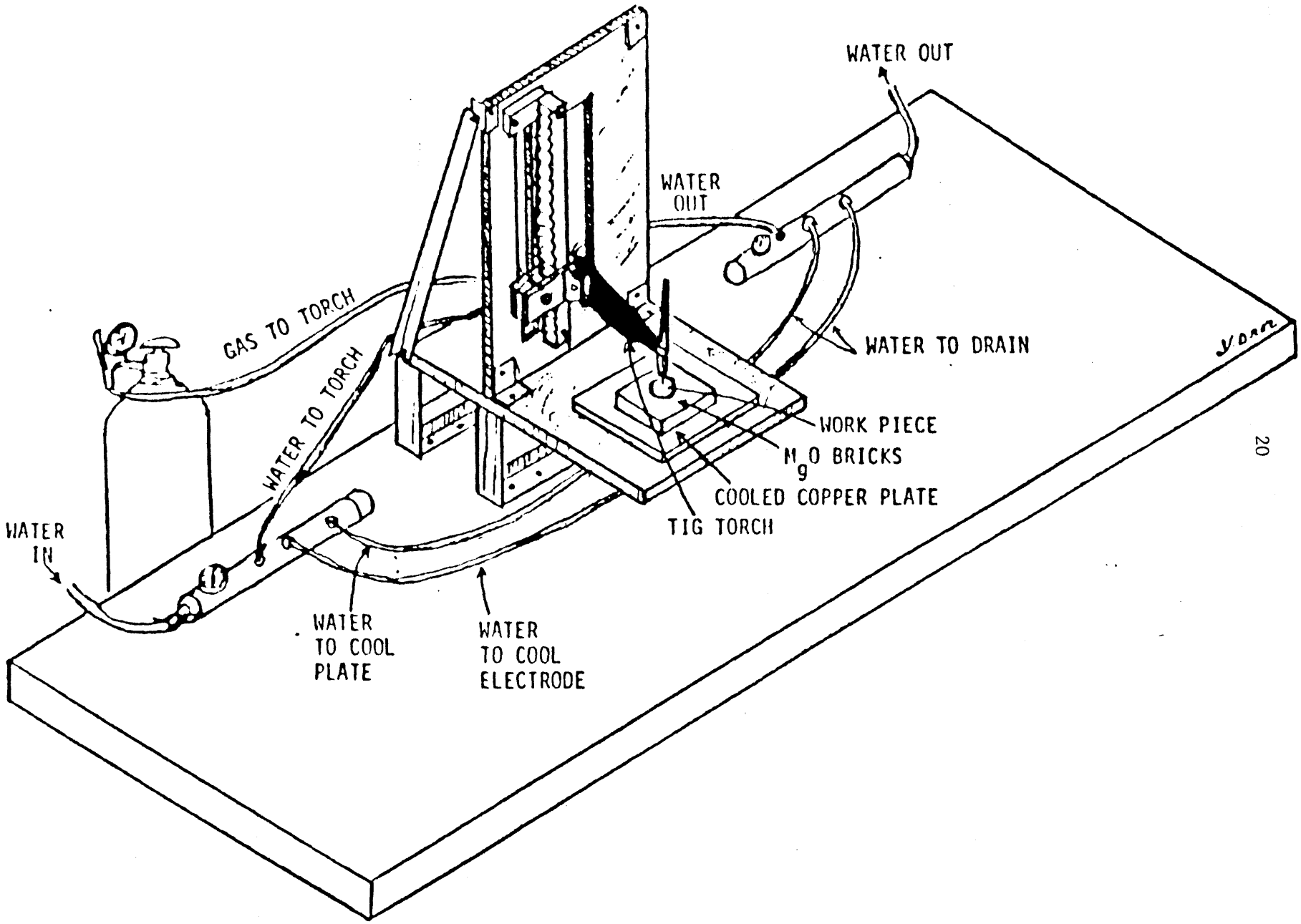

FIGURE 4: OVERALL VIEW OF ARC WELDING EXPERIMENTAL SET-UP

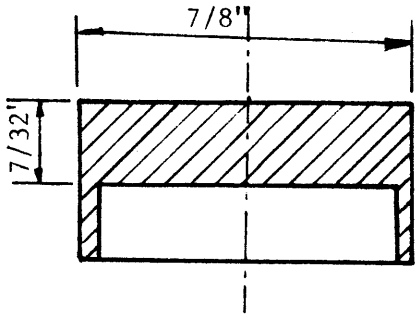

A. workpiece:7/8"*7/32"

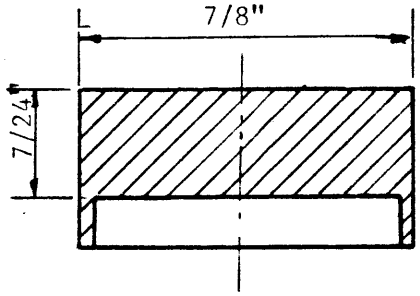

B.workpiece:7/8"*7/24"

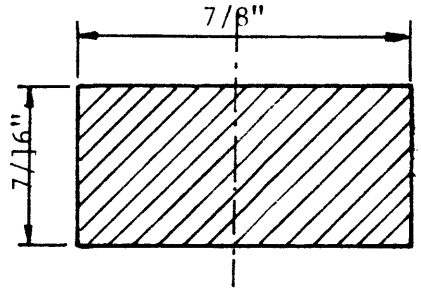

C.workpiece:7/8"*7/16"

FIGURE 5: The workpieces tested

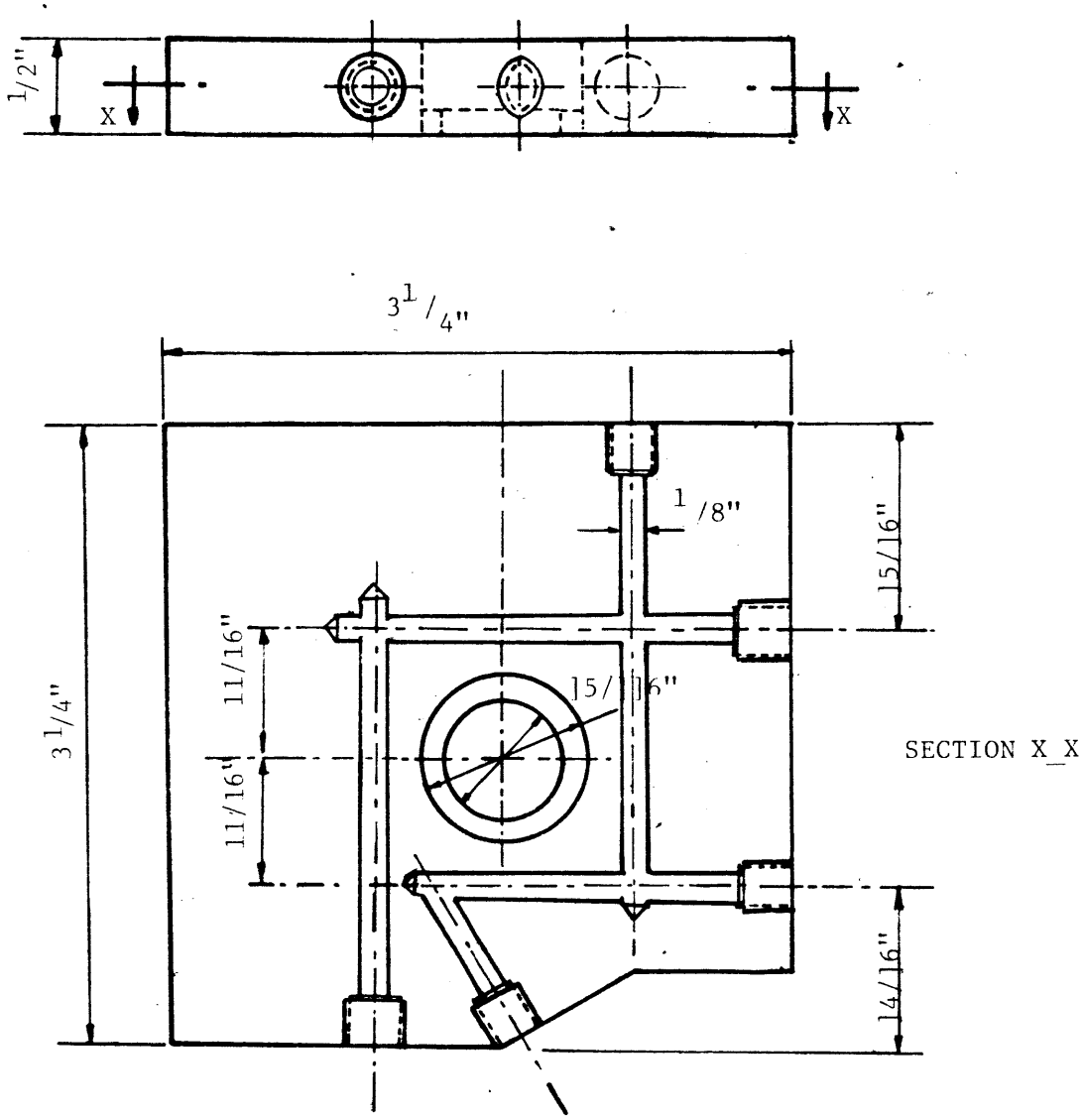

FIGURE 6: The copper plate base

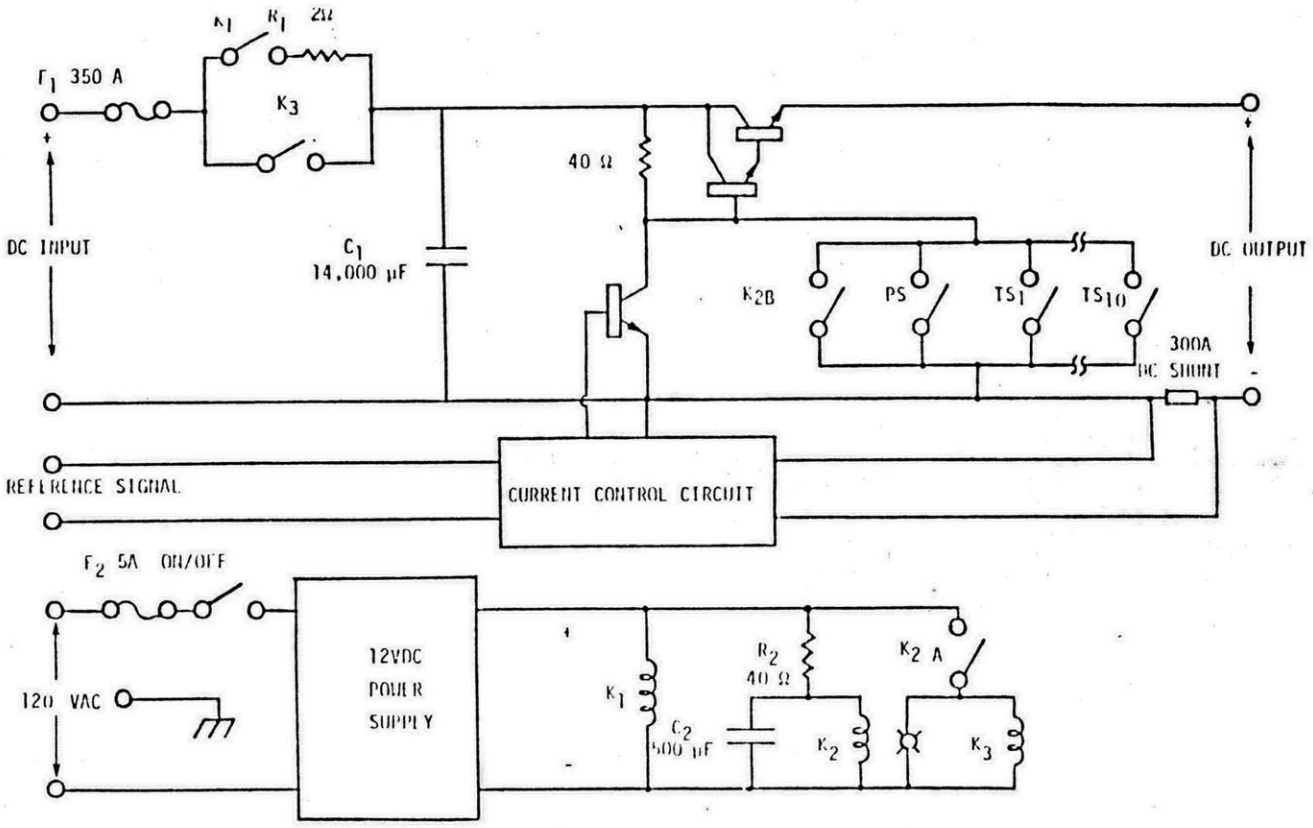

FIGURE 7 : Schematic of the current regulator showing the protection and sequencing circuit.

A computer based data acquisition system called UnkelScope{ M.I.T.,1983} was used to measure, display and store the data from arc current, voltage, temperatures and power input. This system was developed for the M.I.T Department of Mechanical Engineering Undergraduate Laboratory by professor W. Unkel. It is a software data-acquisition package, implemented on a Digital Equipment Corporation (DEC) LSI 11/03 based system operating under RT-11SJ. The analog to the digital converter on UnkelScope was an ADAC Corporation 12 bit converter with programmable gain to give full scale ranges of $\pm$ 10 Volts,$\pm$5 Volts,$\pm$2 Volts and $\pm$1 volts. A hardware clock board manufactured by Data Translation was used to provide synchronization of the data taking process. A DEC RX01 floppy disk drive system was used for mass storage. The CRT display terminal was a DEC VT125,while the hardcopy terminal was a DEC LA50.

3.2 EXPERIMENTS AND RESULTS ON THE ARC V-I CHARACTERISTICS

The product V•I (voltage times current) determines the instanteneous power from the arc, part of which is transferred as a heat input to the workpiece. It is therefore necessary, to establish the precise relation between arc voltage and arc current. In this work V-I measurements were taken for D.C. arcs, but data for A.C. arcs can be found in [11]. The current signal from the 300A shunt and arc voltage readings from the electrode were measured using an amplifier and attenuator, respectively, and recorded by the data acquisition system. A strong dependance of the V-I curve on the arc length was expected, so measurements were taken for three different arc lengths: L= 3.2 ,4.8 ,and 8.8 mm . A non-Ohmic behaviour (see Figure 8) was observed due to the strong dependance of electric conductivity on the temperature. As the current increases the emitted power is increased, the

temperature of the plasma jet also increases and therefore the electric conductivity increases, so the voltage remains approximately constant depending only on arc length.

An empirical relationship was found to correlate very well the experimental data in the two regions, as:

$$V=7.20 \cdot L^{0.3} \cdot \exp\{98.3 \cdot I^{-2.42}\} \qquad (1)$$

when the arc current is in the region from 0 to 85 amperes, and

$$V=3.70 \cdot L^{0.3} \cdot I^{0.15} \qquad (2)$$

when the arc current is in the region from 85 to 250 amperes, and with L in cm.

The solid lines in Figure 8 represent values given by the above equations (1) and (2). These expressions can be used only for argon arcs of approximately commercial purity, since it has been found experimentally that for nitrogen, for example, the voltage drop can be as high as three times the values predicted by the above expressions.

The overall voltage drop measured is the sum of the voltage drop in the vicinity of the anode, the drop in the so called positive column, and the drop which occurs next to the cathode. Electrons are emitted thermionically from the cathode, passing through a potential drop in the immediate vicinity of the cathode before entering a region of low potential gradient, known as the positive column which extends over most of the arc length. At the anode another potential drop occurs, before the electrons enter the anode over a small area the anode spot. In low-current arcs the potential gradient of the positive column is uniform, but in high current arcs the positive column is divided into two parts of different potential gradients. In the positive column, being in equilibrium, the electrons colliding with the gas molecules and raise the gas to a high temperature, estimated at about 5000 K. At this

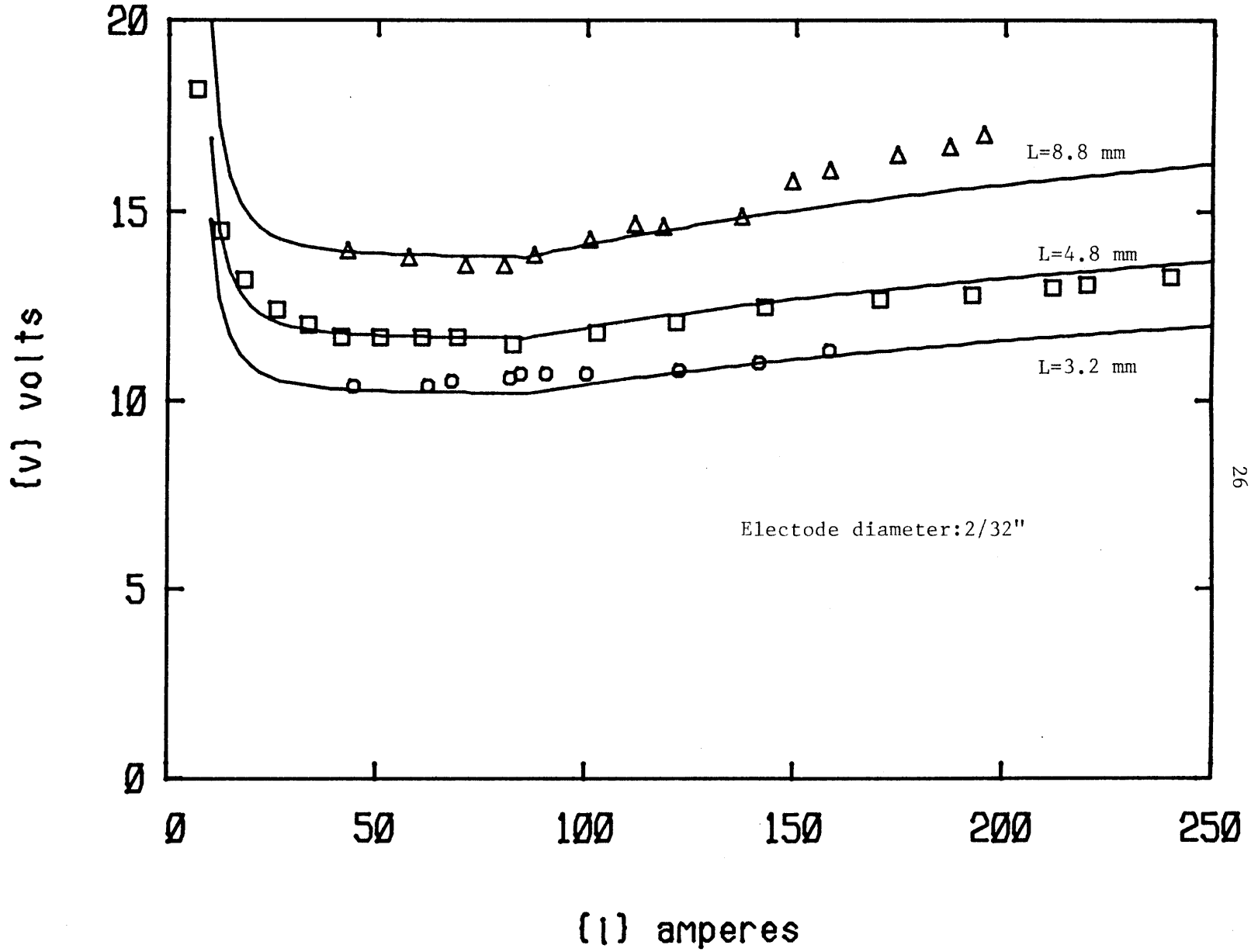

FIGURE 8 : Effect of arc length on the V-I curve

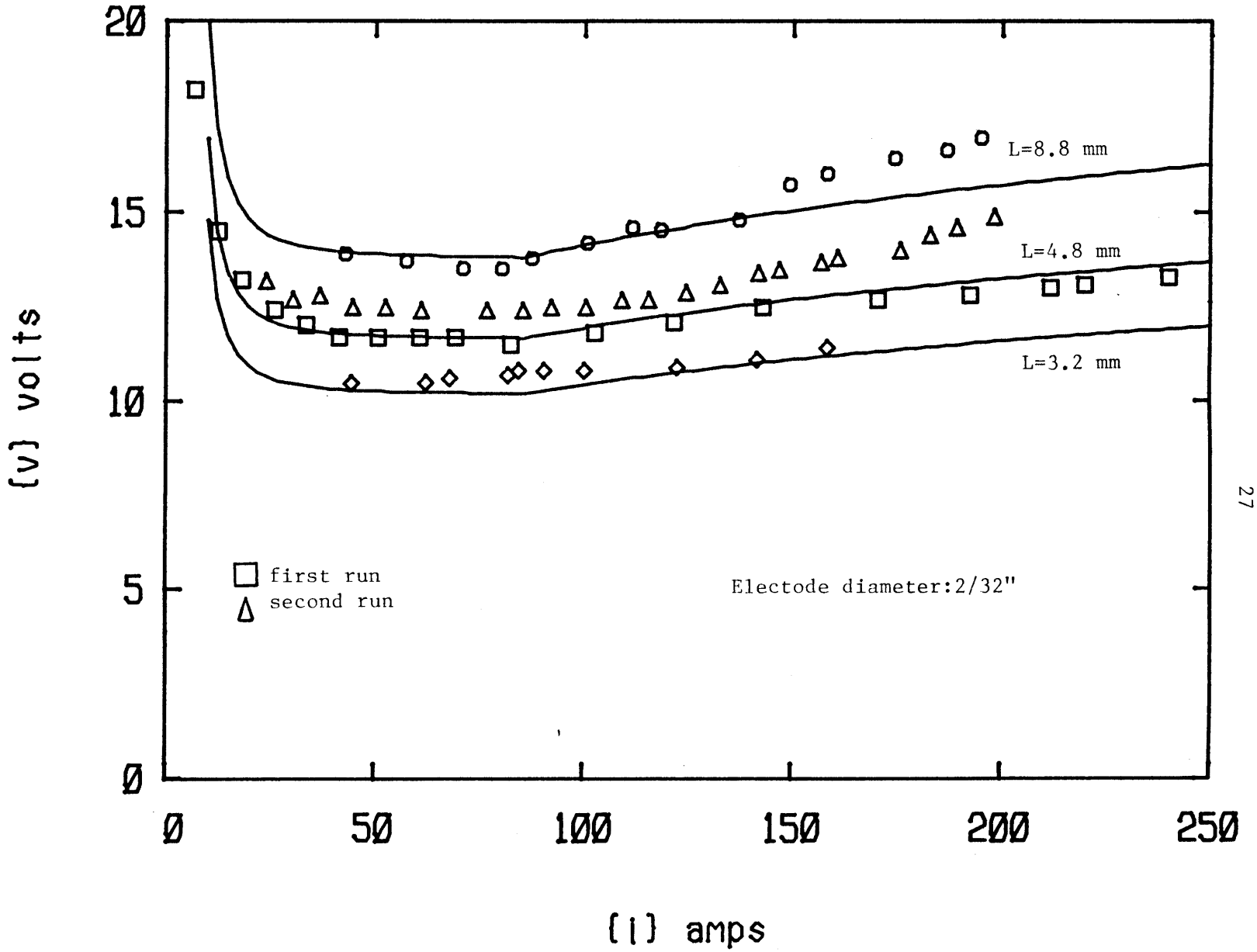

FIGURE 9: Effect of puddle formation on the V-I curve

temperature some of the gas is ionized providing a positive ion current which heats the cathode, but the arc current is largerly carried by the electrons, since although positive ions and electrons exist in approximately equal numbers in the arc column, the mobility of electrons is much greater than that of ions.

The final value of the total voltage drop depends, also, on the formed weld pool. For a pool with a depressed top surface the effective arc length is increased and an increase in voltage should be expected. This is indicated with experimental data plotted in Figure 9 for arc length 4.8 mm. The measurements shown by a triangle were taken in a second run after a pool had been formed in the first run (squares) and as expected has a higher voltage drop because of the larger length.

3.3 EXPERIMENTS AND RESULTS ON ARC EFFICIENCY

The energy transfer to the plates is composed primarily of the electron energy and convective heat transfer with the convection part increasing as the arc current increases, but remaining two to three times less than the electron energy transfer.

The power generated in the arc is not all transferred to the workpiece, and an arc efficiency can be defined as the heat used to melt and heat up the workpiece divided by the total emitted power by the torch. The power not transmitted to the workpiece is dissipated by radiation from the arc or is convected away by the flowing gas or is used to heat up the cathode and subsequently tranferred to the torch cooling water. According to our measurements the heat absorbed by the water cooling the electrode is very small. Even with very low cooling rate very small temperature rise was measured and therefore the losses consist mainly of the radiation from the

luminous gas and the part that is convected away by the gas. It is rather difficult to evaluate analytically or experimentally these losses, and in the literature there is a large discrepancy of data. Results range from an efficiency as low as 40% to as high 90% (Wilkinson and Milner,1960, [12]) have been reported. It is therefore important to measure the heat absorbed by the workpiece. With our experimental set up, in steady state, it is expected that the heat incident on the pool surface will be equal to the heat gained by the cooling water in the copper base plate, since the heat losses from the copper surface are negligible. Thus, the mass flow rate of cooling water, $\dot{m}$, and the water temperature rise ΔT are measured and the heat delivered to the workpiece evaluated as :

$$\dot{Q} = \dot{m} \cdot c_p \cdot \Delta T \qquad (3)$$

where c_p=4,187 j/kg, is the specific heat of water.

To measure the flow rate of water a rotometer was used, operating at different rates as percentage of the total rate at 100%. At the pressure of 30 psi the volume flow rate was 2.5 lt/min, and the calibration curve is shown in Figure 10. To examine how the different cooling rates could change the evaluated arc efficiency, measurements were taken for 70%,50%and 20% flow rates. As shown in Figure 11 for 70% and 50%, no change in the heat input was observed,but in the case of low cooling rate (20%), the measured heat was found to be lower, which should be expected since the overall temperature level of the system (workpiece plus copper plate) was higher and, therefore, the losses from the copper surface start to become important.

The effect of arc length on the arc efficiency was studied next, by taking measurements at two different arc lengths, L=4.8 mm and L=8.8 mm. As shown in Figure 12 in the case of the long arc the losses are larger and this result agrees with the results reported by other investigators. R.C. Eberhart

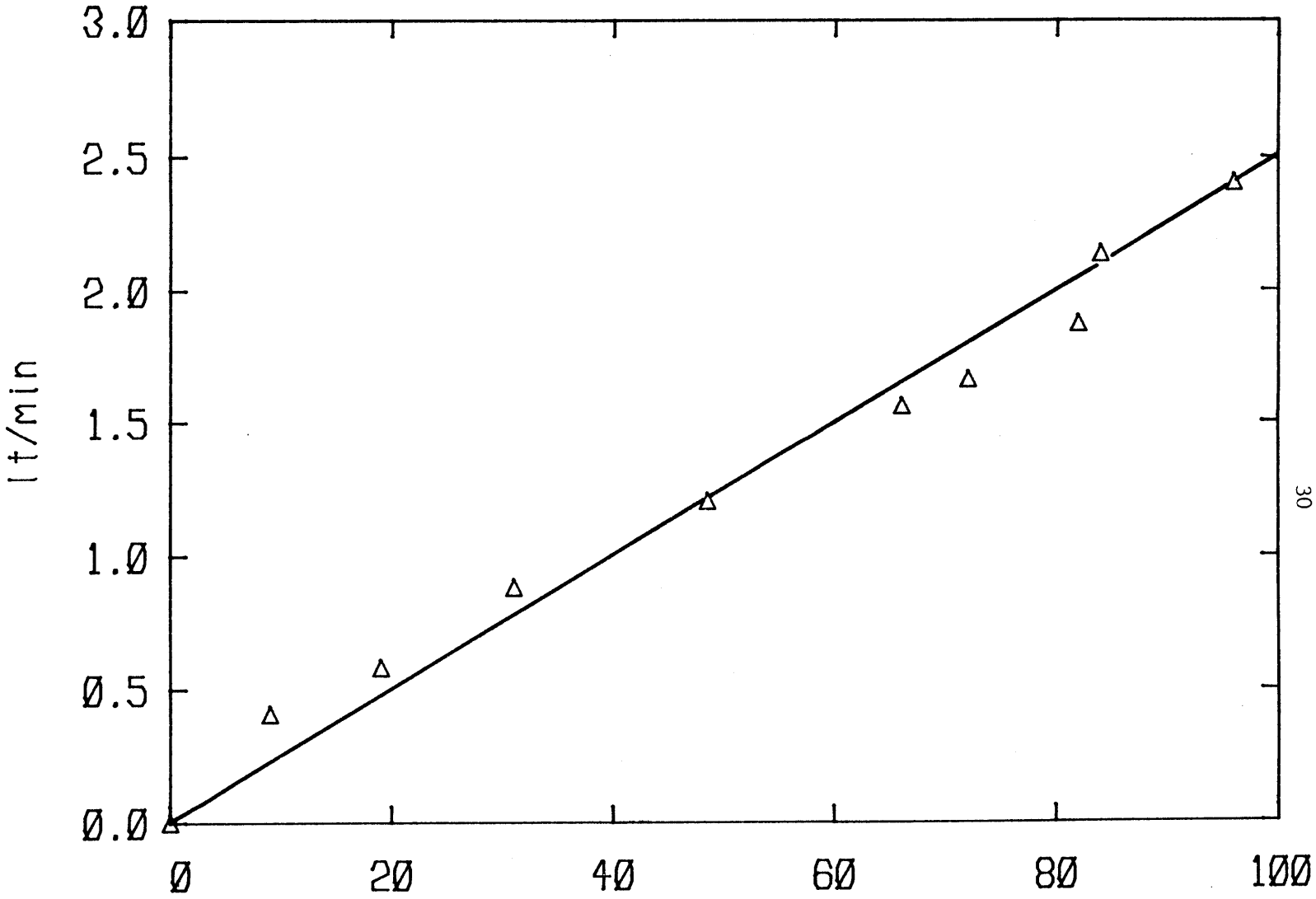

FIGURE 10: Calibration of flow meter

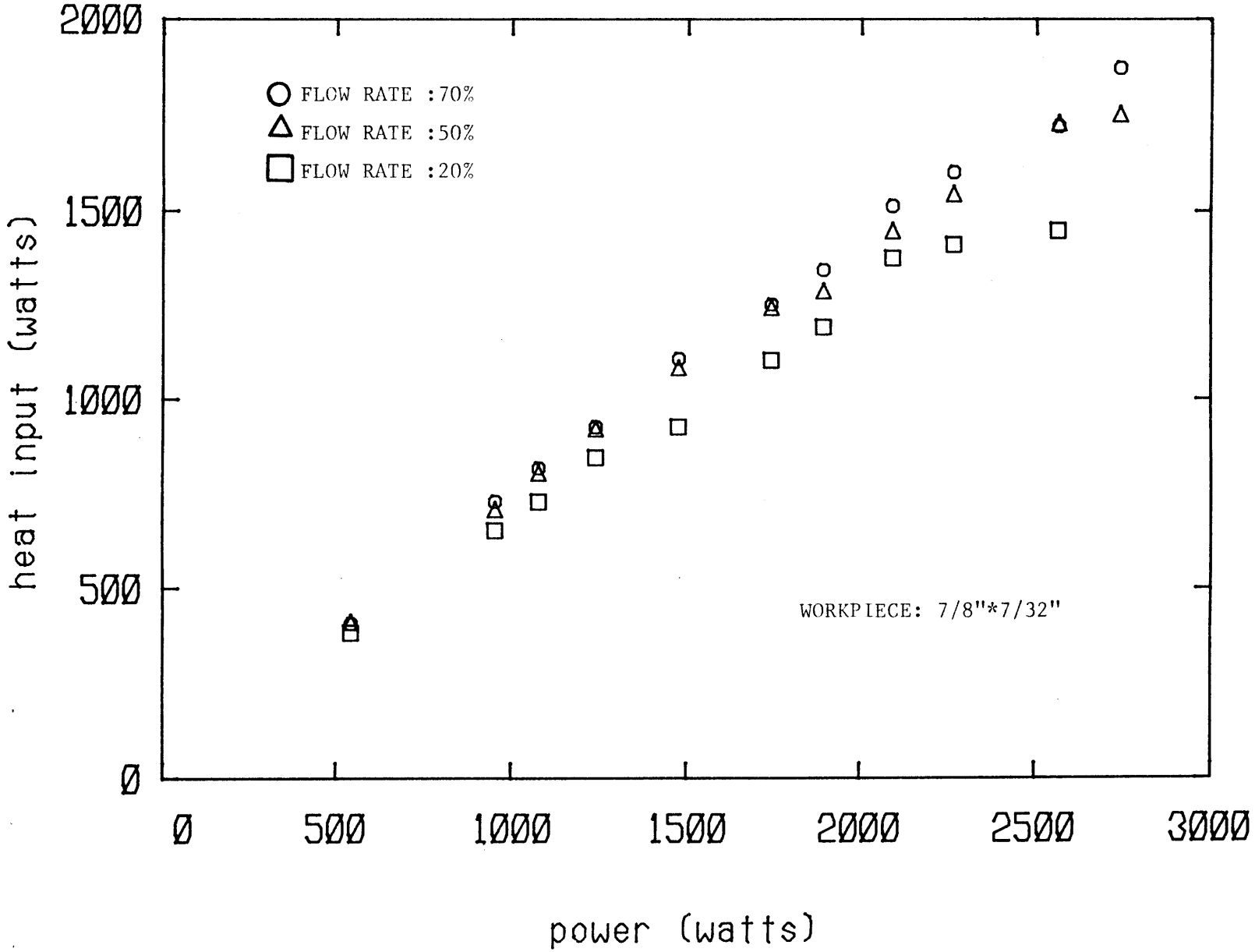

FIGURE 11: Effect of flow rate on arc efficiency

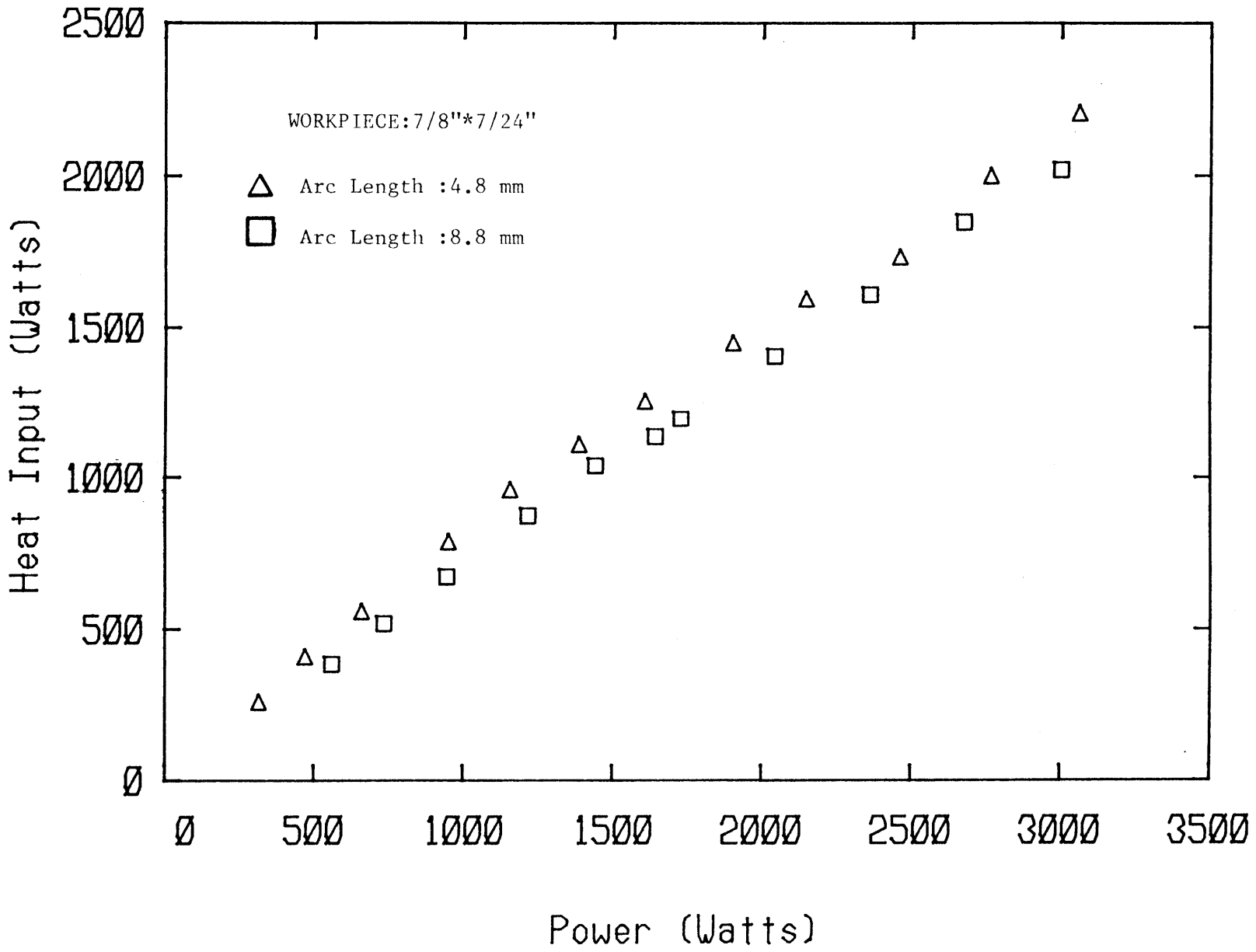

FIGURE 12 :Effect of arc length on arc efficiency

et al [14] have found that the efficiency η is independent of current and depends on the arc length L as :

$$\eta = 0.75/L^{0.13} \quad (L \text{ in cm}) \qquad (4)$$

for currents higher than 200 amperes.

Our results for the three different workpieces indicate that for low current the arc efficiency is, indeed, independent on current, but for higher current values the efficiency decreases as the current increases, and that the dependance on arc length is stronger than that given by [14]. No dependance, however, on the thickness of the workpiece,as it was found by [11] was observed but a rather universal curve for the heat input was obtained depending on the arc length only. The "knee" behaviour for the Q-P curve shown in the Figure 13 observed at, approximately, 1.5 kwatts of emitted power, is explained from the fact that above this critical power a puddle has formed in the metal and the depression in the surface affects the heat input. In addition, the radiative losses become more pronounced for higher current values.

For computational purposes an empirical fitting formula for the two different regions is obtained for the heat input obtained from the experimental data:

$$\eta = 1.20/L^{0.25} \qquad (5)$$

when the average power from the jet is not exceeded the 1500 watts, and as

$$\eta = 0.93/L^{0.25} + 260/\{P\} \qquad (6)$$

when the incident power is in the range of 1500 watts to 3500 watts.

Finally, experiments were conducted to determine the arc efficiency for the promising technique of current pulsing. Although, the data are not extensive, from the plot in Figure 14 the general observation can be made that

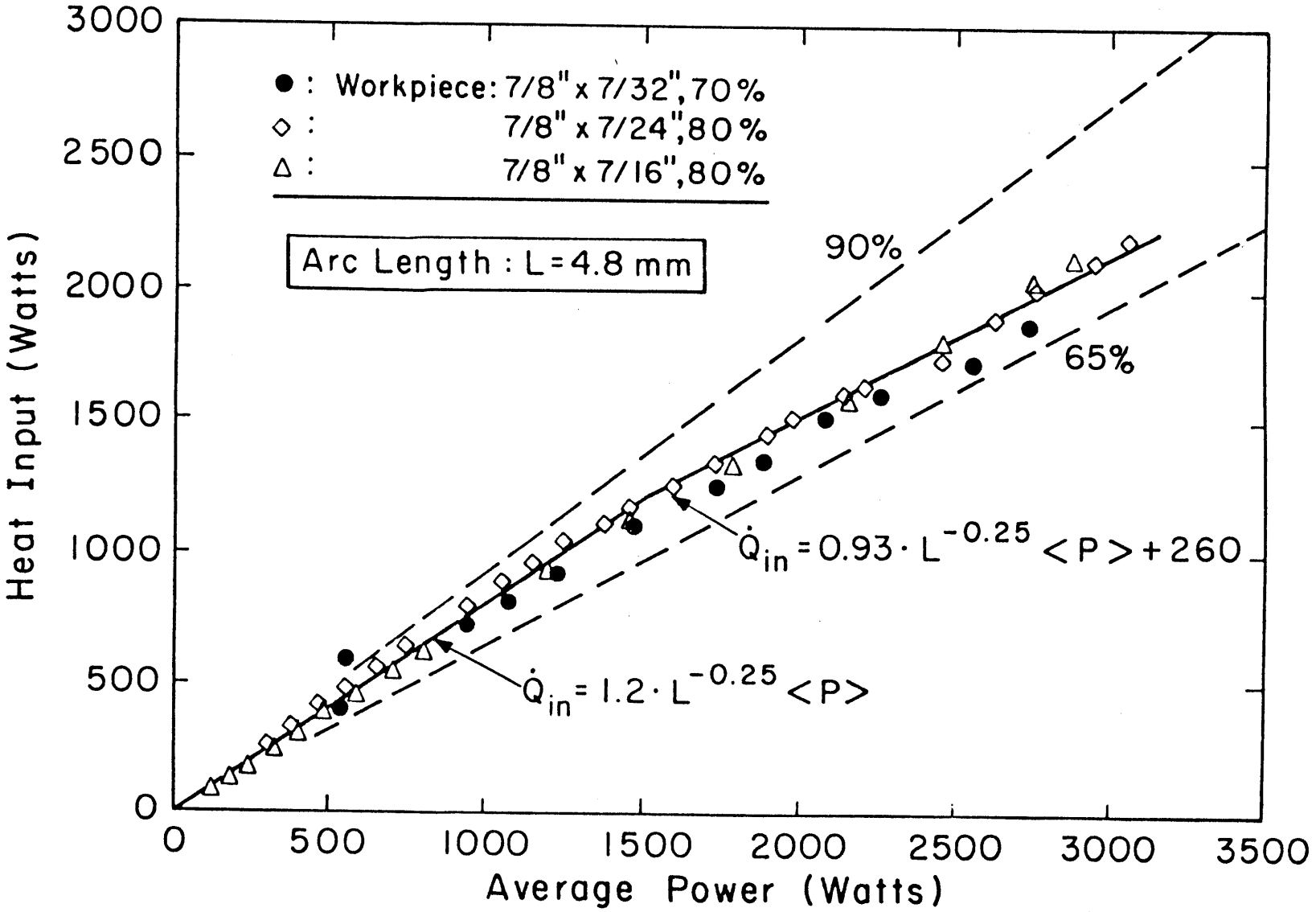

FIGURE 13 : The full problem for a GTA weld puddle

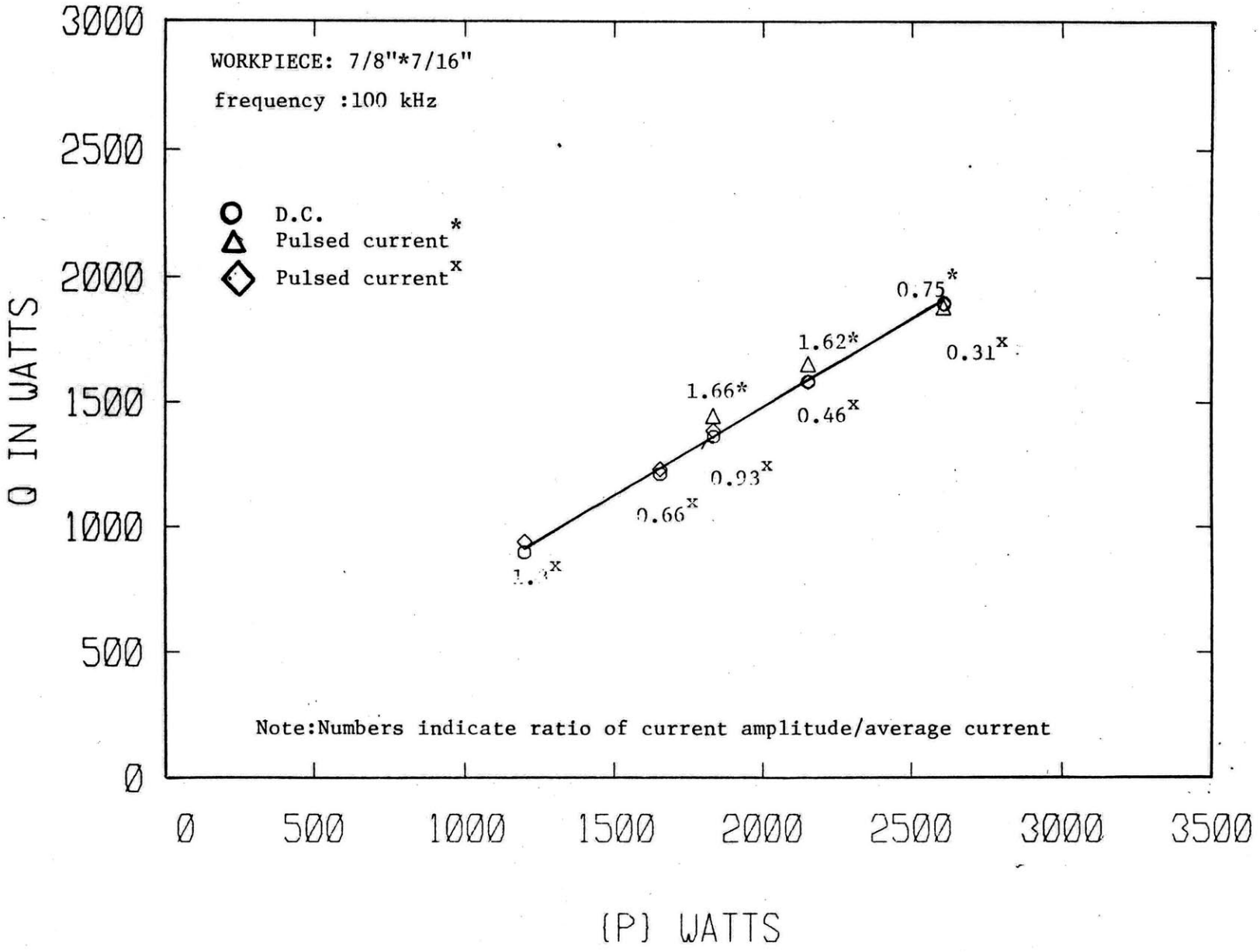

FIGURE 14: Effect of current pulsing on arc efficiency

at high heat inputs and for large current pulsing the effective heat input is slightly larger as it is compared with the D.C. case. For smaller current pulsing no difference in the results was observed. It is expected that in the case of thinner workpieces the small difference observed here will be more pronounced.

To determine analytically the arc efficiency it is a very complicated problem, since the heat that, finally, is delivered to the workpiece is composed of various components, as follows:

$$\dot{Q} = \dot{Q}_{\phi} + \dot{Q}_{e} + \dot{Q}_{c} + \dot{Q}_{r} \qquad (7)$$

where the first two terms on the rhs denote the contribution from the electrons as $\dot{Q}_{\phi}=I\cdot\phi$, where ϕ is the work function, depending on the anode material,for copper, for example, is 4.3 eV, and $\dot{Q}_{e}$ includes the kinetic energy of the electrons and the energy acquired as a result of the accelerated electrons through the anode drop V_a estimated at about 5 V in the current range from 100 to 200 amperes, but V_a probably, varies inversely with the current and ,also,increases with the arc length. Thus, the electronic contribution is:

$$\dot{Q}_{eT} = I\cdot(\phi+V_a+3\cdot k\cdot T/(2\cdot e)) \qquad (8)$$

To calculate the radiation energy transfer $\dot{Q}_{r}$ the diameter of the luminous region of the arc, the absorption coefficient of the anode and the emission coefficient of the gas must all be known. In general, $\dot{Q}_{r}$ is a small fraction (approximately one tenth) of the convective heat $\dot{Q}_{c}$. The convective part $\dot{Q}_{c}$, for low current is a small fraction of the total heat to the anode, but as the current increases $\dot{Q}_{c}$ increases more rapidly than $\dot{Q}_{eT}$, which increases almost linearly with current, since V_a does not change much.

One way to represent the convective heat transfer is to employ an effective heat transfer coefficient h, as

$$\dot{Q}_c = h \cdot \Delta T \cdot \text{Area} \qquad (9)$$

where h can be evaluated for axisymmetric stagnation type flow, as

$$h = 0.76 \cdot (\mu \cdot c_p / k)^{1/3} \cdot (U \cdot d / \nu)^{0.5} \qquad (10)$$

where d is the jet diameter. Then, h can be evaluated to be from 1000 (200) to 1500 (300) W/m^2K ($Btu/hrft^2$).

It is much more difficult to evaluate the temperature distribution and therefore to obtain the temperature potential ΔT. However, it is reported by Converti [10] that ΔT is a weak function of current. The jet velocity has been found to vary linearly with current, and therefore:

Q_c will be proportional to $I^{1/2}$

whereas, Q_e will be proportional to I.

For low current values and arc lengths less than 6 mm it has been found [14] that Q_c is always less than 25% of the convective flux and therefore the total heat input will increase roughly linearly with current.

3.4 TEMPERATURE MEASUREMENTS

Thermocouples were spot welded on the workpiece surface at various locations and temperatures were recorded using the data acquisition system and an Omega digital thermocouple thermometer.

The centerline backside temperature is expected to be a good indication of the size of the weld pool and therefore a good measure for comparison with the values predicted by the model; this temperature was measured for the three workpieces. For the thin workpiece (7/8"•7/32") and the medium thickness workpiece (7/8"•7/24") the topside temperature at a distance 7.4 mm from the centerline was measured. The thermocouples were shielded to eliminate the effect of the very strong radiation from the arc, which otherwise could alter significantly the thermocouple signal. For the third workpiece the backside

temperature at a location 5.0 mm from the centerline was also measured; a copper/constantan thermocouple was used, since the range of this temperature was not expected to exceed 700 degrees Celcius.

To check the effect that the water cooling rate could have on the temperature level of the system, experiments were conducted with different cooling rates, 70%,50% and 20% of the maximum flow rate. As shown in the Figure 15 the cooling rate has no effect in the measured temperature, except in the case of very low flow rate, for which a strongly assymetric cooling results. In such cases the water temperature rise is more than 20 degrees C for relatively high heat inputs.

All the measurements were being taken after waiting at least one minute in order for the system to have enough time to equilibrate at steady state. The time constant, as it can be shown either from the transient measurements or from analytical calculations was less than 15 seconds.

The arc length is also an important factor upon which the temperature of the system depends. In Figure 16 the centerline temperature for the second (medium thickness) workpiece is plotted against the effective heat input, the heat delivered to the cooling water. In the case of the long arc a large temperature drop was recorded for emitted power above 1 kw, after the puddle is formed. Such a temperature drop should be expected, although probably, not so dramatically, since the anode spot of the heat input is expected to increase with the arc length and therefore the heat input is not as focused as in the case of shorter arc lengths.

In the next Figure 17 the centerline back temperature is plotted as a function of the effective heat input for the three plates. The centerline back temperature is very sensitive to the heat input with the slope $dT/d\dot{Q}$ increasing as the penetration increased. Near full penetration the changes

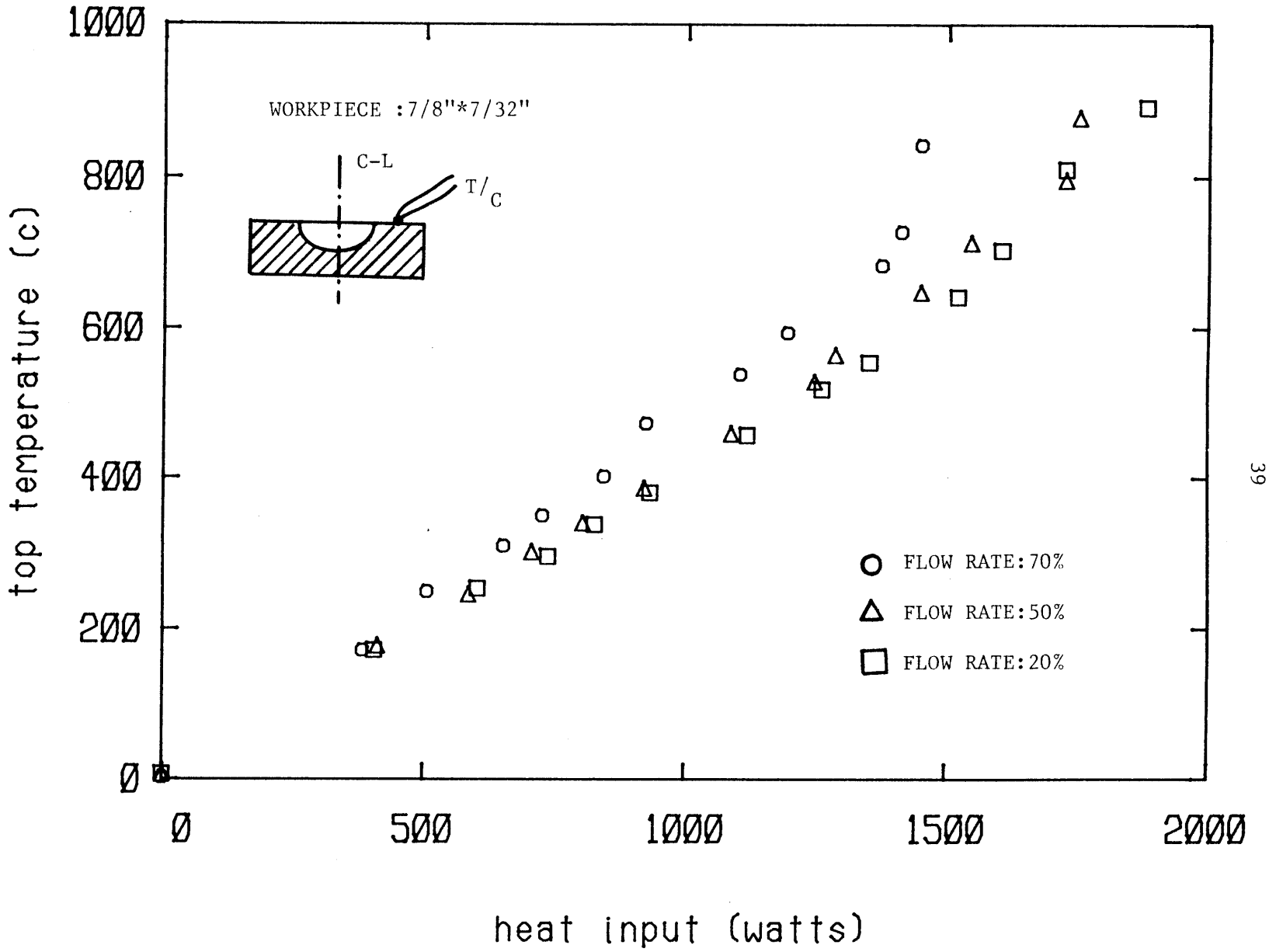

FIGURE 15 :Effect of flow rate on top temperature

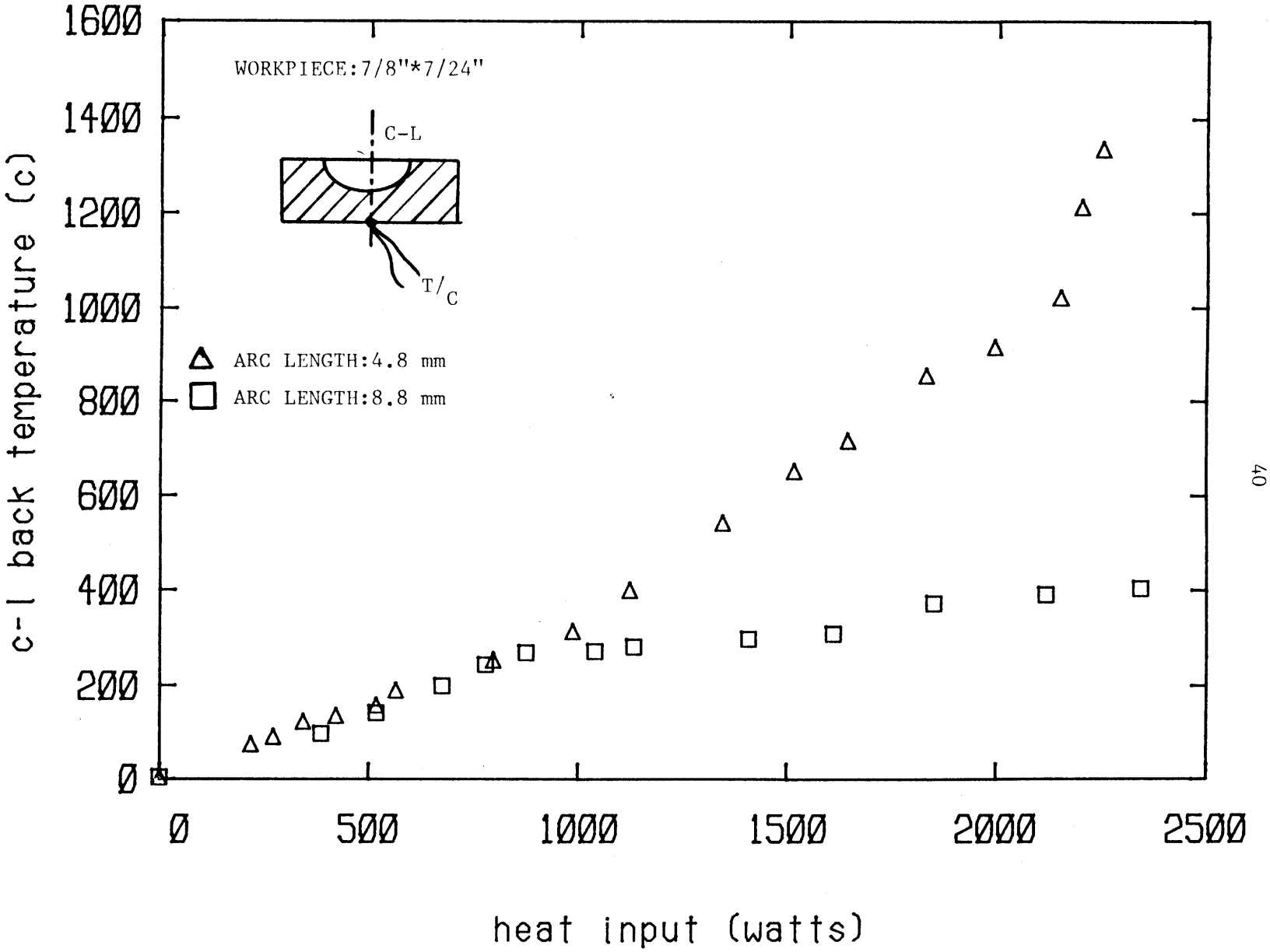

FIGURE 16: Centerline back temperature for different arc lengths

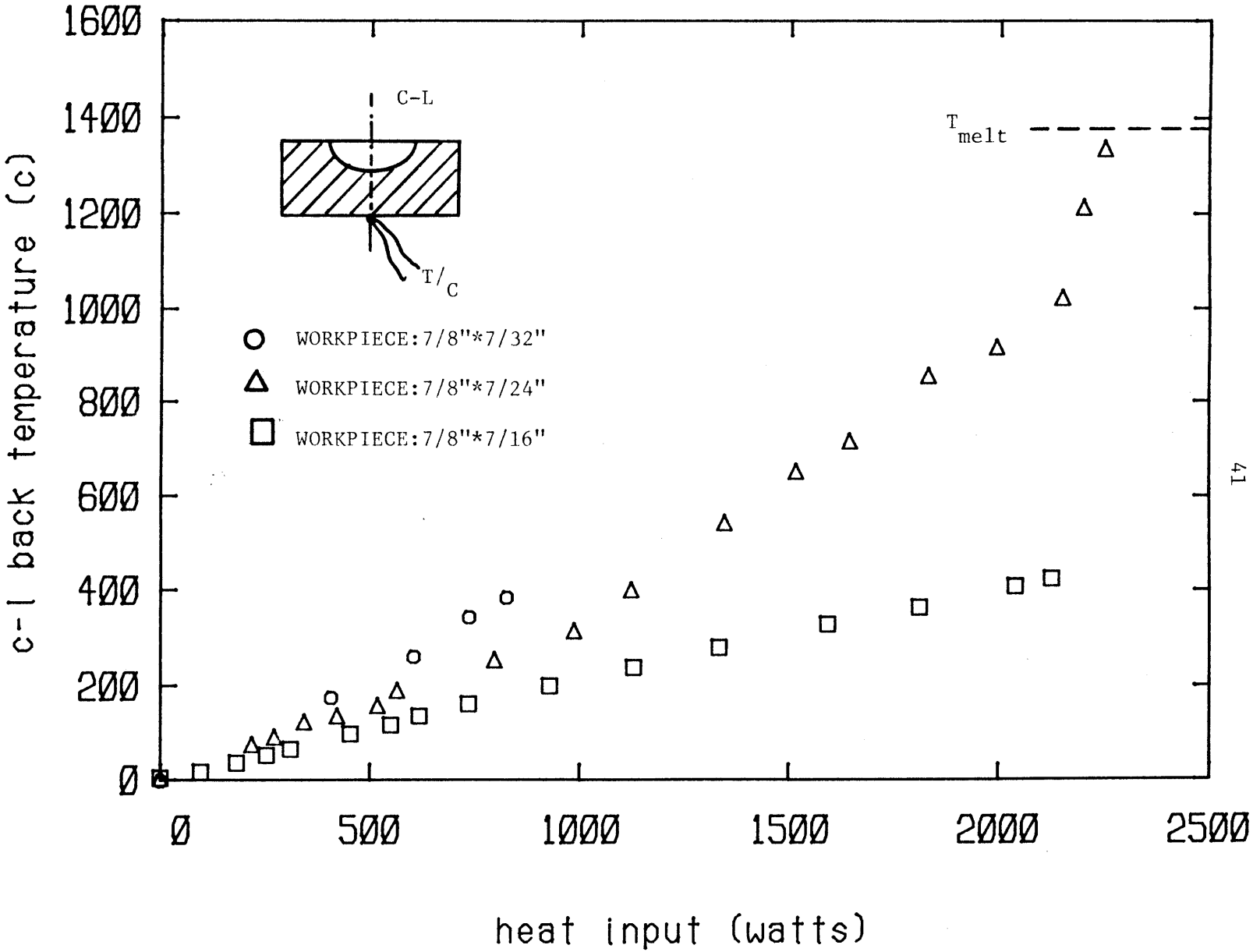

FIGURE 17: Centerline back temperature for different workpieces

are extremly rapid. For the thick workpiece for which full penetration is expected to occur only above 4 kw effective heat the centerline back temperature varies almost linearly with the heat input with a change of 50 degrees C for 500 watts. For the medium thickness workpiece the corresponding change is 250 degrees C per 500 watts. It is seen that a very detailed recording of the centerline temperature was obtained for the second workpiece with a chromel/alumel thermocouple responding up to nearly the melting temperature. The maximum temperature recorded just before the full penetration was 1337 degrees C, the melting temperature of mild steel being at 1347 degrees C. Unfortunately, with the thin workpiece the constant/copper thermocouple used did not respond above 500 degrees C and the data are very limited in this case. Finally the experiments for the thick workpieces were repeated three times to ensure that the measurements taken were correct since their magnitude was rather low. In Figure 18 the top temperature for the small and medium thickness workpieces are presented with the thinner workpiece experiencing higher temperature. That the effect of the strong radiation from the arc was completely eliminated using insulated chromel/alumel thermocouples could easily be observed during the experiment, since when a signal from the emitted radiation heat is picked up the thermometer intications are very unsteady, but no such fluctuation were observed.

For the thick workpiece the back temperature was measured instead of the top temperature at a distance 5.0 mm from the center, as shown in Figure 19. It is seen that the slope $dT/d\dot{Q}$ is not larger that the slope of the centerline back temperature, which was also low as it was compared with the thinner workpieces. The linear response at small values of heat input is expected, since at low heat input pure conduction occurs with no puddle formed yet and also the losses from the back surface due to radiation and natural convection (hot plate facing downwards) are small.

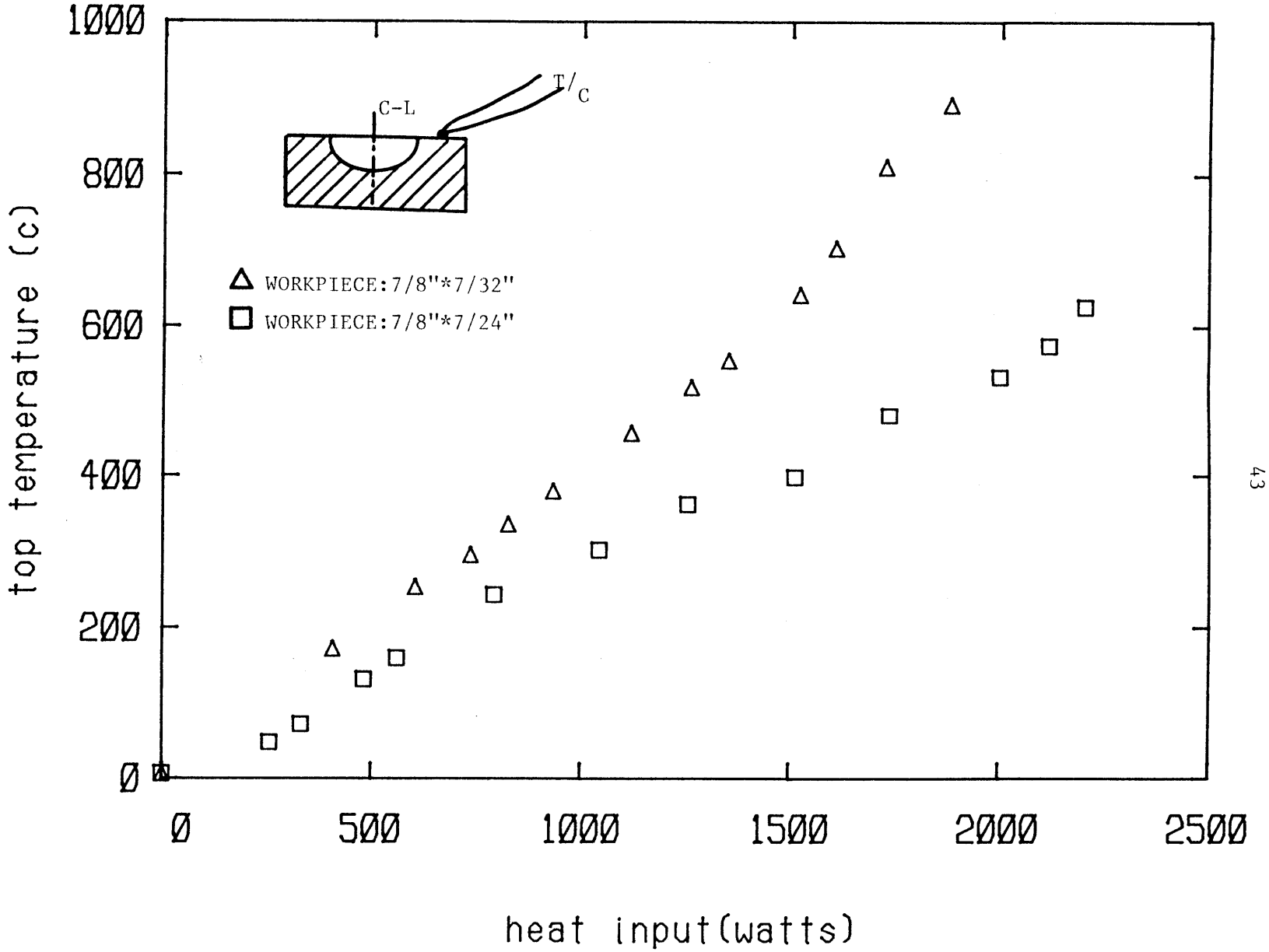

FIGURE 18 :Top side temperature versus effective heat input

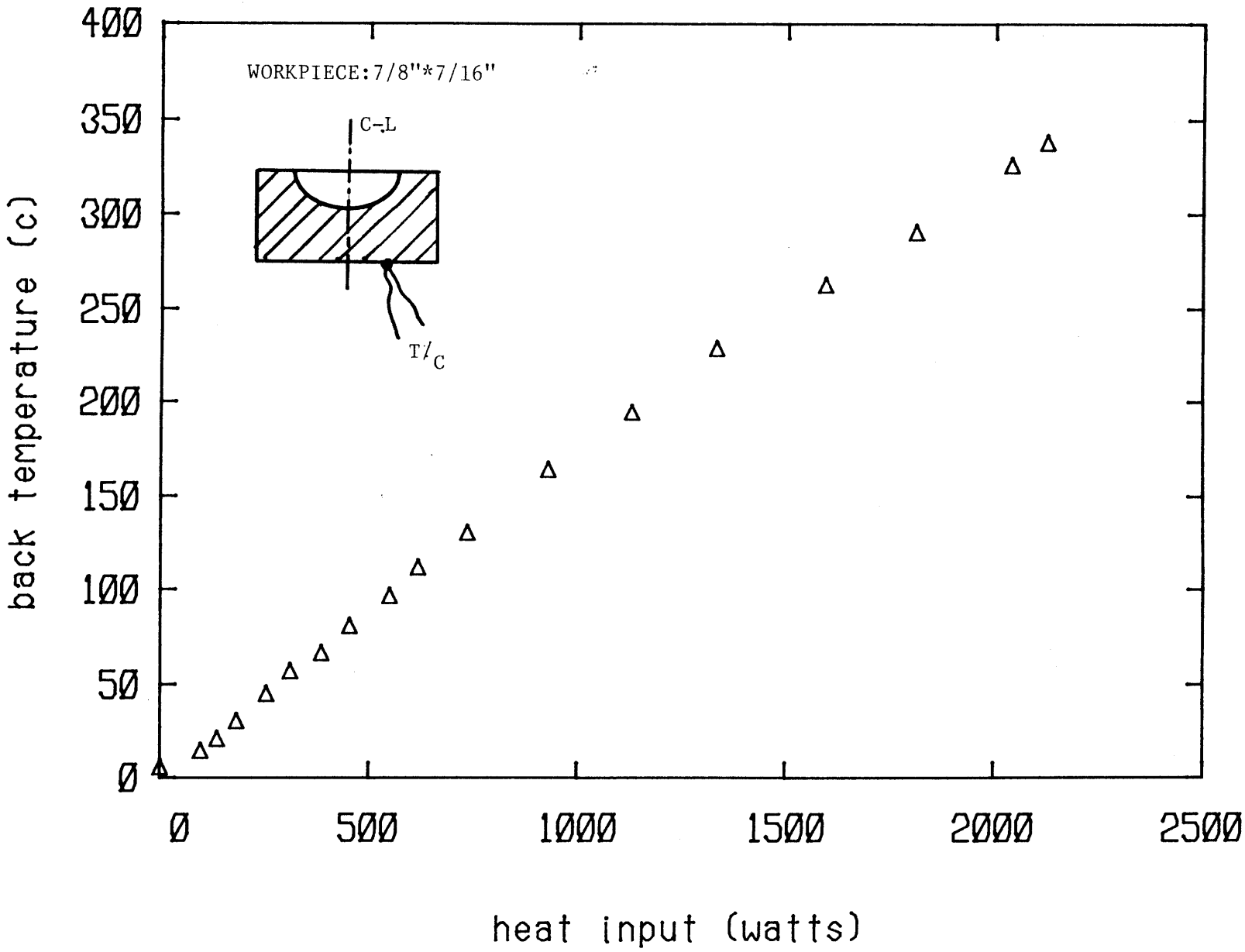

FIGURE 19:Back temperature versus effective heat input

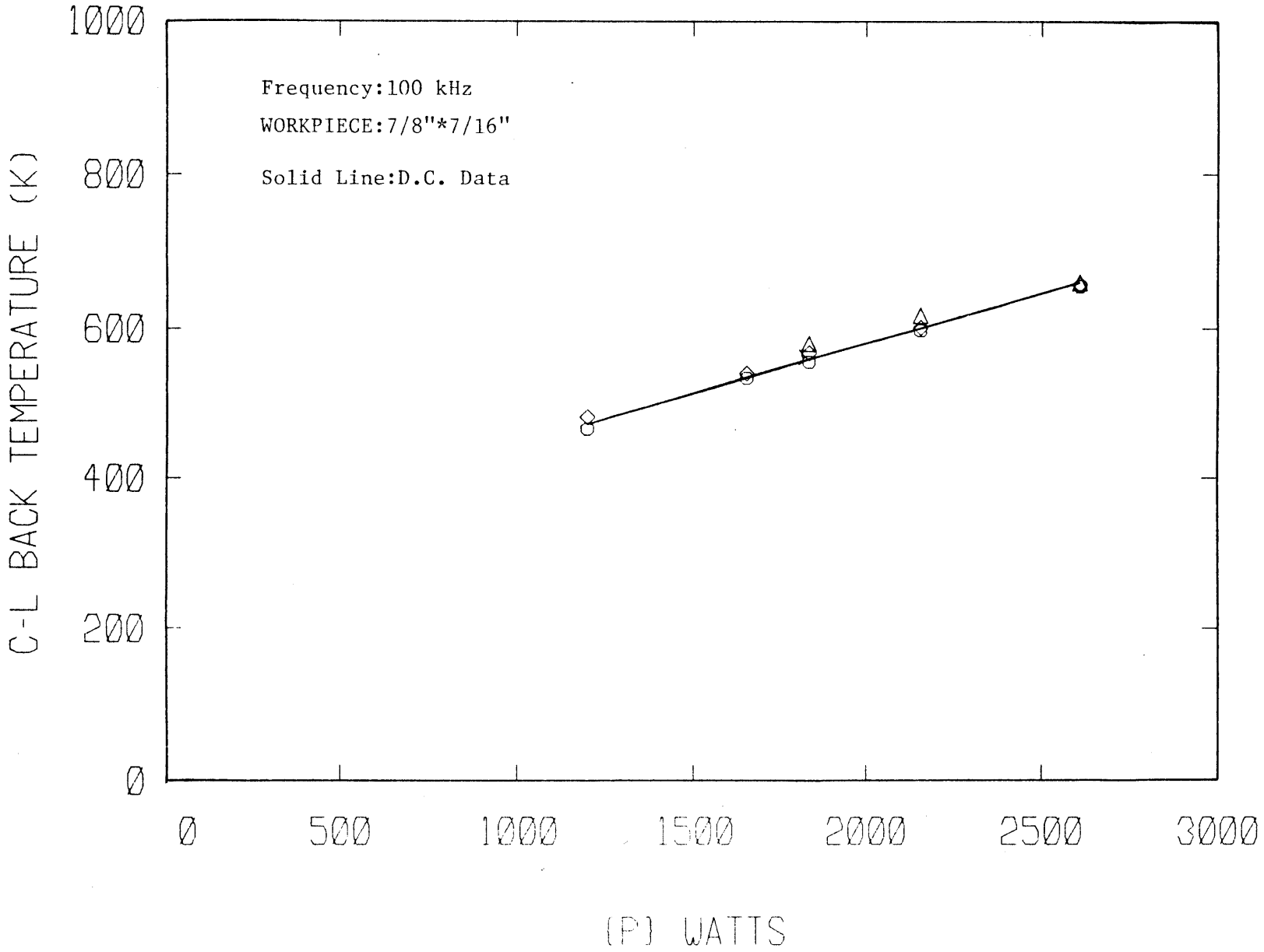

FIGURE 20 :Effect of current pulsing on the centerline back temperature

To examine the effect of the current pulsing on the temperature level of the system the centerline back temperature was measured for the thick workpiece and plotted in Figure 20, where a comparison is being made with the case of D.C. For ratios of current amplitude over average current larger than unity slightly higher temperatures were measured, but no difference was observed for this ratio being less than one. It is expected that in the case of thinner workpieces a different respond would occur.

3.5 VELOCITY MEASUREMENTS

The difficulties involved in the measurement of velocities within a puddle of high temperature melt are self evident. In addition to this the very small dimensions of the weld pool make this task almost impossible. On the other hand, it is very important for heat transfer calculations to establish a realistic order of magnitude for the Reynolds number inside the pool and furthermore the velocity field.

To determine the direction of the flow inside the pool a tungsten colored node was inserted into the hole drilled into the workpiece of dimensions 7/8"•7/24" at about 8 mm deep from the side and 1.5 mm from the top at a location, where a molten steel puddle was expected to be formed. After the experiment was finished the workpiece was cut at exactly this position ,but the tungsten node was not there, apparently moved to another place by the flow.

This attempt along with other investigators attempts to estimate the velocity of the interior flow show that direct measurements of the flow in the real system is a rather unsolved problem, at least at the present time.

There have been reported, however, indirect measurements of the pool surface velocity in the real system, or in similar systems, by taking a time

exposure photographs of a small bead of material (glass, for example) as it was swept across the surface. This, of course, gives no indication of the flow underneath, which can even have the opposite direction, and on the other hand the reported values of surface velocity for almost the same conditions with GTAW vary from a few millimiters per second to one meter per second. It has been reported by Woods and Milner working with pools of mercury that the observed intensity of motion was varying as the square of the arc current, increasing also, with the melting point for different materials.

Mercury at room temperature has a viscosity of 0.00161 $Nt \cdot s/m^2$, close to that of molten steel and so the room temperature mercury pool may be expected to show similar behaviour to that of large high temperature melts. However, to keep in the same conditions in the simulation experiments as in the real case is very difficult. For instance, a crust of mercury oxide forms on the pool surface, and this layer likely alters the surface tension characteristics of the melt. For the mercury, thermally induced motion can be large, whereas for the real system this effect is almost negligible. This problem encountered by Sadoway et al [15], who conducted experiments with molten salts, a binary mixture of KCl and LiCl, using a Laser doppler anemometer to measure velocities in this transparent materal. The problem was that the flow induced was caused not by electromagnetic forces from the applied current through the metals, but by the dominant buoancy forces.

To keep the same real welding conditions in the simulation experiments a complete set of simulation criteria, as determined from the equation of motion and the electromagnetic field, must be met.

If the effect of velocity of the metal on the magnetic field is neglected (a reasonable assumption since the magnetic Reynolds number for welding conditions of steel plates is much less than unity) a complete set of similarity parameters for the steady state is as follows:

$$\Pi_1 = \rho \cdot U \cdot l^2 / \mu_0 \cdot I^2 = \text{inertia force /em force}$$

$$\Pi_2 = \mu_m \cdot U \cdot l / \mu_0 \cdot I^2 = \text{viscous force/em force}$$

$$\Pi_3 = \rho \cdot g \cdot l^3 / \mu_0 \cdot I^2 = \text{gravity force/em force}$$

where μ_0 is the magnetic permeability, μ_m the dynamic viscosity of the melt and l is a characteristic length. To keep only the two parameters Π_1, Π_2 constant with a mercury pool (2) instead of the real system of the molten steel (1), two constraints should be fullfilled:

Π_1 = constant, therefore $I_1/I_2 = 5$

Π_2 = constant, therefore $U_1 l_1 / U_2 l_2 = 7$

The above relations indicate that 100 amperes of arc current for the real system correspond to only 20 amperes to the Hg system, but still it is not sure if the mercury with a boiling point of 357 degrees C will not evaporate. Gallium with boiling point of 2205 degrees is suitable for this use, since all its other properties are similar but it has a very high cost.

3.6 CROSS WELD SECTIONS

After each experiment, the molten metal was removed from the weld pool by suddenly applying a very high water cooling rate, as the arc was turned off. The rapid cooling prevented the melt from binding with the solid material so the solidified content of the pool could be removed with a screwdriver. After the pool material was removed the workpiece was cut across the centerline and was grounded and polished.

The experiment with the thick workpiece was repeated three times, so three different weld cross sections were produced under slightly different welding conditions. The very shallow puddle, shown in Figure 21.a, was produced by applying a rather low d.c. current and very high cooling rate, whereas the very uniform parabolic melting boundary shown in Figure 22.a was

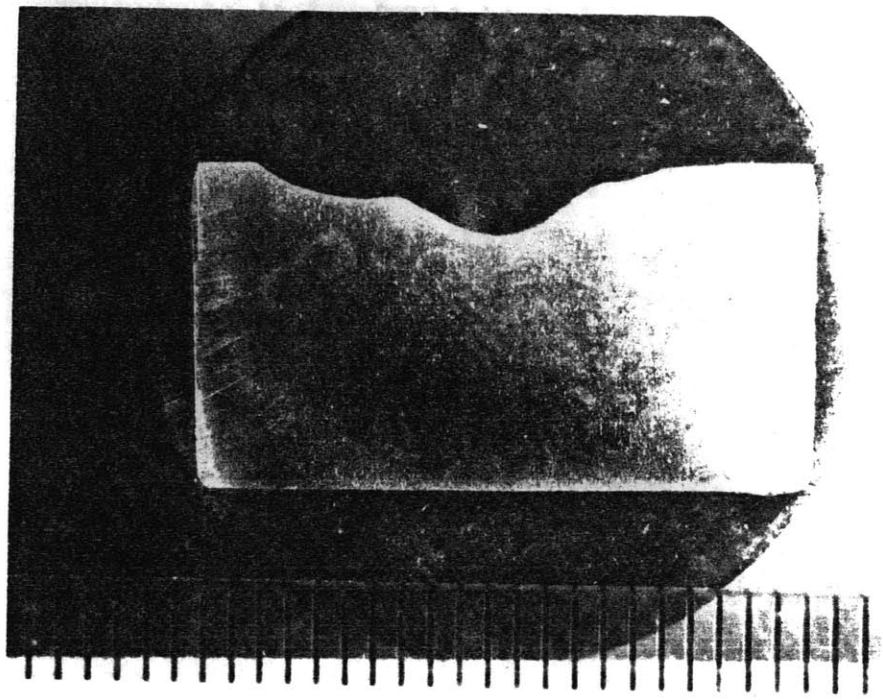

FIGURE 21 a:Shallow puddle for workpiece 7/8"*7/16"

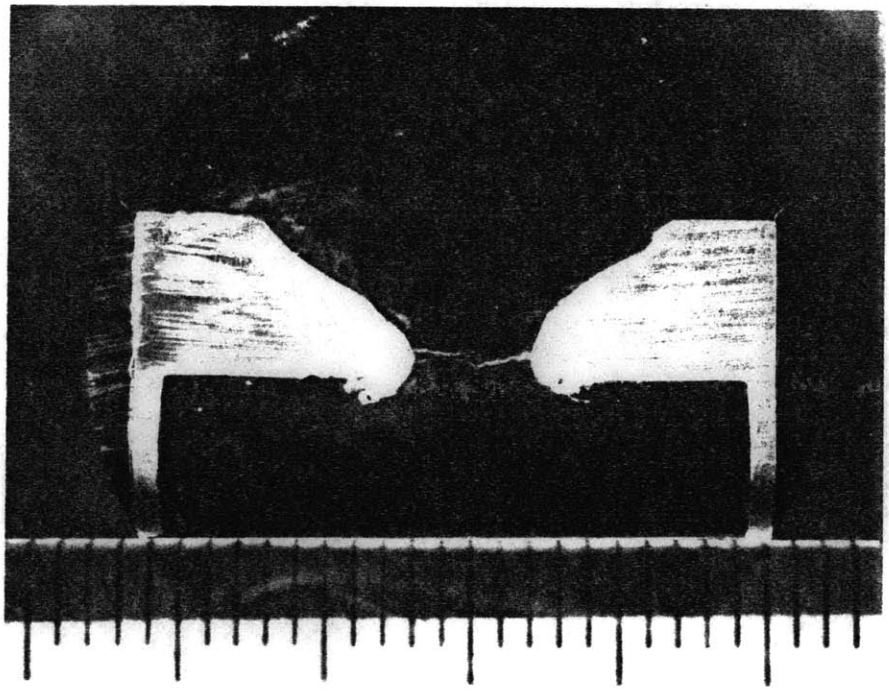

FIGURE 21 b:Full penetration for workpiece 7/8"*7/32"

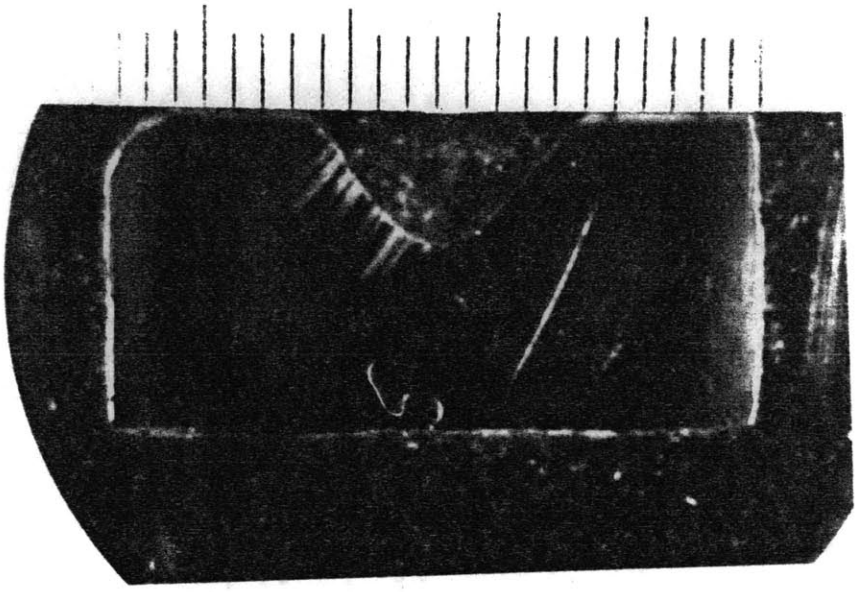

FIGURE 22 a : Parabolic boundary

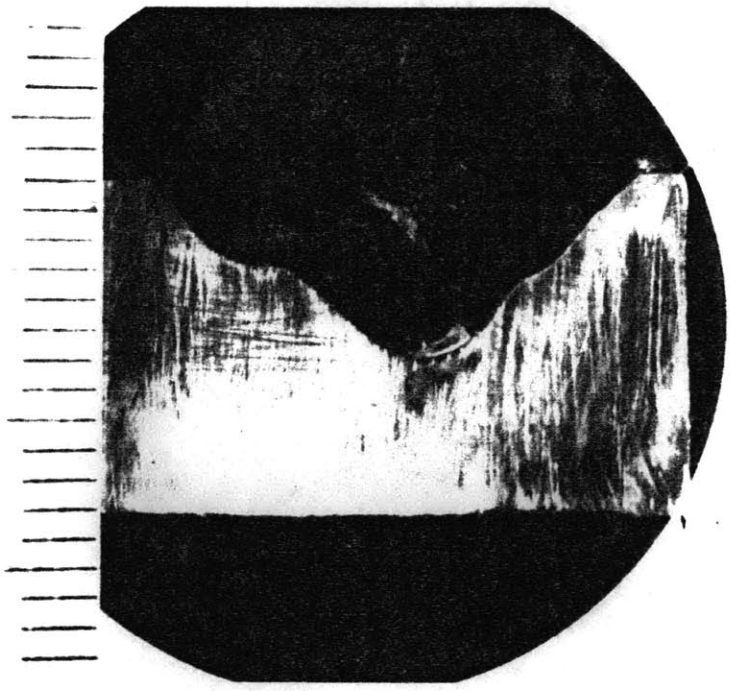

FIGURE 22 b : Double shape boundary

produced by applying current up to 240 amperes and 80% cooling rate. To demonstrate the effect of the concetrated impurities three small holes were symmetrically drilled from one side of the disk workpiece and a small amount of green powder of Cr_2O_3 was put in the holes as well as in the pool surface bounded in place by using a paint as an organic binder. The effect of Cr_2O_3 is twofold. First it changes the surface tension characteristics of the molten steel and therefore affects the intensity of the motion with more heat flowing outwards to the cold edge so that a more shallow puddle is produced. Second, it changes the wetting angle and this affects again the radial surface flow. The resulted weld pool is shown in Figure 22.b.

The two other workpieces were fully penetrated the first (thin), Figure 21.b, at arc current of 190 amperes and the second at 210 amperes.

3.7 MEASUREMENT OF T_{MAX}

An attempt was made to measure the maximum temperature in the weld pool expected at the centerline of the pool just underneath the electrode tip. A CCD array was used purchased from E.G.and G. with 256 elements. The CCD array was focused on the centerline of the pool to pick up the radiation emitted from the very hot pool surface. Although a diaphragm and an infrared filter was used to reduce the light intensity from the arc its effect were not completely eliminated and the final recorded signal was not sure if it caused by the radiation emitted by the high temperature pool surface.

More work is needed to first calibrate the CCD array according to a standard temperature scale in the high range from 1500 degrees and above. By selecting the proper infrared filter since the spectral scan of the hottest part of the argon shows strong peaks in the red and infrared region, it should be possible to measure the maximum temperature of the pool, the importance of

which is self evident, since it is expected to be a very precise indication of the weld pool size and one of the variables to be sensed in the real contol applications when no access in the backside of the plates for the measurement of the temperature is possible.

3.8 SUMMARY

To summarize, in this chapter the experimental apparatus was described first and data on the arc voltage-arc current relation, on the arc efficiency and on the surface temperature were then presented. A universal curve was found to correlate the experimental data for the arc efficiency with lower efficiency measured at higher current values. The effect of impurities was also studied and the addition of Cr_2O_3 on the molten steel was found to alter dramatically the weld pool shape.

CHAPTER FOUR

THEORETICAL ANALYSIS

4.1 INTRODUCTION

Within the context of control systems for weld geometry it is important to understand and develop computationally simple models to predict the puddle size. The model must be capable of predicting the effect of a variety of parameters, such as the heat input, the welding torch speed, the arc length, and the impurities in the pool.

Since the motion in the pool cannot be ignored in the heat transfer calculations it is essential to investigate the possible mechanisms, which give rise to motion. Stirring type fluid motion in the puddle can be caused by several such mechanisms including electromagnetic stirring forces, surface tension forces resulting from the nonuniform surface temperature, shear and normal forces exerted on the puddle surface by the plasma flow and the buoyancy forces resulting from the large temperature gradients within the pool. All these forces, which may reinforce each other or conflict with each other are responsible for the directionality of the heat flow in the pool as compared with what would be expected from pure conduction only. The overall effect is the formation of very shallow weld puddles when the fluid and heat flow radially outwards in the pool surface or deep puddles when the main motion is radially inwards.

If the heating was from a point source in the case of a thick block of metal and there was no interior motion the melting boundary would be hemispherical as it is predicted by the conduction heat transfer theory. In the real case the shape of the pool is not known and it is a very difficult

problem to determine both the precise shape and the size (dimensions) of the pool. The approach adopted in this work is to solve the coupled fluid flow and heat flow field with a free boundary (melting interface) by postulating the shape of the boundary to be generally consistent with the puddle shapes observed from our experimental data and the results of other investigators and then determining from the model the size of the pool for a specified set of conditions. Results for a two shape parameter model have been completed and work on a three shape parameter model have been started.

The solution technique is to split the problem into three regions (a) the arc (b) the solid material and (c) the molten metal region and then solve iteratively since the physical phenomena occuring in these three regions are coupled.

A numerical model for a GTA arc has been developed by Converti [10] and in this work only experiments were conducted to determine the arc-voltage relation and the arc efficiency. The mode of heat transfer through the solid material is conduction, a well posed problem with the outer edge of the plate at prescribed temperature. In the liquid region the enhanced heat transfer is taken into account by determining first the motion of the melt and then apply the principles of heat convection. After the solution in the convection and conduction sides have been obtained, the heat fluxes at the solid/liquid boundary are tested to see if they match. If the results for the convection side and conduction side do not match a new boundary is specified (by its depth and width) and the solution procedure repeated.

4.2 CONDUCTION IN THE SOLID

For the stationary configuration used in this work the full problem for the weld puddle formed is displayed in Figure 23.a. Axisymmetry allows reduction to the half width (two dimensional) geometry as shown in Figure 23.b. The outer face of the workpiece is in contact with the cooled copper base which is kept at the coolant temperature 10 ^{0} C. The lower and upper surface are assumed to radiate as a grey body with a specified emissivity. The effect of natural convection from the surfaces was included using a temperature dependent heat transfer coefficient. To show the importance of the heat losses, adiabatic bottom and top surfaces have also been examined . The conduction problem is linear when the boundary conditions are adiabatic, but radiation and natural convection introduce nonlinearities which can increase the computational time by a factor of two.

4.2.1 FINITE ELEMENT MESH EMPLOYED

The conduction solution was obtained with a general purpose heat transfer finite element code ADINAT [21], developed at M.I.T. For steady state various finite element meshes were tested before the final mesh selection. Optimization requires that with a minimum number of nodes and elements a good agreement for the computed heat fluxes at the nodes common to more than one element to be obtained. In the meshes shown in Figures 24 through 27, 24 isoparametric elements with 98 nodes were used. The size of the elements is changed automaticaly as the mesh is deformed to capture any shape of the weld pool. In the first mesh, shown in Figure 24, the weld pool boundary is a parabola, in comparison to Figure 25 where the pool shape is simulated by a combination of an ellipse in the uppermost element and a parabola bound the

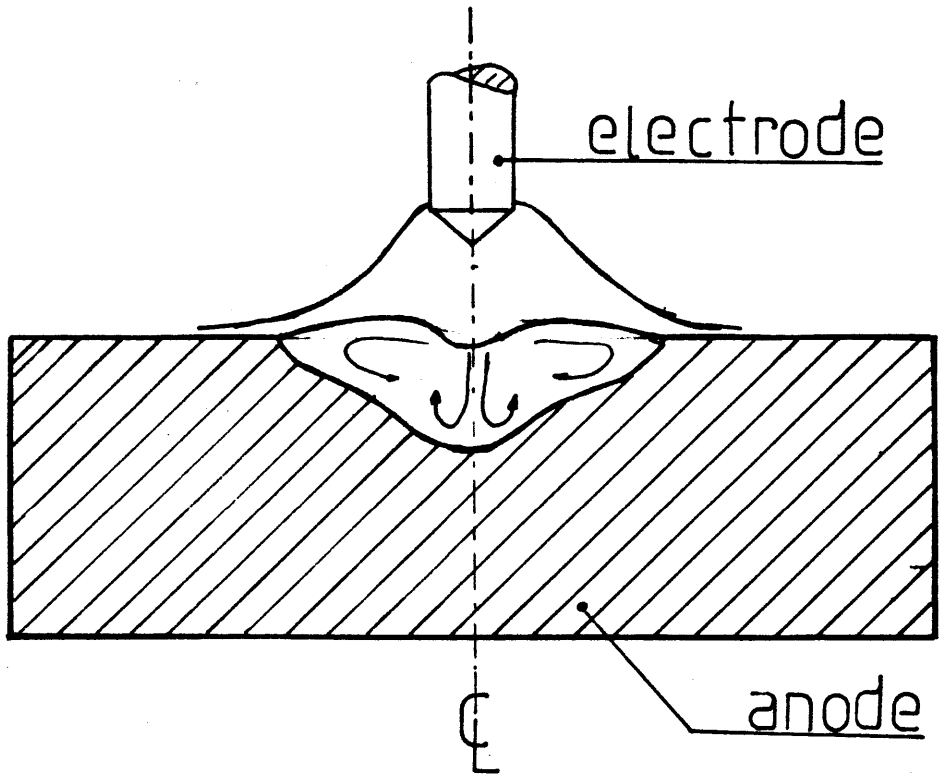

FIGURE 23 a:Demonstration of axisymmetric conditions

FIGURE 23 b:Reduction to half width geometry

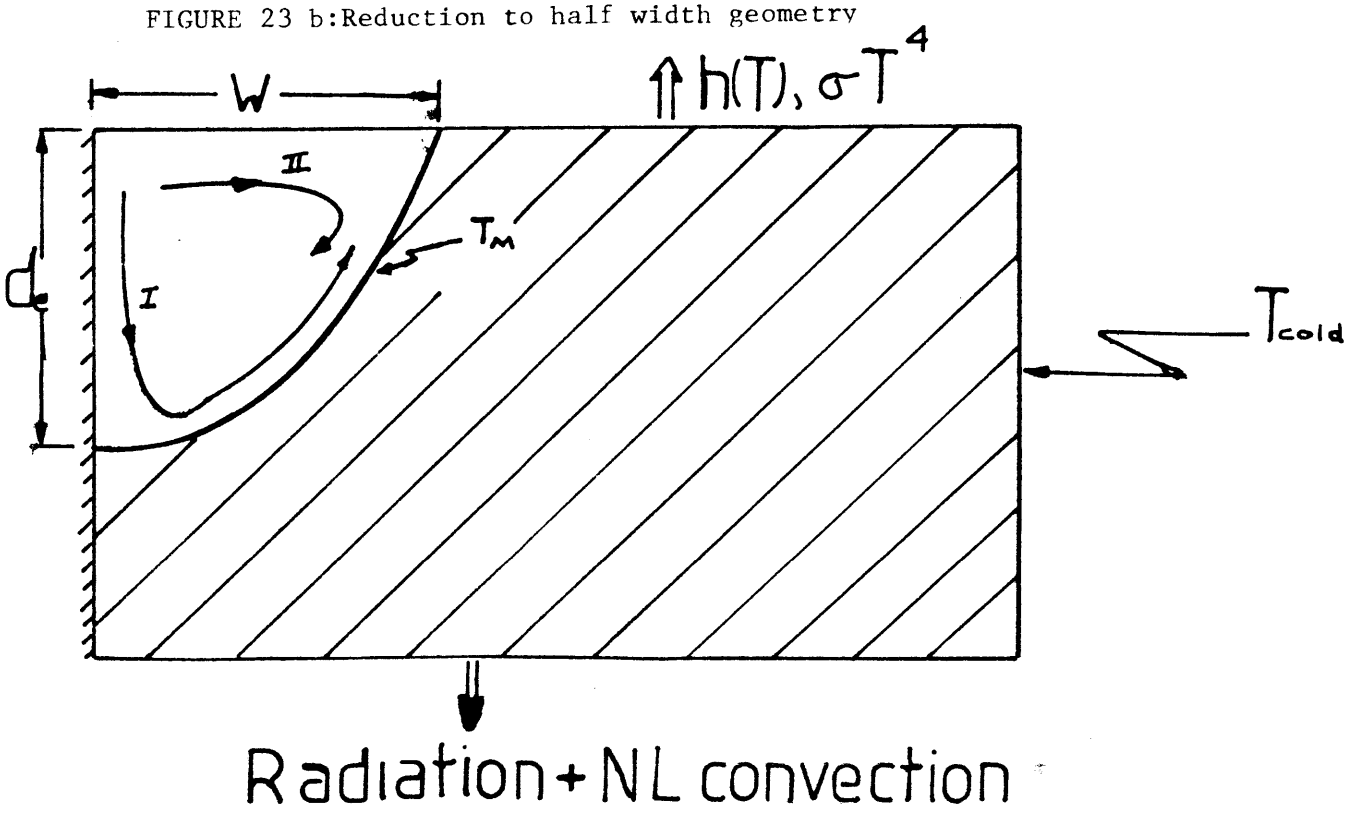

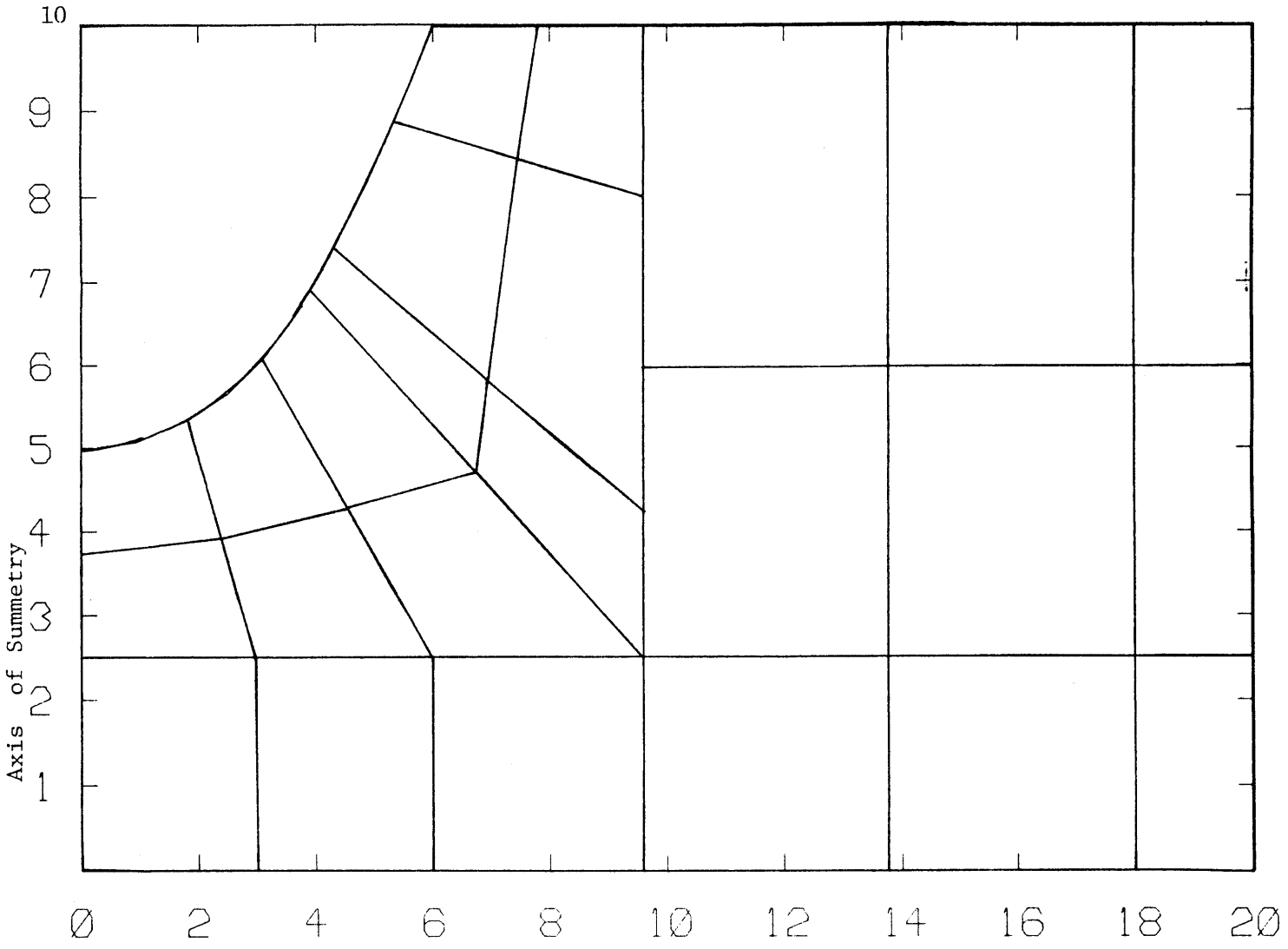

24 -Isoparametric Elements

FIGURE 24:FEM mesh employed with a parabolic boundary

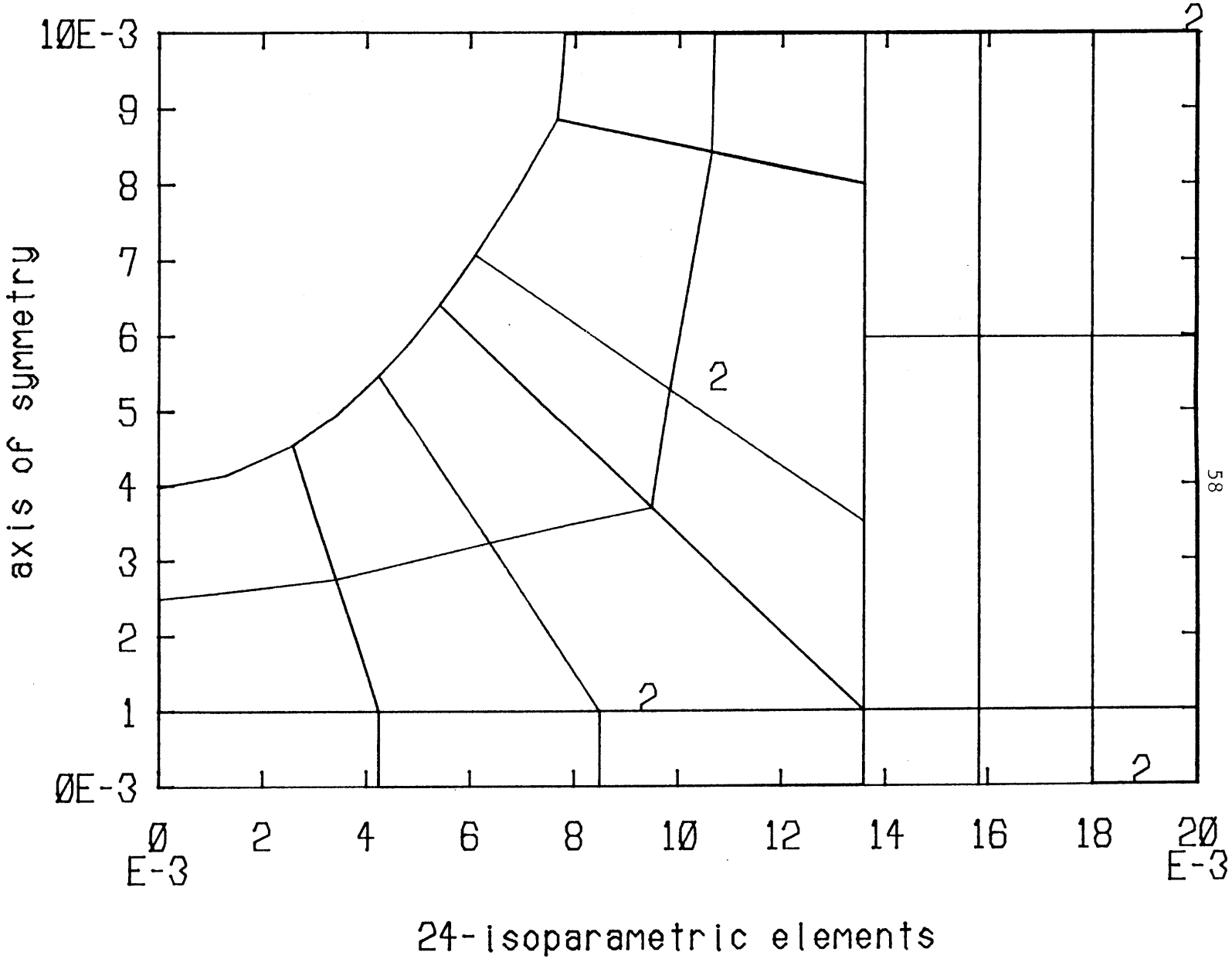

FIGURE 25:FEM mesh employed with a parab+elliptic boundary

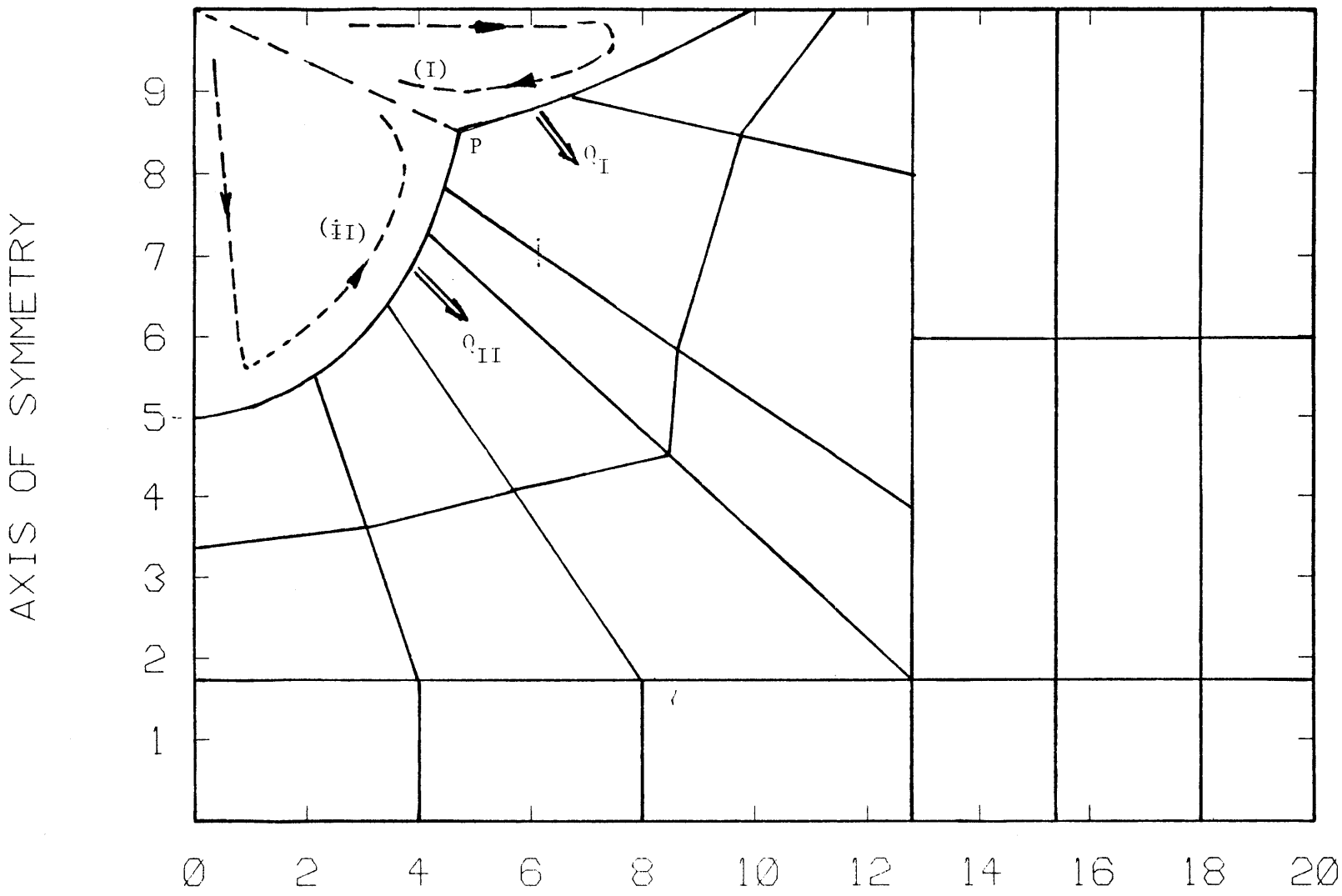

FIGURE 26: FEM mesh for the three parameter model

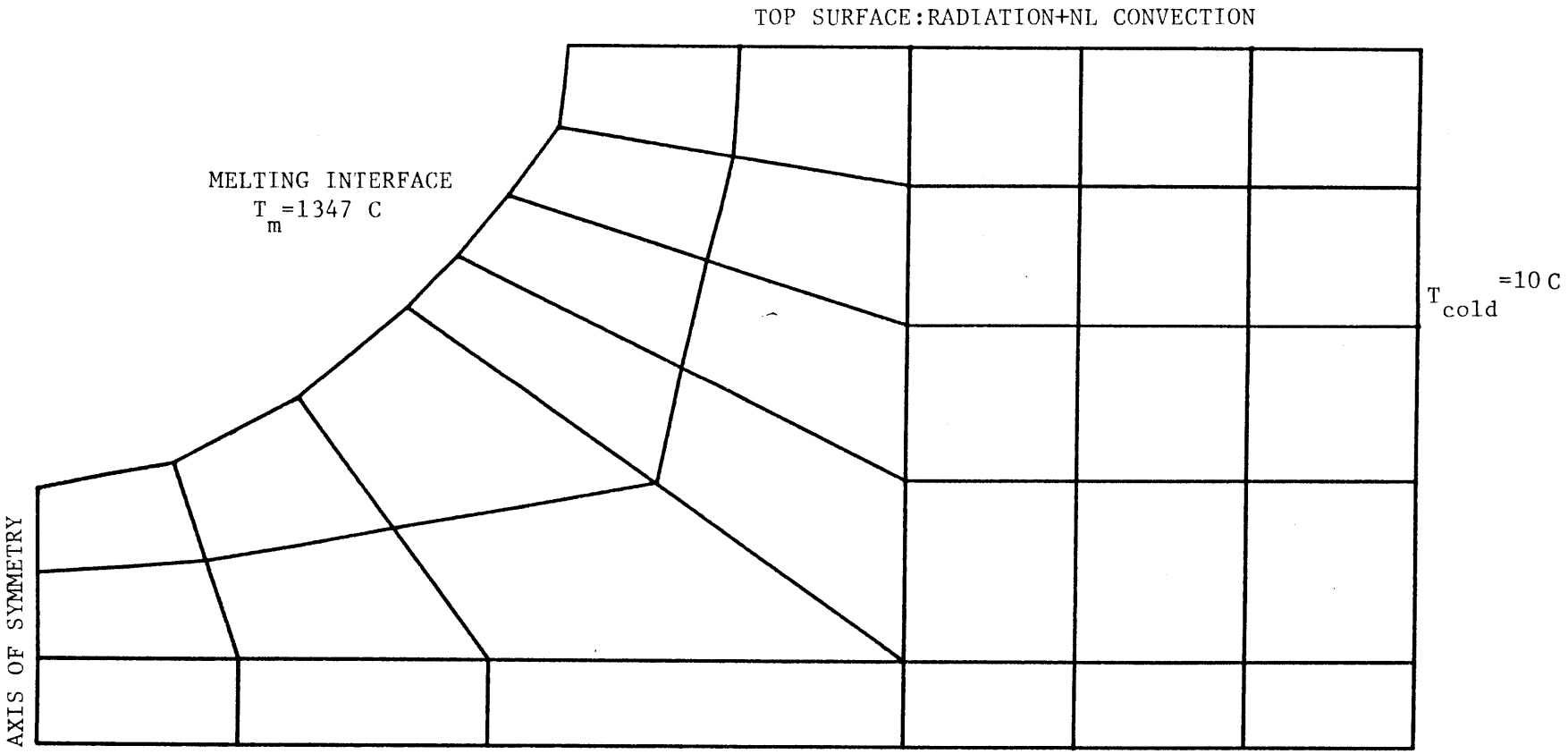

FIGURE 27: An improved finite element mesh with 32 isoparam elements

adjacent interface element. With the second mesh the computed values of the heat flux were smoother, as indicated by the better agreement of fluxes at common nodes. This is expected because in the first case there is a possible singularity at the non-orthogonal corner of the upper element and this results in a large discontinuity in the computed heat flux at the corner node. The mesh shown in Figure 26 was developed for a more advanced model where a double cell flow structure is used to represent cases where the effect of surface tension is such that very shallow puddles are produced (see also photograph at Figure 22.b).

An improved modification of the first mesh is shown in Figure 27, where 32 isoparametric elements with 123 nodes are used. This mesh is superior beacuse in spite the increased number of nodes the required CPU time is not increased by much.

4.2.2 HEAT FLUX CALCULATIONS

For a given depth and width of the pool and a postulated shape the conduction solution can be obtained using the ADINAT code. If the assumed size and shape of the pool were the correct one a perfect matching of the two solutions (conduction and convection) for the heat fluxes at the melting interface would be obtained. To easily check the results of the finite element program various plotting subroutines were developed to plot the heat fluxes at the melting interface and to plot the surface and bottom temperature distributions. In Figure 28, results for one representative case are shown. Two runs are compared for the same depth of the weld pool but different weld pool widths. For these results adiabatic conditions at the surface and bottom of the plate were used. The redistribution of the heat flux toward the bottom of the pool for the smaller aspect ratio of the weld pool is clearly shown.

To examine the importance of convection and radiation losses, the two extreme cases were tested. First, radiation with emissivity of one and thermal convection and second, with no losses at all. As shown in Figure 29, although the way that the heat flux is distributed along the interface does not change significantly, at least in this particular case, its magnitude has changed considerably. The temperature level, although lower when losses are included did not change significantly.

Finally, the effect of the shape of the interface has been examined to show the resulting difference in predicted values of heat flux. For the same dimensions of the pool (depth and width) two shapes were considered, one with an elliptic interface and the second with a parabolic one. The results, plotted in Figure 30, verify that no appreciable difference occurred due to change of boundary. This strongly supports the proposed approach of this work for predicting the weld puddle size, given a reasonable assumed interface shape.

4.2.3 TOP SIDE TEMPERATURE SENSING

One measurable parameter, especially useful when no access in the backside of the plate is possible (as it is the case of pipe welding) is the top side temperature. Although its relation to the penetration is not expected to be a simple one since other factors such as concetrated inpurities in the pool which can change dramatically the interior flow pattern and therefore the heat transfer and the temperature level, it is useful to investigate just how much can be inferred from the top surface measurement using the conduction solution only. For a workpiece of dimensions 40 mm x 10 mm and pool width of 5 mm the penetration was varied keeping an elliptic boundary. The top temperature at various locations and the back temperature

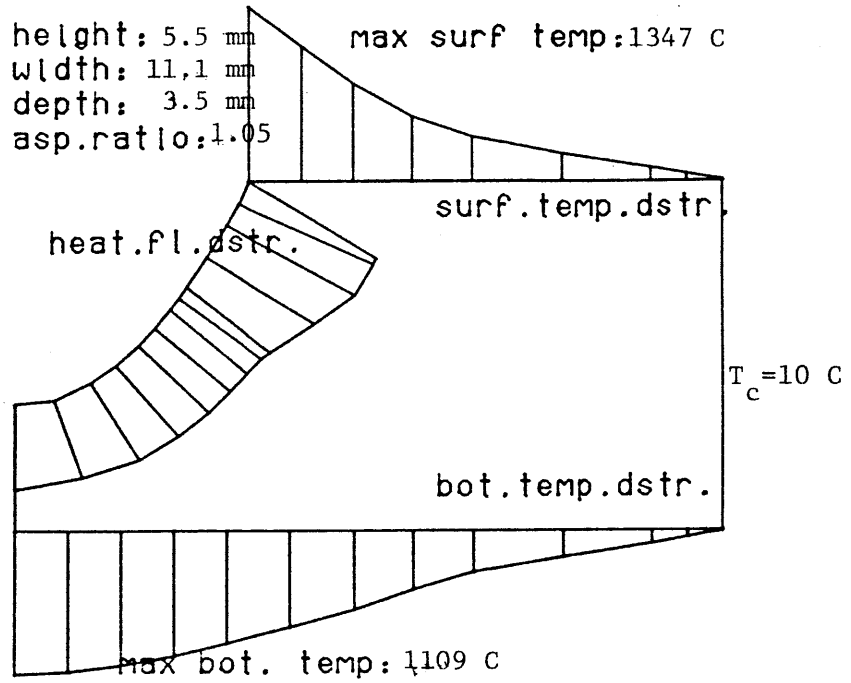

ASPECT RATIO: 1.05

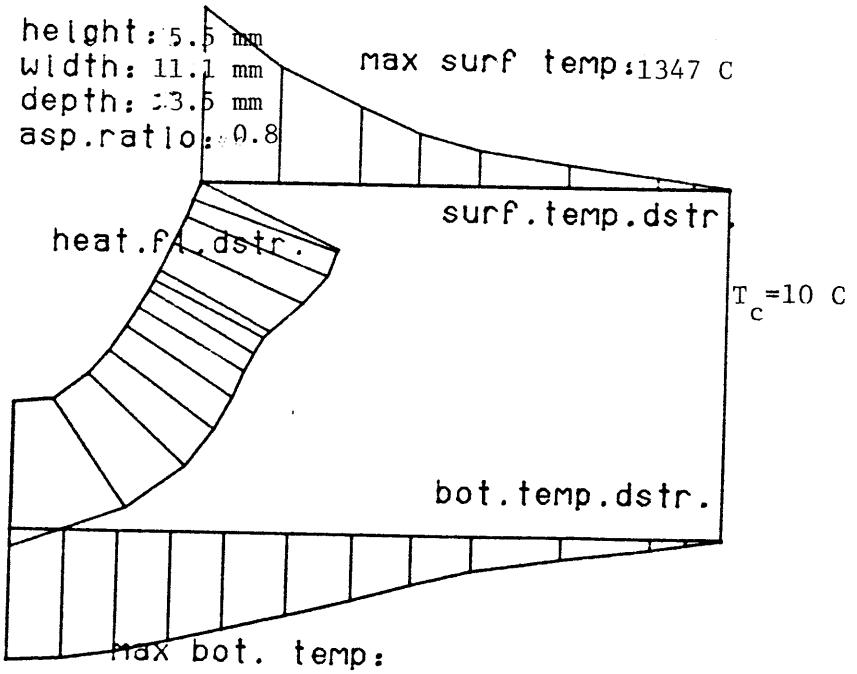

ASPECT RATIO :0.8

FIGURE 28: Comparison of heat fluxes for differ.. pool aspect ratios

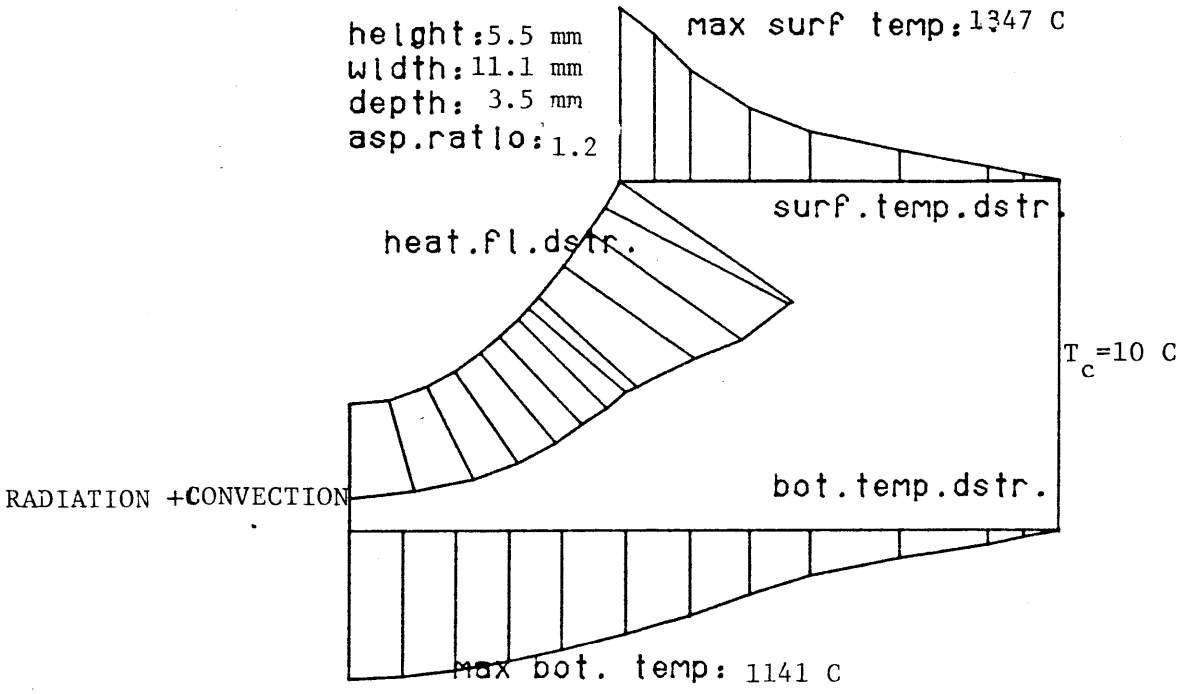

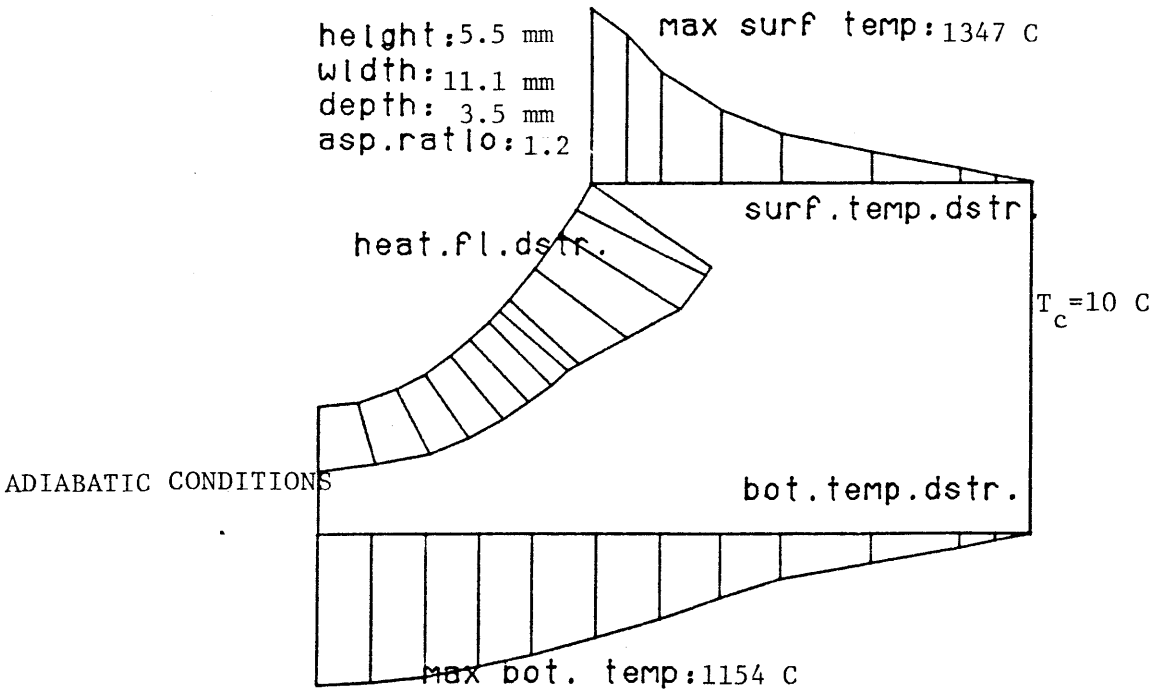

FIGURE 29 :Comparison of adiabatic and heat radiated plate surface

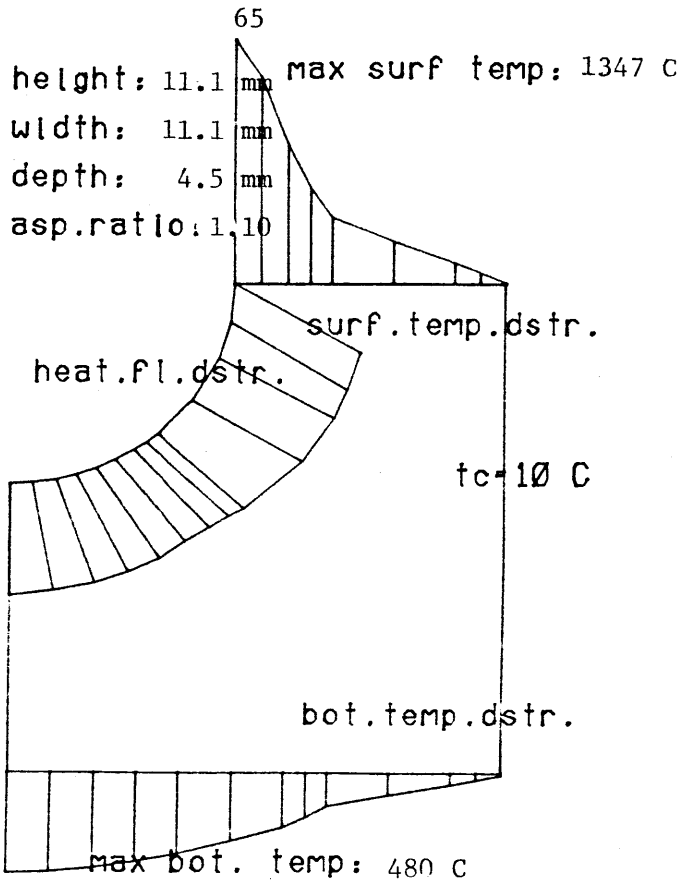

ELLIPTIC BOUNDARY

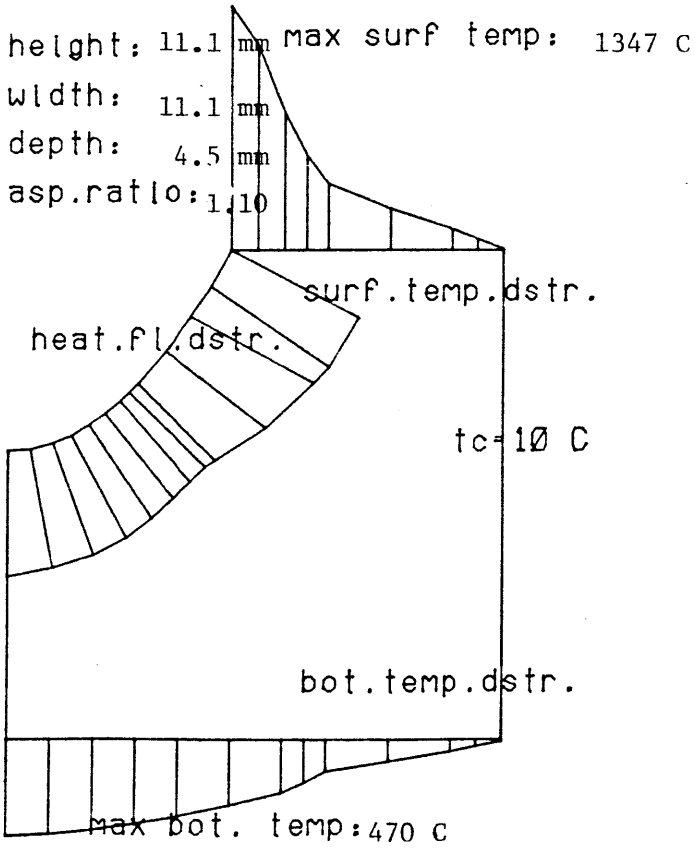

PARABOLIC BOUNDARY

FIGURE 30 : Comparison of different boundaries

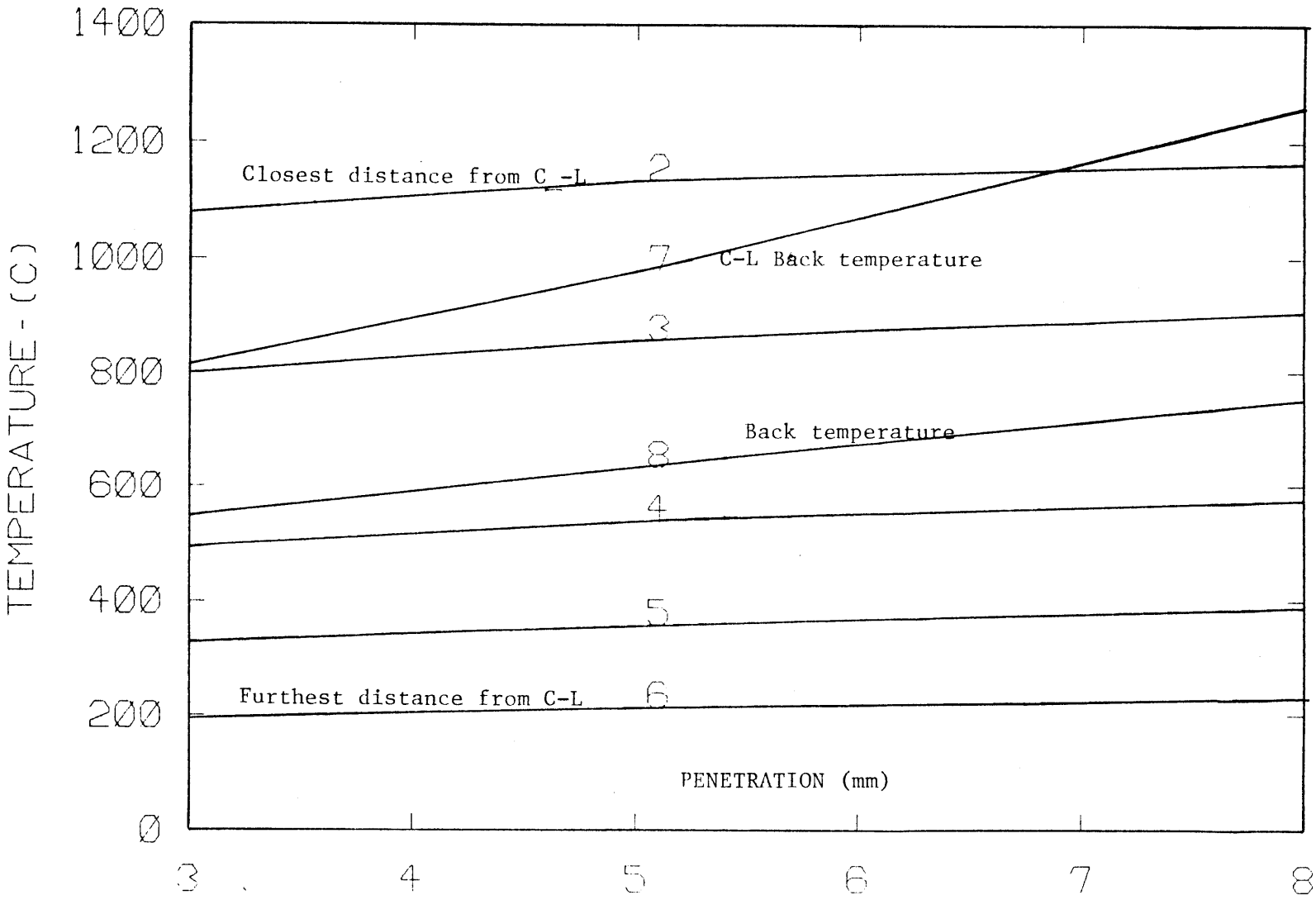

FIGURE 31: Top temperature sensing

at the center and at 5 mm from the centerline were computed using the ADINAT code. It is seen in Figure 31 that the top temperature (curves (2),(3),(4),(5),and(6)) shows extremely small changes as the penetration changes. In contrast, and as expected, the centerline back temperature changes rapidly with 100 degees C rise corresponding to an increase of one millimeter in penetration. These results are representative of many conditions and clearly show that the top side temperature is not a strong enough function of penetration to make the temperature a good candidate for an on line technique for penetration sensing. The opposite is true for the back side temperature, which, unfortunately, in many applications cannot be measured. However, it should be recognized that this conclusion is true only in this particular problem, where with the side of the plate kept constant at the temperature of the ccolant and the temperature of the weld pool boundary at the melting point of the material the intermediate computed temperatures are bounded to remain between this range. In other words, the above conclusion is not necessary true in the real welding sitution where no steady state and no cooling of the welding plates are applied.

4.3 CONVECTION IN THE WELD POOL

4.3.1 ELECTROMAGNETIC DRIVEN FLOW

It has already been mentioned that several mechanisms cause motion in the weld puddle. When electric current enters a region of fluid through an interface, a magnetic field is produced and this gives rise to rotational magnetic body forces, which must cause motion of the fluid. It is the rotationality of the magnetic force that determines the motion, at least if compressibility is unimportant and the fluid has no free surfaces and uniform

density. For the current flowing in an axisymmetric manner the magnetic field B is purely azimuthial and therefore the direction of curl jxB is as shown in Figure 32.a . This holds whatever the direction of j is, since B reverses if j does. The most active region is near the origin, where the fluid gains most of its vorticity and thus is accelerated, but viscosity and turning losses finally provide a brake and a steady state in the velocity field is established. The rotational jxB force field has the effect of sucking fluid in sideways and ejecting it as a jet normal to the interface. A solution for the magnetic field and the corresponding jxB force can be found in appendix A for the case when a simple radial current distribution is assumed to originate from a point current source. This rotational force per unit volume driving the melt inwards at the near the origin region is proportional to the square of the arc current and varies as the inverse of the cube of the distance from the origin producing a net counter-clockwise motion. The relative importance of the electromagnetic forces over the opposed the motion viscous forces is given by the Sozu's constant defined as:

$$K = \frac{\mu_o I_o^{\,2}}{2\,\pi^{\,2}\rho\,\nu^{2}} \qquad (11)$$

When the viscous effects are neglected a "back of the envelope" solution reveals that the velocity in the puddle varies linearly with the current,since

$$jxB \text{ is proportional to } I_0/L^3$$

and

$$\rho \cdot U \cdot \partial U/\partial x \text{ is proportional to } \rho \cdot U^2/L$$

and the two left hand side terms are of equal order of magnitude in the equation of motion,so that

$$U \propto I_0/L \cdot (\mu_0/\rho)^{0.5} \qquad (12)$$

When the flow is characterized as viscous similar arguments gives that

$$\mu \cdot \partial^2 U/\partial y^2 \propto jxB$$

and therefore

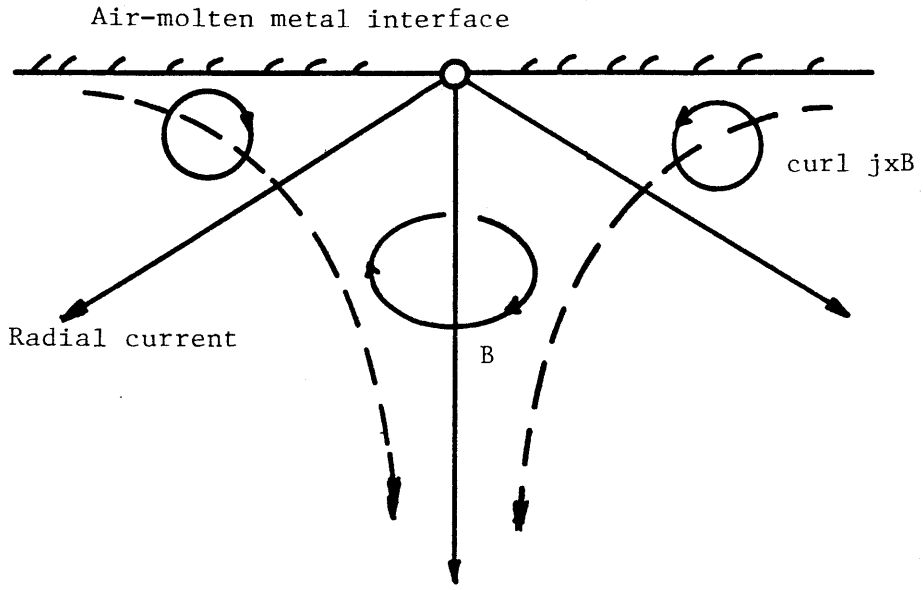

FIGURE 32 a: Motion induced by the e.m. field B

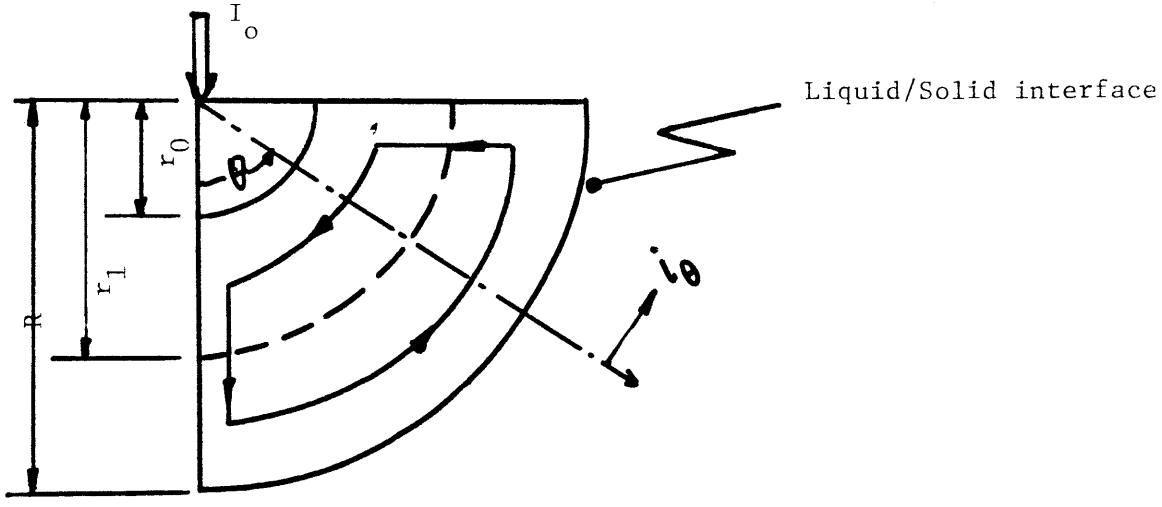

ϕ Azimuthial Angle

θ Cone Angle

FIGURE 32 b: Idealized system for the e.m. driven flow

$$U \propto I_0^2/L \cdot \mu_0/\mu_m \qquad (13)$$

where L is a characteristic length of the pool. The above expression shows that that the velocity varies with the square of the current when viscous losses are significant.

Various solutions have appeared in the literature for the problem of fluid motion induced by Lorentz forces solving the linear or nonlinear equation of motion, but the main parameters, which must be determined experimentally, are the current anode spot size or more precisely the disribution of the current to the pool surface. For the present model a rather simple expression for the velocity was used obtained from the linearized equation of motion:

$$V_{em} = \frac{I_o^2 (1 + \lambda)}{10^{10} \pi \mu_m \lambda d} \qquad (14)$$

where λ is the ratio of pool surface radius over the penetration d and μ_m is the viscosity of the molten metal, and all the parameters in S.I. units.

4.3.2 SURFACE TENSION DRIVEN FLOW

In the absence of concentrations of surface active elements the surface tension of most molten metals and alloys decreases with temperature (for pure iron, for instance, $\partial\sigma/\partial T$ is $-0.49 \cdot 10^{-3}$ Nt/m). Since large temperature gradients exist along the weld pool surface, a flow is induced by surface tension with direction from the hot center of the pool radially outwards. However, the presence of even small quantities of active elements can lower the surface tension gradient and in extreme cases could even change its sign and therefore producing an inward motion assisting the e.m. driven motion. Although Selenium has been reported [16] to reduce the surface tension of the

molten steel significantly, no general agreement exists for the effect of addition of aluminum (Al) and its oxide or for the effect of Cr_2O_3 on the molten steel. In this work as it has already been mentioned in the chapter with the experimental results it was found that the addition of concentrated quantities of Cr_2O_3 in the molten pool results in a more shallow puddle, which implies that Cr_2O_3 actually increases the gradient of the surface tension of the system with temperature causing a more intense radially outwards motion.

An estimate of the surface tension driving force can be found from the expression:

$$F_{ST} = (\partial\sigma/\partial T)\cdot(\partial T/\partial r)\cdot\pi\cdot w^2 \qquad (15)$$

where w is the radius of the pool surface. For pure iron properties and $\Delta T/w = 250\ ^{\circ}K/3$ mm the force is computed to be at 2 mN; This value is almost the same magnitude as the Lorentz force computed with an arc current of 100 amperes.

The velocity field produced by the surface tension force as a driving force and the viscous forces opposing this motion was solved approximately and the solution is given in appendix B. The relative magnitude of the surface tension force over the viscous forces is given by the Marangoni number defined as:

$$Ma = \frac{\frac{\partial\sigma}{\partial T}\,\Delta T\,\ell}{\rho\,\nu\,\alpha} \qquad (16)$$

where ℓ is a characteristic length, ν is the kinematic viscosity and α is the thermal diffusivity of the steel melt. Substituting the typical values for these parameters used above, the Marangoni number is about 20,000 ,indicating a rather strong surface tension driven flow.

3.3.3 PLASMA STREAM SHEAR FORCE

An additional cause of motion comes from the action of the arc plasma jet streaming on the surface of the weld pool. Although the contribution of this force in establishing a precise flow pattern has been ignored so far by other investigators, a simple order of magnitude calculation shows that its magnitude is comparable with the Lorentz force and surface tension force for a jet velocity of the order of 100 m/s. For an axisymmetric stagnation type flow a friction coefficient can be calculated and thus the local shear as well as the total shear force exerted on the pool surface can be calculated (Appendix C).

4.3.4 BUOYANCY FORCE

The effect of buoyancy driven force has been neglected in this analysis. In spite of the large temperature gradient existing within the pool, the thermally induced velocity depends on the cube of the characteristic length, whereas the surface tension caused velocity is linerly dependent on the length. Thus, for the very small weld pool dimensions the contribution of the buoyancy force is insignificant. The relative importance of the buoyancy forces over the viscous forces is given by the Grashof number

$$Gr = \beta \cdot g \cdot \Delta T \cdot L^3 / \nu^2 \qquad (17)$$

Substituting typical values, the Grashof number is of the order of 10, indicating that buoyancy force is relatively very small.

4.3.5 VELOCITY FIELD

After the velocities induced by each of the above considered driving forces are obtained, the final velocity of the melt in the pool is obtained by simply superimposing the three velocity fields as :

$$V = V_{em} + V_{st} + V_{shear} \qquad (18)$$

This neglects the inertial contribution which would cause a more intense motion and thus the proposed model, is expected to underpredict, although not by much, the velocities.

4.3.6 FLOW STRUCTURE:Two and Three parameter model

The flow in the weld pool is considered to be laminar, since for the very small size of the pool a Reynolds number smaller than the critical one should be expected. The direction of the flow, however, can be changed, and a counter-clockwise or clockwise motion can be established, depending on which of the driving forces dominates. The analytical solution [19] even with the electromagnetc force only considered, predicts in some cases a two cell flow of opposite directions as shown in Figure 33.b. This result is a possible explanation for weld pool boundaries such as shown in Figure 33.b or in photograph of Figure 22.b where a sudden discontinuity in the boundary occurs and the pool is divided into two regions,the upper where a strong surface tension driven flow with radially outwards direction is established, and the lower region where the jet-like flow driven by the Lorentz force has the opposite direction with the two streams flowing in parallel in the contact area.

To simulate these two different flow structures in the weld pool two models were developed corresponding to the two different geometries expected. In the first model one motion loop is considered, but with a variable direction (radially inwards or radially outwards). For this case the postulated shape, a combination of an elliptic and parabolic arc is specified by the two free parameters (depth and width). Figure 33.a shows this two parameter and single cell model. In the other one model the double

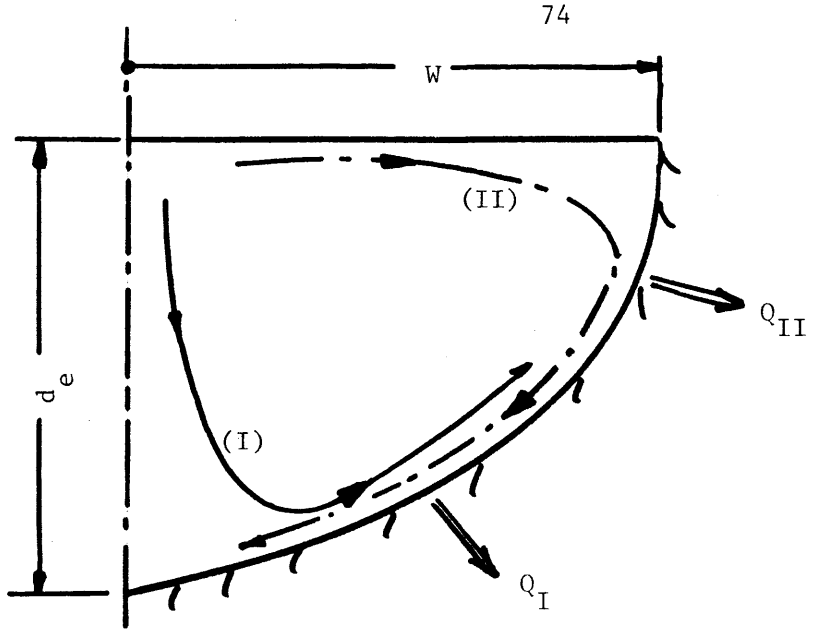

(I):e.m. driven flow

(II): surf tension flow

FIGURE 33 a: Two parameter model

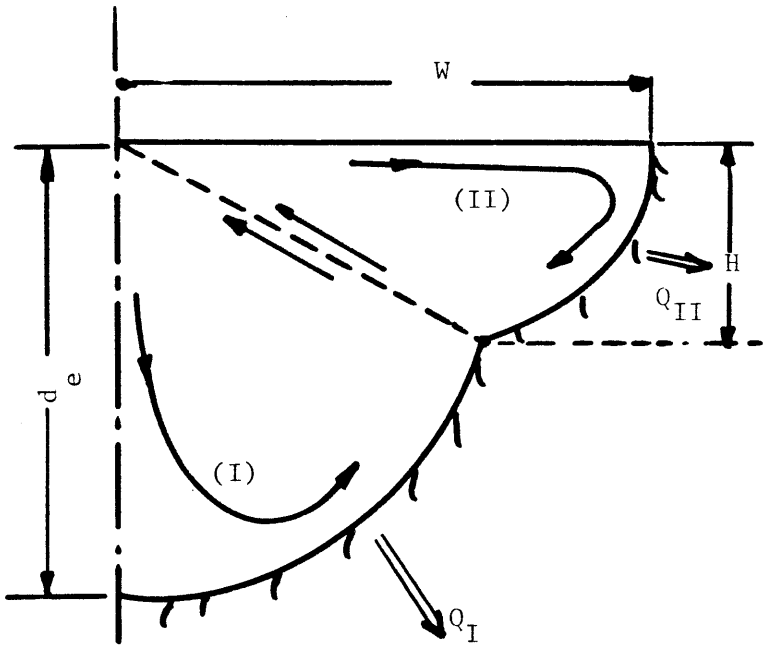

(I):e.m. driven flow

(II):surf.driven flow

FIGURE 33 b: Three parameter model

circulation flow character is considered by choosing the boundary of an ellipse (lower part) intersecting a parabola (upper part) and specified by the width, the depth and the distance of the intersection from the pool surface. The three parameter-double cell model is shown schematically in Figure 33.b.

4.4 TEMPERATURE FIELD IN THE WELD POOL

The velocity field is coupled with the temperature field in the pool, since the surface tension driven flow is temperature dependent. The stream of hot melt flowing either from the bottom center of the pool upwards or from the upper edge towards the bottom delivers heat through the melting interface to the solid. This heat is then conducted through the material and is delivered to the cooling water. The stream of fluid flowing next to the origin gains this heat from the arc, the majority of which is carried by the flow and the remainder which is conducted across the relatively stagnant central region of molten metal to the lower flowing stream of smaller temperature. This convected by the motion and cross-conducted heat flow was modelled using a simple analogy of heat exchange between a flowing stream and two reservoirs, the source being the region with the maximum temperature in the top center of the pool and the sink being the solid liquid interface, kept at the melting point temperature, as shown in Figure 34. The calculations for the heat fluxes at the boundary to match with the fluxes computed from the conduction solution, the pool was divided into twelve elements and a heat balance was written for each element. The effective heat transfer coefficient was based on the axisymmetric, stagnation type heat teransfer flow with a constant thermal boundary layer [20]. No correction for molten metal flows is required since the Prandtl number of molten steel is 0.23, much larger than the Prandtl number of other liquid metals. The Nusselt number is calculated as :

$$Nu_R = 0.93 \cdot Re^{1/2} \cdot Pr^{0.4} \qquad (19)$$

where the Reynolds number is based on the geometric mean of the depth and width of the pool, that is

$$R = \sqrt{d \cdot w} \text{ and } Re = V \cdot R/\nu \qquad (20)$$

A heat balance for the n^{th} element shown in figure (34) yields:

$$\dot{m}\, c_p\, (T_n - T_{n+1}) = h_t \frac{T_n - T_{n+1}}{\ln \frac{T_n - T_m}{T_{n+1} - T_m}} A_n + \left(\frac{k}{S_n}\right) \frac{T_n - T_{n+1}}{\ln \frac{T_n - T_{max}}{T_{n+1} - T_{max}}} A_n$$

where (k/S_n) is an effective heat transfer coefficient taken care of the cross conducted heat flow.The parameter S_n depends on the shape of each particular element has been chosen to be:

$$S_n = (r_n + r_{n+1})/2 \qquad (21)$$

where r is the local radius.

Defining

$$ex_n = \exp\left\{- \frac{h_t}{\frac{\dot{m}\, c_p}{A_n} - \frac{k/S_n}{\ln \frac{T_{max} - T_n}{T_{max} - T_{n+1}}}}\right\} \qquad (22)$$

the temperature T_n is obtained as:

$$T_n = T_m + (T_1 - T_m) \cdot ex_1 \cdot ex_2 \cdots ex_{n-1} \qquad (23)$$

The boundary condition at the free boundary requires the heat delivered to the solid material to be the total heat convected in the pool,so:

$$\dot{Q} = \sum_{1}^{12} \frac{h_t\, (T_n - T_{n+1})}{\ln \frac{T_n - T_m}{T_{n+1} - T_m}} A_n \qquad (24)$$

and the temperature at the node (1) can be obtained as:

$$T_1 = T_m + \dot{Q}/(h_t \cdot SM) \qquad (25)$$

where

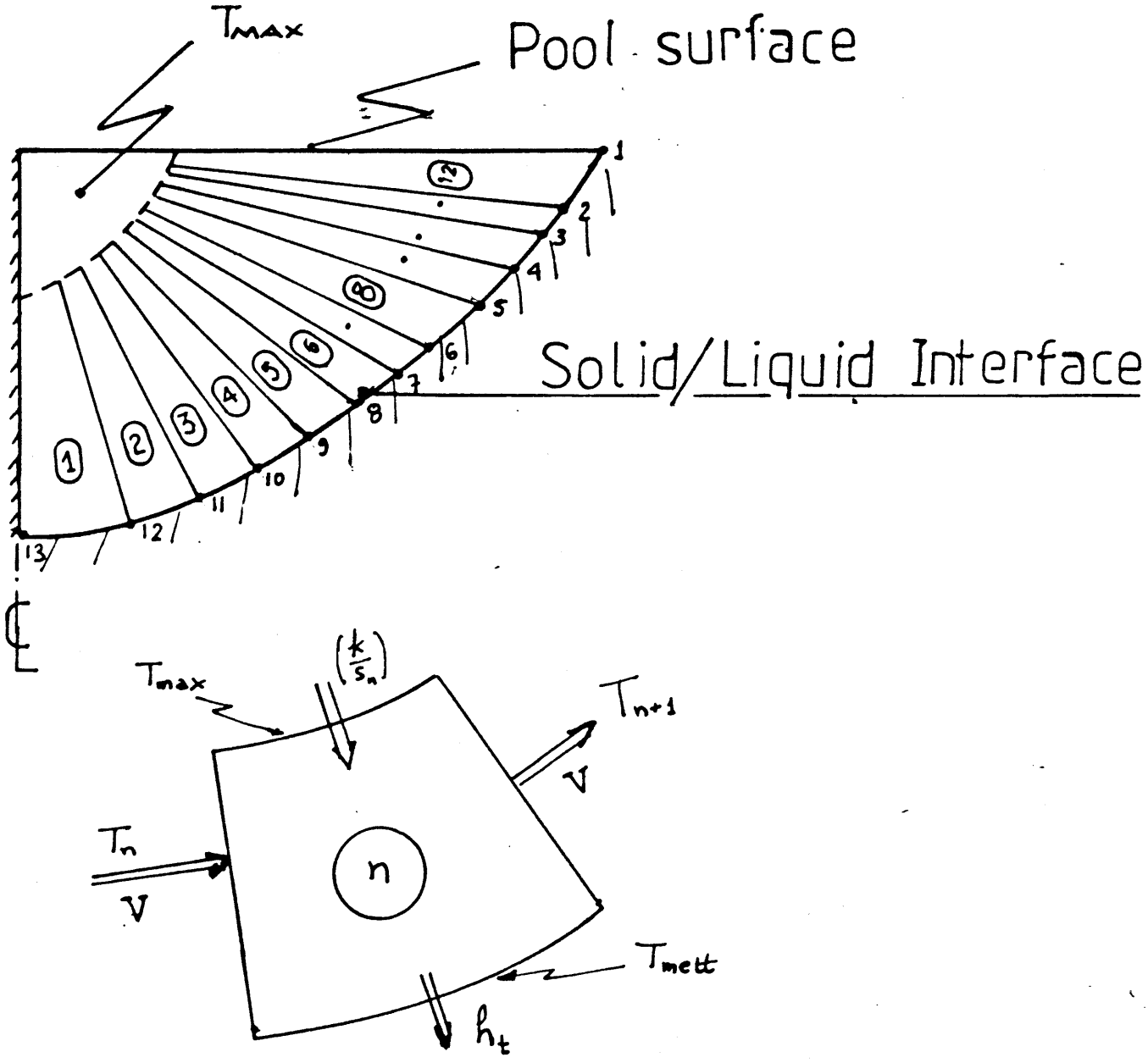

Isolated n^{th} element

FIGURE 34 :Convection heat transfer calculations

$$SM = \sum_{1}^{12} \frac{ex_1\ ex_2 \ldots ex_{n-1}(ex_n - 1)}{\ln(ex_n)}$$

After the temperatures at all nodes in the boundary have been obtained the maximum temperature in the pool can be computed as:

$$T_{max} = T_{min} + \dot{Q}/(m \cdot c_p)$$

where T_{min} is the temperature at the node (1) or (13) depending on the direction of the flow.

4.5 MATCHING OF CONDUCTION/CONVECTION SOLUTION

A computer code "CONVECT" was developed to perform all the calculations for the velocity and temperature field of the pool for a given size of the pool. If the correct size of the pool for the interface boundary had been chosen a perfect matching of the steady state heat fluxes from the convection and conduction sides would be obtained along all the points in the boundary. Since the pool shape and size are specified by only two parameters in the first model, the boundary condition of equal fluxes can be applied only at two points. So by dividing the boundary in two regions the boundary condition is specified on the average as follows:

$$\sum_{1}^{7} \frac{h_t\ (T_n - T_{n+1})}{\ln \dfrac{T_n - T_m}{T_{n+1} - T_m}} A_n = \int_{node\ 1}^{node\ 7} k_{solid} \frac{\partial T}{\partial n}\ dA_n$$

and the same equation applies in the region from node (7) to node (13). These two additional equations close the problem and the two free parameters, penetration and width can be determined.

In the three parameter model the matching of integrated heat fluxes at three regions of the weld pool boundary must considered. The CPU time

required is much higher for the three parameter model. The final selection of accuracy versus speed is a consideration in the development of an actual control strategy.

CHAPTER FIVE

5.1 PREDICTED WELD POOL GEOMETRY

The model developed to predict the weld pool geometry requires only the workpiece geometry and the arc power characteristics. For the three different plates used in the experiments the code "CONVECT" along with the ADINAT finite element code was used to infer the geometry of the pool and compare directly not only the dimensions of the resulted pool but also the temperatures at various locations with the experimental data discussed in the earlier chapter.

The variation of predicted penetration and width with heat input are shown in Figures 36, 37 for the thin and medium thickness workpieces. For conditions close to to full penetration (thin workpiece) a large increase in penetration is obtained with only slight increase in the heat input, whereas the width of the pool remains almost constant. With the thick workpiece a slightly different behaviour is observed, Figures 38, 39, where the penetration varies almost linearly with the heat input but still the width remains almost constant at 7.2 mm as the penetration increases in conditions close to those of full penetration.

To examine how sensitive the centerline back temperature is to the heat input, predictions were made for the three different workpieces and the results are plotted in Figure 40. This temperature is bounded by the melting point of the steel at 1347 °C. In Figure 41 values of the temperature at the top surface of the plate 7.4 mm from the centerline were predicted. No such results were obtained for the third workpiece for which the back temperature was measured instead, 5 mm from the centerline.

The developed computer code is very general including the case of current pulsing. Several runs were made and the geometry of the pool resulted

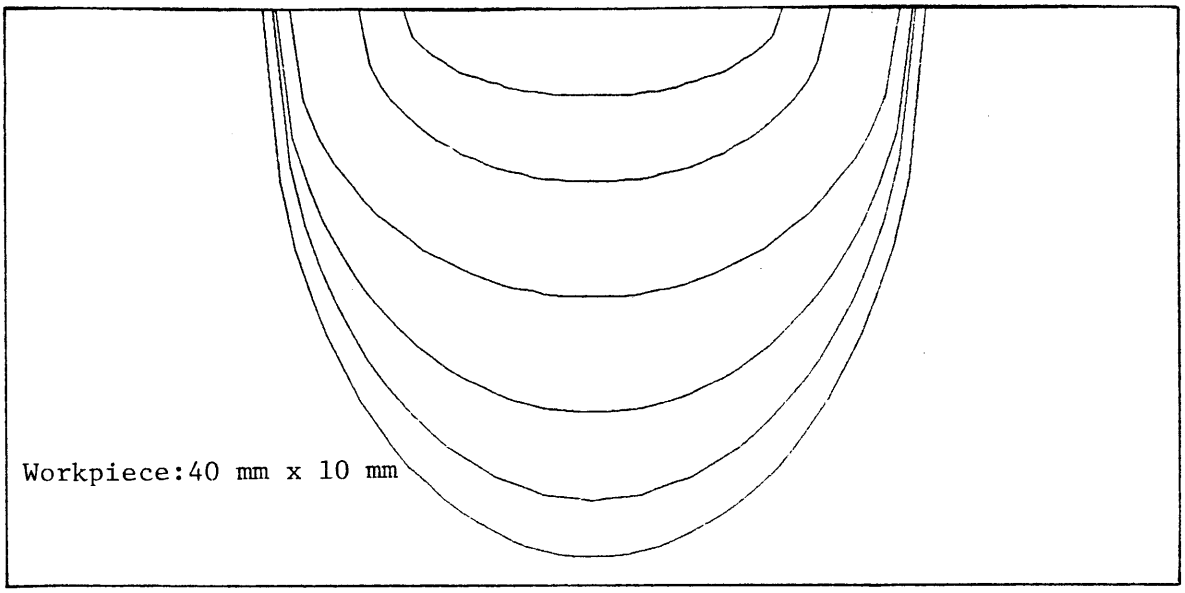

FIGURE 35 a: Current pulsing developed weld puddles (Ratio:1.44)

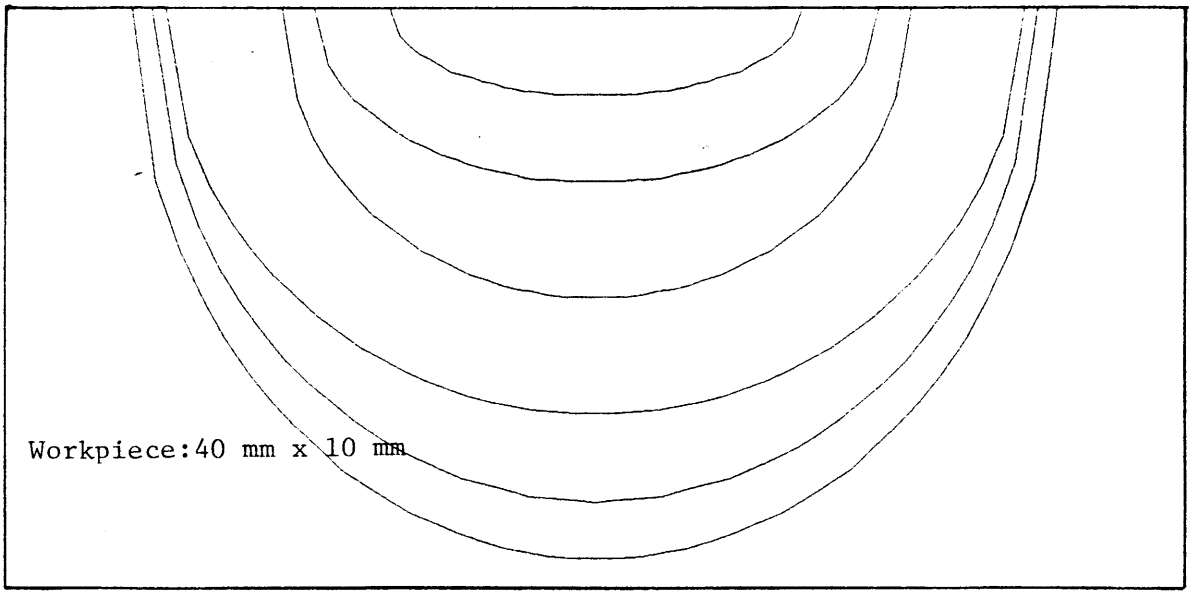

FIGURE 35 b: Direct current developed workpiece

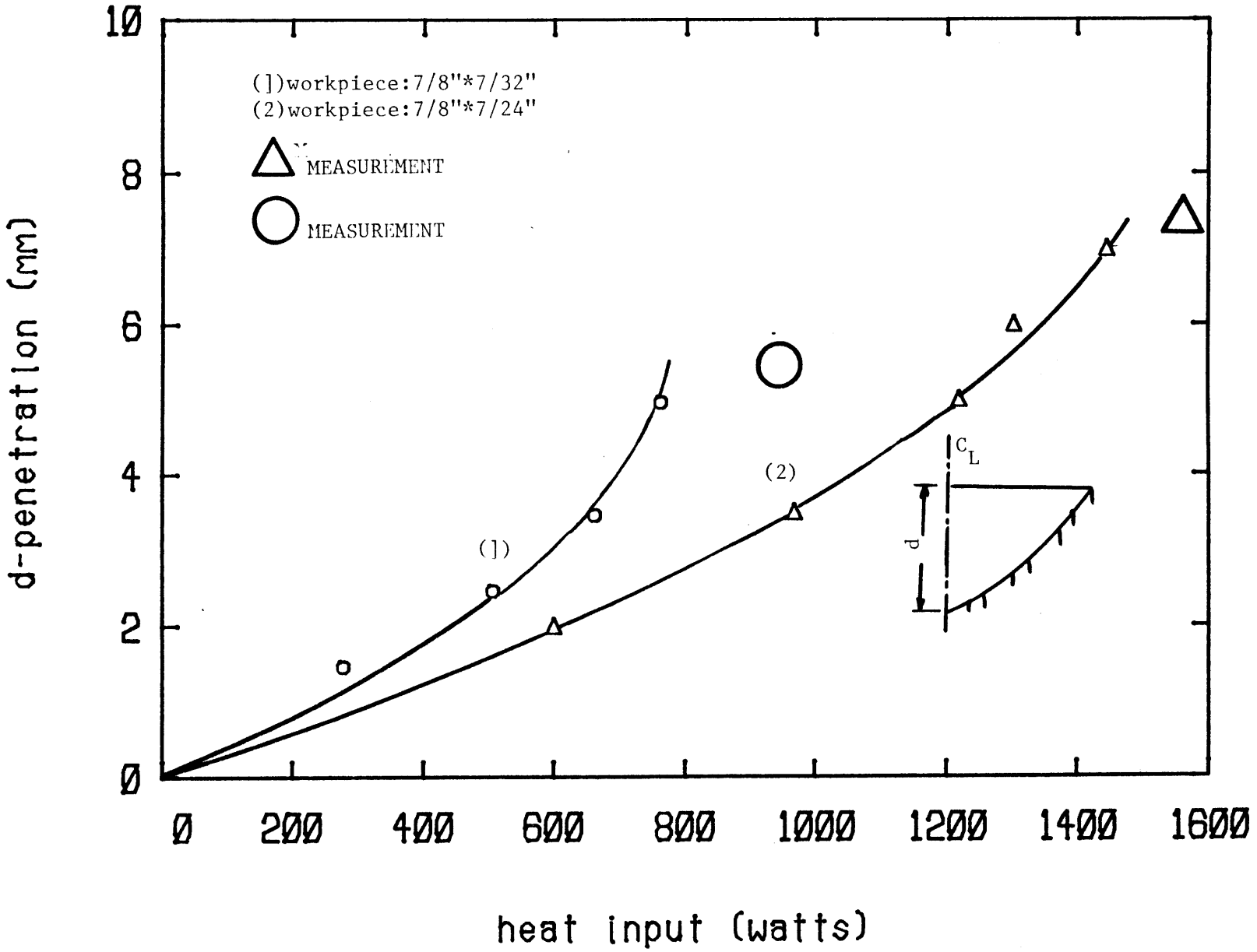

FIGURE 36: Predicted and measured penetration

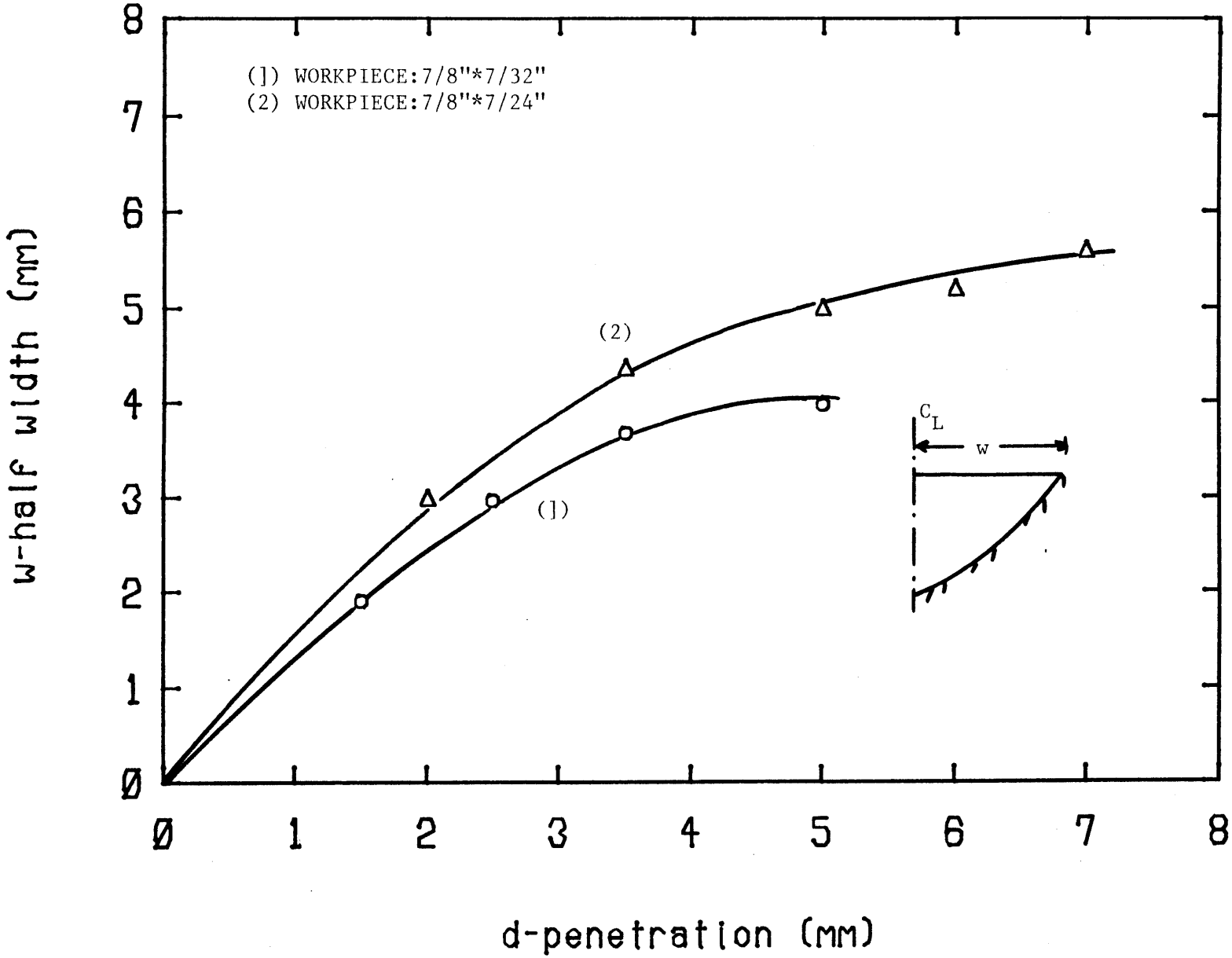

FIGURE 37 :Predicted weld pool width versus penetration

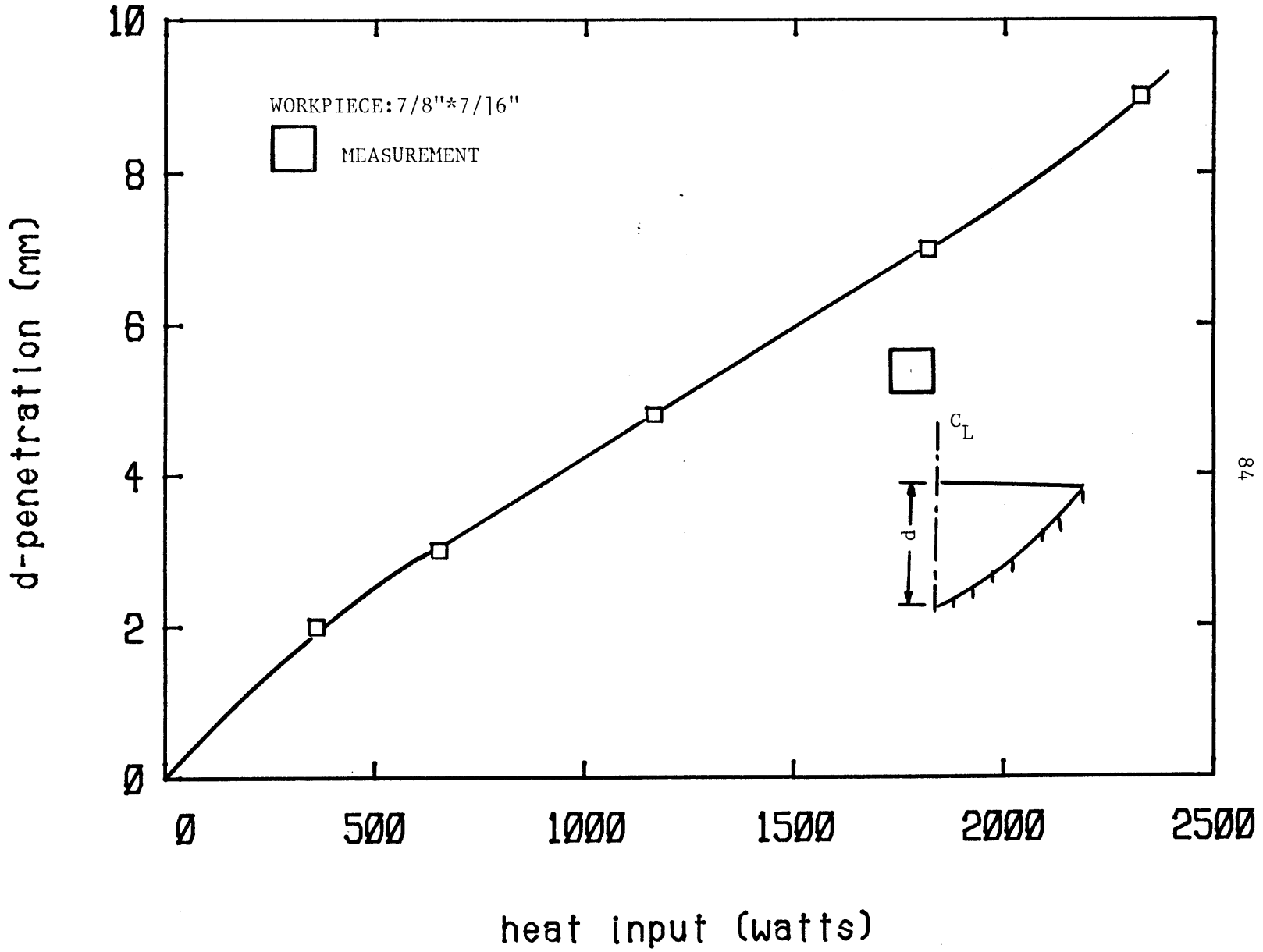

FIGURE 38: Predicted and measured penetration for the thick workpiece

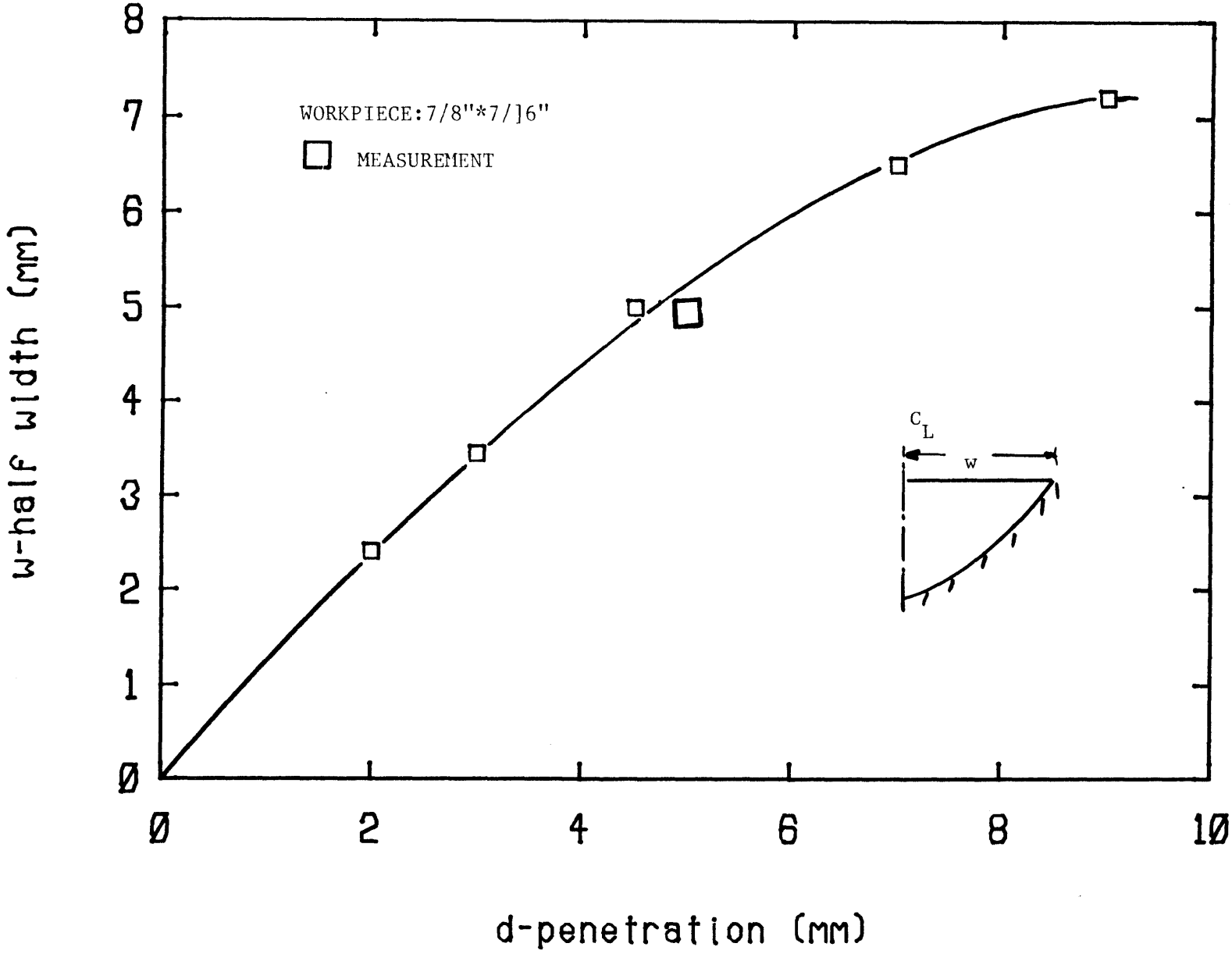

FIGURE 39 :Predicted and measured width versus penetration

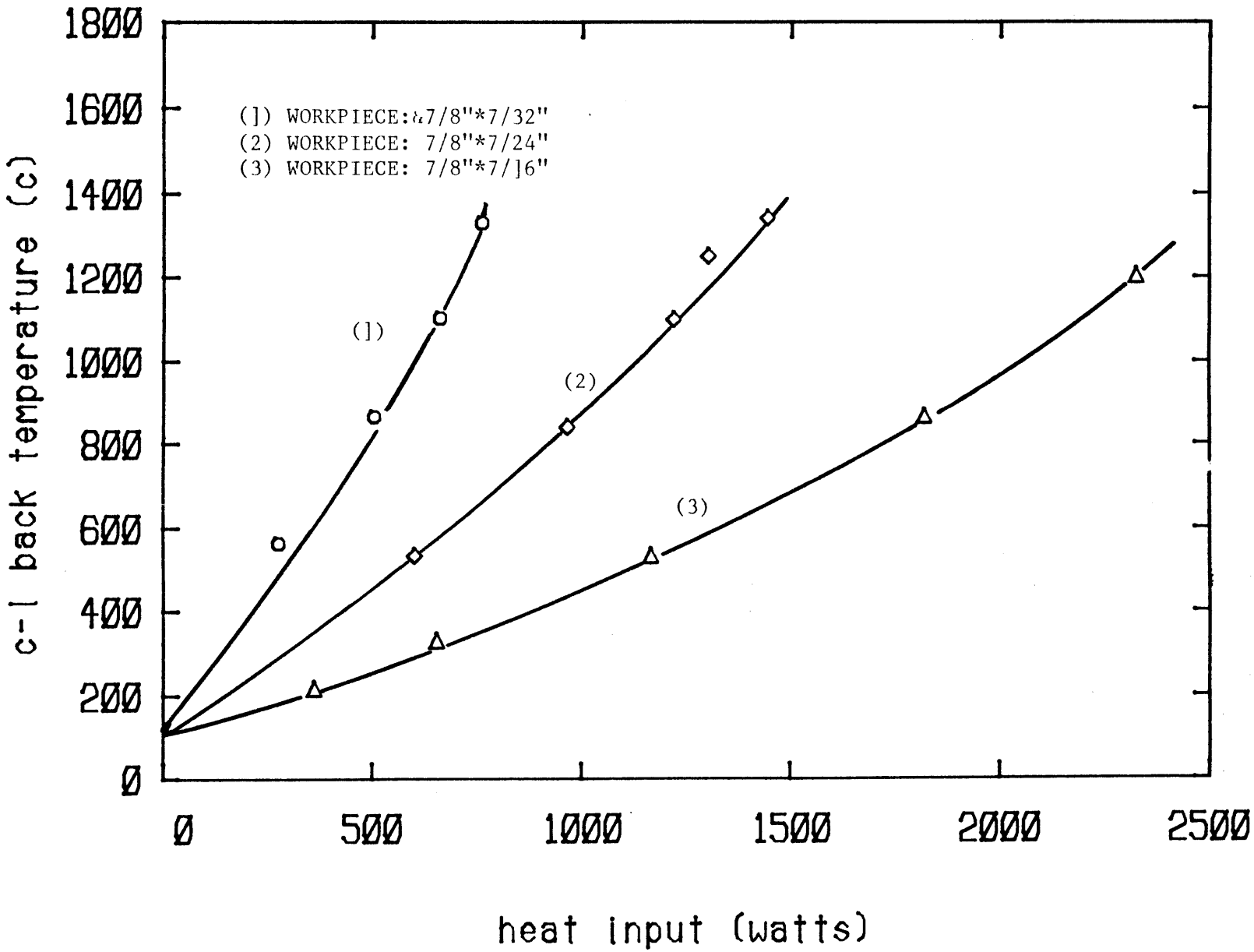

FIGURE 40 : Predicted centerline back temperature

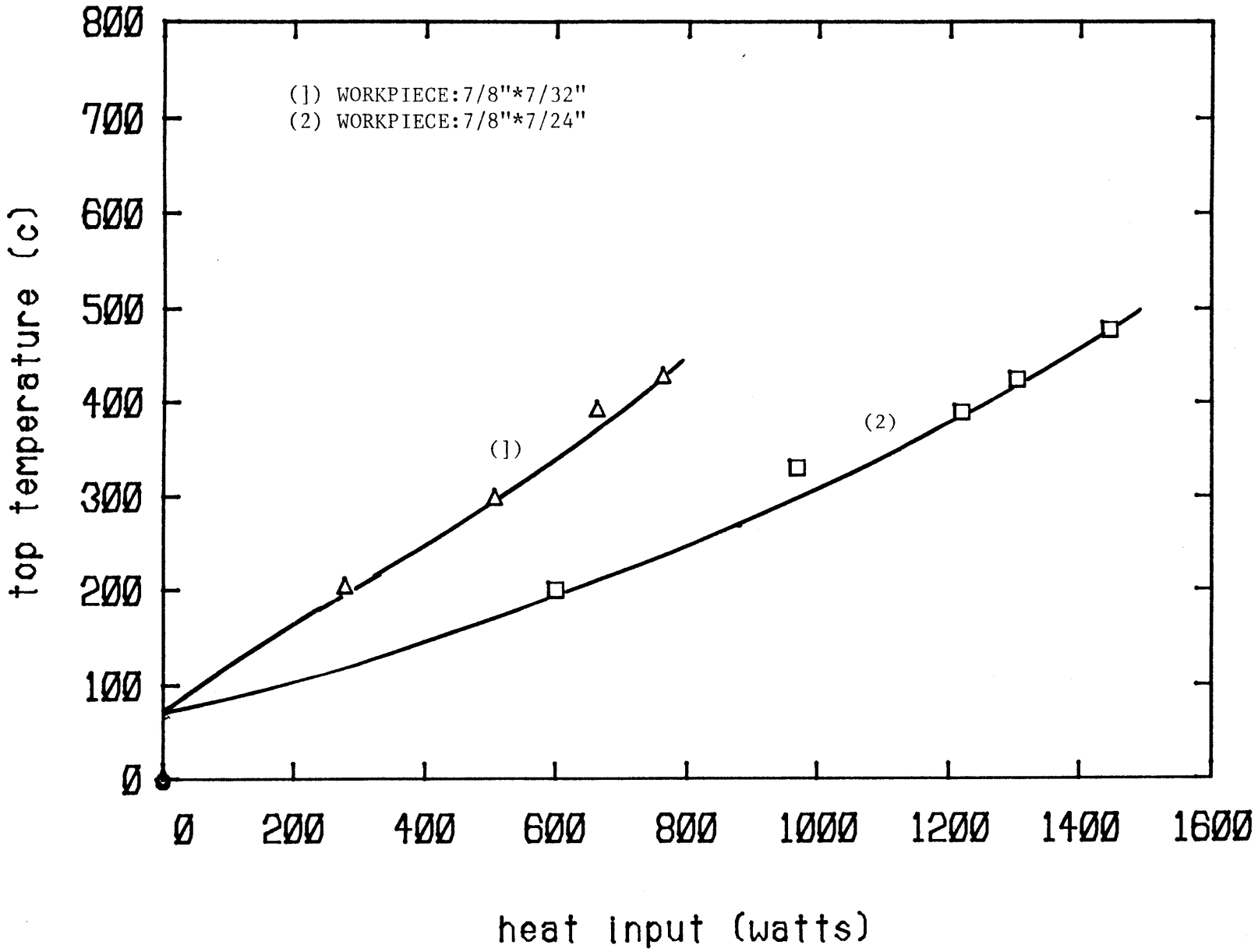

FIGURE 41 : Predicted top temperature

with pulsed current was compared against the geometry predicted with direct arc current. In general, deeper weld pools were predicted with the current pulsing as shown in Figure 35, which shows the positive effect of current pulsing, result which agrees with experimental data found in [11].

5.2 COMPARISON OF RESULTS PREDICTED BY THE MODEL WITH EXPERIMENTAL DATA

To test the validity of the developed model, comparisons of the predicted values for the size of the weld pool and for the top and bottom temperature with the experimental data obtained under similar conditions was attempted.

Only the depth and width of the pool for the last current level were measured, since it was very cumbersome and time consuming the direct measurement of intermediate depths. This comparison is shown in Figures 36 to 39. In all these cases the model overpredicts the weld pool size for a certain heat input. Similar is the comparison for the surface temperature (Figures 42 to 44) where it is seen that the predicted temperatures are higher than the measured ones. Note that all the analytical results shown so far were obtained with the conduction solution employing adiabatic conditions. To examine the effect of the radiation and convection losses from the plate surface, additional calculations were performed assigning an emissivity of one to the steel plate surface. The top side temperature was used as a measure of comparison and the results are shown in Figure 45 and compared to the experimental measurements. In this case the model underpredicts the temperatures of the real system in contrast with the first case where only adiabatic conditions were considered.

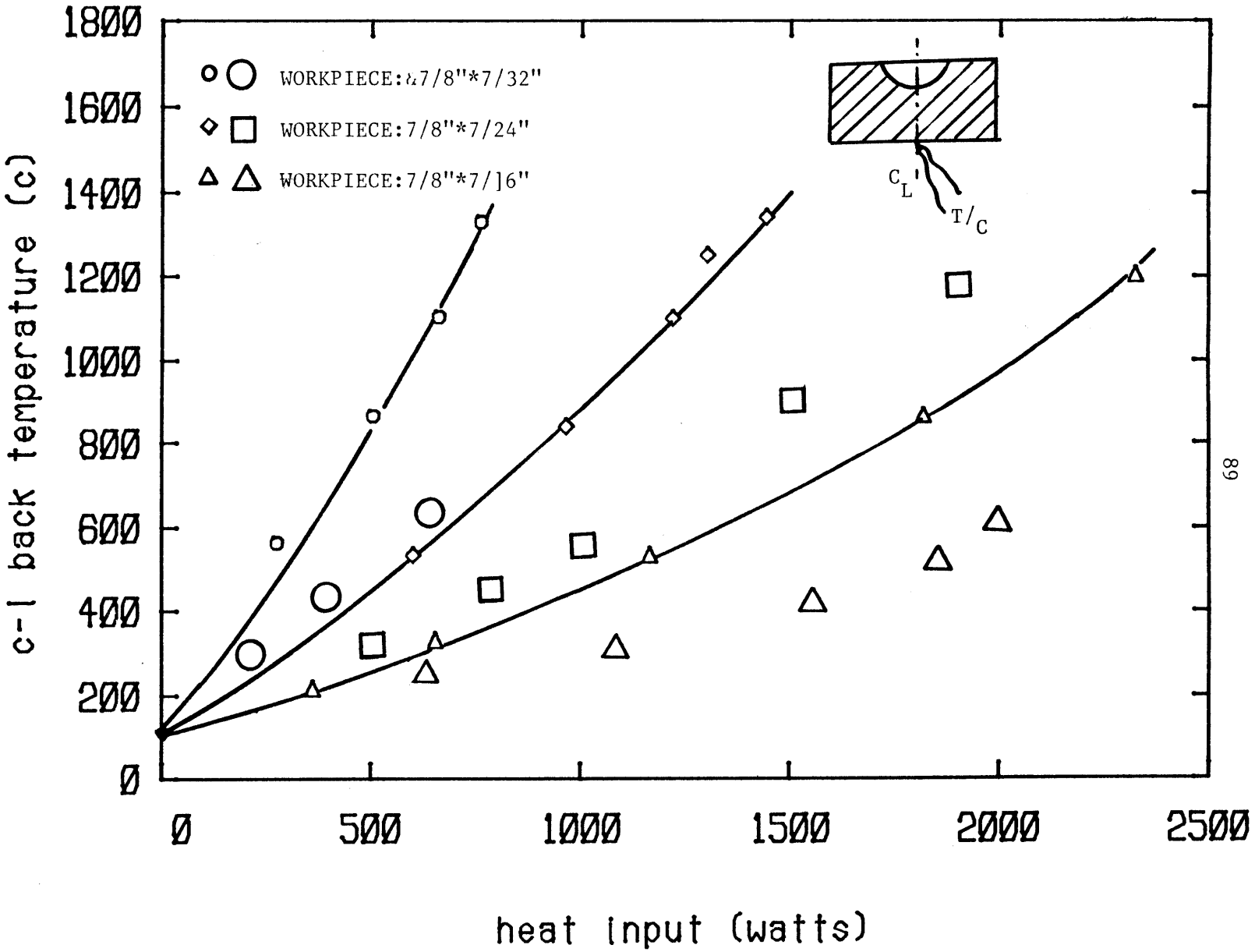

FIGURE 42 : Comparison of predicted and measured c-1 back temperature
(Adiabatic conditions)

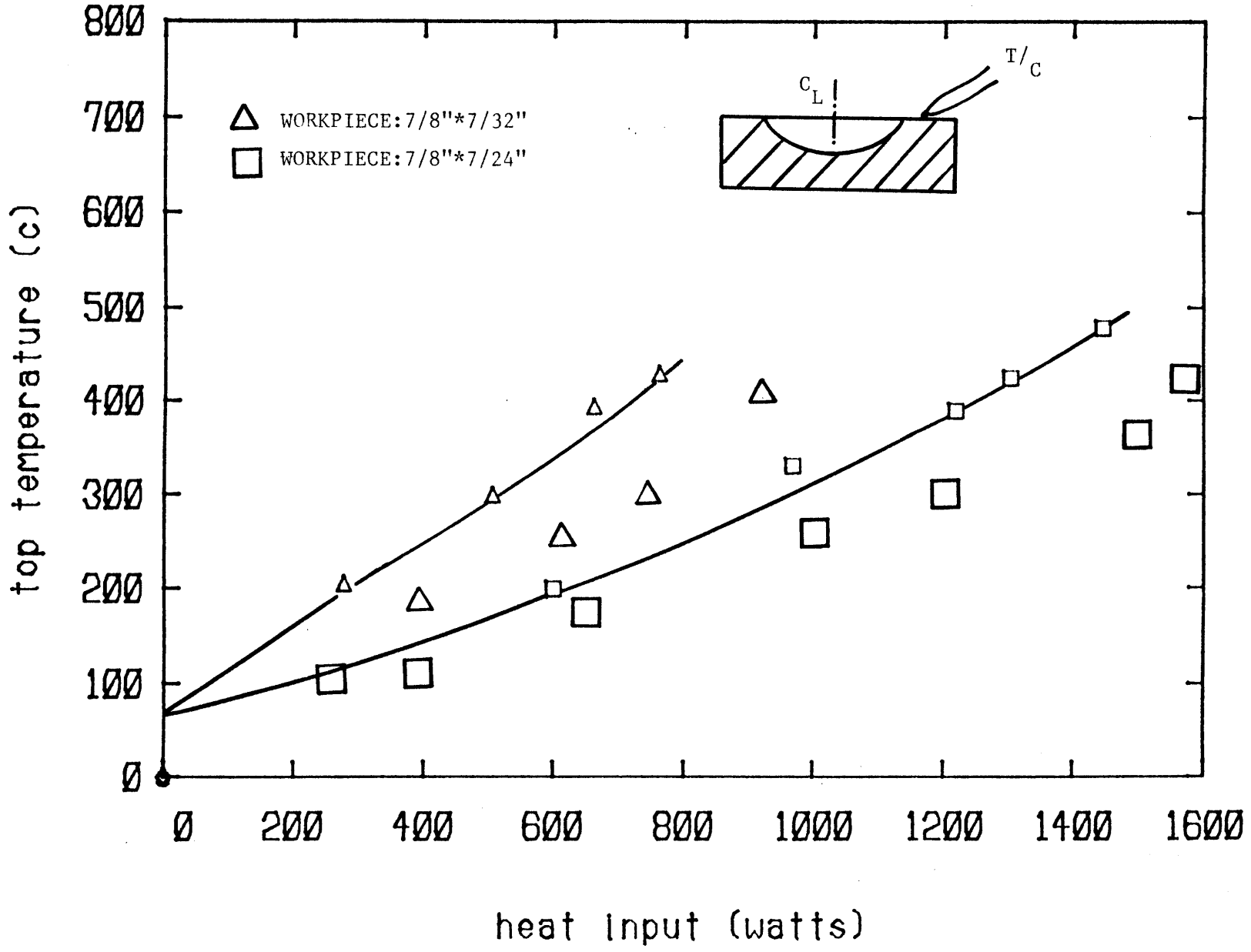

FIGURE 43 : Comparison of predicted and measured top temperature
(Adiabatic conditions)

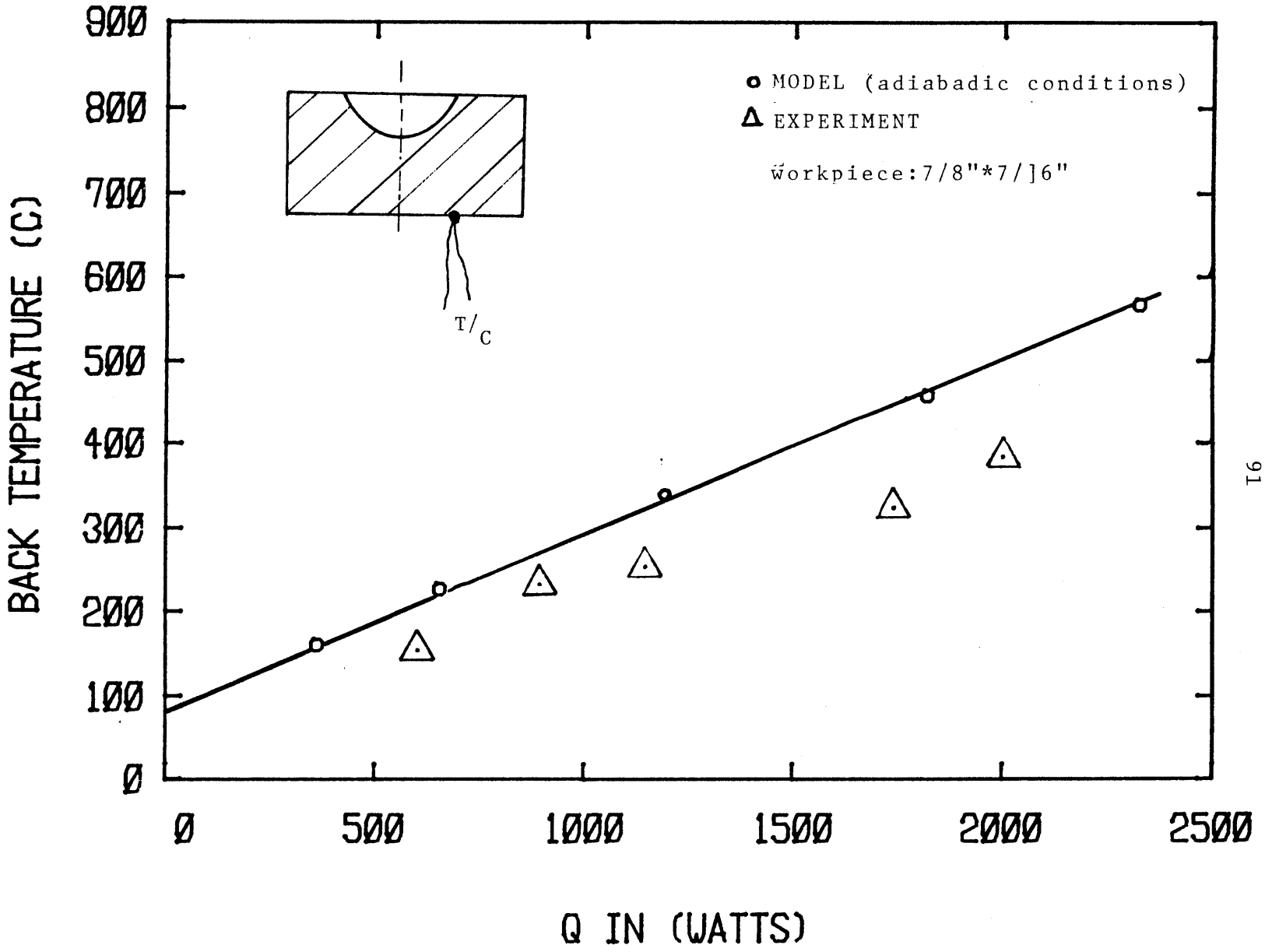

FIGURE 44 : Comparison of predicted and
(Adiabatic conditions)

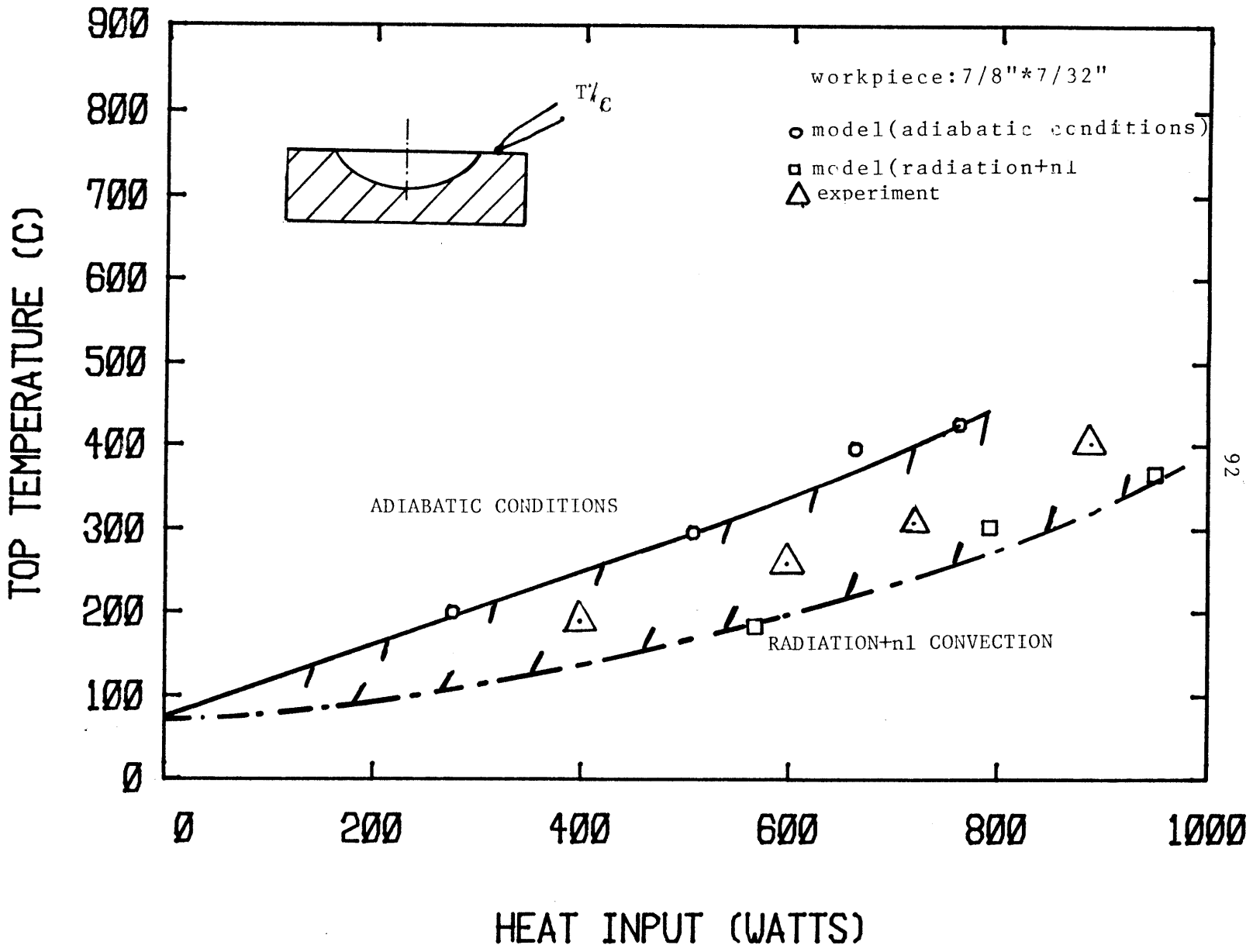

FIGURE 45 : Comparison of solutions corresponding to different plate surface boundary conditions

CHAPTER SIX

SUMMARY, DISCUSSION AND RECOMMENDATIONS

A predictive model for the stationary weld pool geometry has been developed and validated by comparison with experimental results. In contrast to previous work the model considers all the significant physical phenomena present in the pool, in the solid material, and in the arc. The model is developed in the context of a control system for welding devices and is therefore designed to have modest computational time and requires a minimum of inputs, most of which can be measured in real time.

The model is composed of three parts : An arc-molten pool interface model, a model for the fluid and thermal behaviour of the pool and a model for the heat transfer in the solid material. These components are joined in a supervisory program that iterates to find the weld pool shape for a specified workpiece geometry and arc power characteristics. For the arc, the input information regards the heat dissipated in the torch, and the efficiency of energy transfer to the workpiece. Empirical expressions were obtained for the torch efficiency from experiments in a stationary welding simulation rig. The mode of heat transfer through the solid steel is conduction and solutions for this part of the problem were obtained using the ADINAT computer code with an optimum, deformable mesh consisting of 32 isoparametric elements. Three main mechanisms were considered to cause motion in the pool:

(a) The electromagnetic force which tends to produce a counterclockwise motion,

(b) The surface tension force, which gives rise to a surface radially outwards flow, and

(c) The plasma stream shear force with the same direction as the surface tension force.

The heat transfer in the pool was modelled as a heat exchanger type of flow with a cross-conduction heat transfer term accounting for the conductive heat flowing through the relatively stagnant central region of the pool.

The predictions follow the expected qualitative results that motion of molten metal outward from the anode spot serves to make the pool shallow, while increased electromagnetic forces tend to deepen the pool. Direct comparison of analytical and experimental results for the surface temperature of the plate below the torch and other locations indicated that the experimental results lie between results obtained with no heat losses considered from the plate surface and results obtained with convective and radiative (with emissivity one) included. Other experimental results show the importance of impurity concentration in the melt. In this work the addition of Cr_2O_3 in the melt was found to drastically modify the weld pool shape.

One useful extension of the study of the weld pool behaviour is the quantitative investigation of the effect of impurity concentration present in the pool. A concentrated impurity existed in the pool is not only diffused through the melt, but also is convected by the flow to other locations within the pool. Since this motion is not strong enough in order the convective dispersion to dominate, the complete problem for study should include both the effect of diffusive and convective dispersion, the so called Taylor dispersion. The convective model developed here could be one component of such a model of weld pool impurities.

While additional measurements are necessary under various welding conditions, for a stationary weld pool configuration, for a complete validation of the developed predictive model, the results presented here, are extremely encouranging and suggest that the same approach can be applied with

success in the moving torch situation. An intermediate step would be the study of the transient instead of the steady state considered in this work.

REFERENCES

[1] Rosenthal, D., "The Theory of Moving Sources of Heat and Its Application to Metal Treatments", Trans. Amer. Inst. Min. Mech. Eng., 1946, vol.68, pp. 849-865.

[2] Wells, A. A., "Heat Flow in Welding", Welding J., 1952, vol.31, pp. 263s-266s.

[3] Prokhopov, N. N., "Cracking Resistance of Welded Joints in Solidification", Moscow, Metallurgiya, 1979, p.248.

[4] Friedman, E., Glickstein, S. S., "An Investigation of the Thermal Response of Stationary Gas Tungsten Arc Welds", Welding J,, 1976, vol. 55, pp. 408s-420s.

[5] Woods, R. A., Milner, D.R., "Motion in the Weld Pool in Arc Welding", Welding J., vol. 50, pp. 163s-173s.

[6] Shercliff, J. A., "Fluid motions due to an electric current source", J. Fluid Mech., 1970 , vol. 40, part 2, pp. 241-250.

[7] Sozu, C., "On Fluid Motions induced by an Electric Current Source", J. Fluid Mech., 1971, vol. 46, part 1, pp. 25-32.

[8] Sozu, C., Pickering, W., "Magnetohydrodynamic Flow due to the Discharge of an Electric Current in a Hemispherical Container", J. Fluid Mech., 1976, vol. 73, part 4, pp. 641-650.

[9] Operer, G. M., Eagar, T. W. and Szekely, J. "Convection in Arc Weld Pools", Welding J., 1983, vol. 62, pp. 307s-312s.

[10] Converti, J., "Plasma Jets on Arc Welding", Ph.D. thesis, Mech. Eng., July 1981, M.I.T. .

[11] Chung Sun Kang, "Control Parameters for the Arc Weld Pool Boundary", S.M. thesis, Mech. Eng. ,June 1983, M.I.T. .

[12] Wilkinson, J. B., Milner, D. R., "Heat Transfer from Arcs", British Welding J., 1960, February, pp. 115-128.

[13] Apps, R. L., Milner, D. R., "Heat Flow in Argon-Arc Welding", British Welding J., 1955, October, pp. 475-485.

[14] Eberhart, R. C., Seban, R. A., "The Energy Balance for a High current Argon Arc", J. Heat Mass Transfer, 1966, vol 9, pp. 939-949.

[15] Sadoway, D., Szekely, J., "A Neaw Experimental Technique for the Study of Turbulent Electromagnetically Driven Flows", Metall. Transaction B,1980, vol. 11B, pp. 334-336.

[16] Heiple, C. R., Roper, J. R., "Effect of Selenium on GTAW Fusion Zone Geometry", Welding J., 1981, vol.60, pp. 143s-145s.

[17] Heiple, C. R., et al. "Surface Active Element Effects on the Shape of GTA, Laser, and Electron Beam Welds", Welding J., 1983, vol. 62, pp. 72s-77s.

[18] Birikh, R. V., "Thermocapillary Convection in a Horizontal Layer of Liquid", Zhurnal Prikladnoi Mekhaniki i Teckhnichskoi Fiziki, 1966, No. 3, pp. 69-72.

[19] Atthey, D.R., "A Mathematical Model for Fluid Flow in a Weld Pool at High Currents", J. Fluid Mech., 1980, vol. 98, part 4, pp. 787-801.

[20] Kays, W. M., Crawford, M. E., "Convective Heat and Mass Transfer", 2nd Ed., Mc Graw-Hill, N.Y., p. 211.

[21] Bathe, K. J., "ADINAT-A Finite Element Program for Automatic Dynamic Incremental Nonlinear Analysis of Temperatures", Reoprt AE 81-2, Acoustics and Vibrations Lab., Mech. Eng., M.I.T., September 1981.

APPENDIX A

ELECTROMAGNETIC FORCE j x B

An approximate solution can be obtained by assuming that the current through the pool is purely radial in which case

$$j_\phi = j_\theta = 0$$

where θ and ϕ are the azimuthial and cone angle of a spherical coordinate system respectively. For reasonable values of the velocity of the molten metal the magnetic Reynolds number is much less than unity and the magnetic field induced by current can be directly determined from:

$$j = \nabla \times H \qquad (1)$$

For this situation the only non-zero magnetic field is in the azimuthial direction and equation (1) reduces to the scalar relationship

$$-r\, j_r \cos\theta \,\Big]_0^\theta = H_\phi \sin\theta \,\Big]_0^\theta \qquad (2)$$

where r is the radial coordinate, H_ϕ the azimuthial component of the magnetic field and j_r the current density in the radial direction. Symmetry imposes the condition that $H_\phi = 0$ at $\theta = 0$ and the current density can be related to the total current I_0 as

$$j_r = \frac{I_0}{2\pi r^2} \qquad (3)$$

Combining Equation (3) with the boundary conditions yield the final result for the magnetic field as

$$H_\phi = \frac{I_0}{2\pi r} \frac{1 - \cos\theta}{\sin\theta} \qquad (4)$$

The Lorentz force on the fluid can then be expressed as

$$j \times B = j_r i_r \times \mu_0 H_\phi i_\phi \qquad (5)$$

where i_r and i_ϕ are unit vectors in the r and ϕ directions and μ_0 is the permitivity of the material. Substituting expressions for j_r and H_ϕ the resulting body force per unit volume is

$$F''' = j \times B = - i_\theta \frac{\mu_0}{4} \left[\frac{I_0}{\pi r^2}\right]^2 r \frac{1 - \cos\theta}{\sin\theta} \quad (6)$$

The spatial distribution of the body force is shown in Figure 32.b with the resulting circulatory flow; the body force is higher near the center of the pool than that toward the periphery. To estimate the driving force for the circulatory flow, a simple flow pattern is assumed, as shown in Figure 32.b, and the average force determined by averaging over the assumed forward and backwards paths designated I and II.

$$-(F_{em})_I = \iiint F'''_{em} dV = \mu_0 \frac{I_0^2}{4\pi^2} \int_{r_0}^{r_1} \int_0^{\pi} \int_0^{\pi/2} \frac{1 - \cos\theta}{r^3 \sin\theta} r^2 \sin\theta \, dr \, d\theta \, d\phi$$

where the limitis of integration are such as to include a hemispherical shell from radius r_0 to radius r_1 and the negative sign indicates that the force tends to rotate the fluid in a counterclockwise direction relative to i_ϕ. The approximate solution where j_r is taken stricktly radially indicates a singularity as $r \to 0$. This will not occur in the real situation since the anode spot size is finite; for an approximate value r_0 can be chosen to be the anode spot size.

The result of integration is

$$-(F_{em}) = \frac{\mu_0}{4} \frac{I_0^2}{\pi} (\pi/2 - 1) \ln (r_1/r_0) \quad (8)$$

For the region II the result is

$$-(F_{em}) = \frac{\mu_0}{4} \frac{I_0^2}{\pi} (\pi/2 - 1) \ln (R/r_1) \quad (9)$$

where R is the radius and the positive sign indicates that this force acts opposite the motion imposed by region I. The resulting net force for circulation is

$$F_{net} = \frac{\mu_0}{4} \frac{I_0^2}{\pi} (\pi/2 - 1) \ln (R/r_0) \qquad (10)$$

The square law dependance of the net circulation force on the current is clearly established and the modest dependance on the ratio of arc spot size to molten pool size is also shown. For I = 200 amps and R/r_0 =5 the net force is calculated to be 3.7 mN.

APPENDIX B

A SIMPLE SOLUTION TO THE 2-D STEADY THERMOCAPPILARY MOTION.

The flow at the surface is driven by surface tension. Since the net flow rate is zero there must be a line of zero velocity above which the velocity profile is assumed to be linear and below which a pressure driven Poiseuille plane flow is considered to simulate the real flow conditions.

At the surface, for a linear velocity profile, Figure 46:

$$\mu \frac{V_s}{\gamma h} = \frac{\partial \sigma}{\partial x} \rightarrow \quad V_s = \left(\frac{\partial \sigma}{\partial x}\right) \frac{\gamma h}{\mu}$$

where γh is the distance from the free surface to the line of zero velocity and h is the depth of the liquid layer.

In the lower flow (Poiseuille);

$$U_x = -\frac{1}{2\mu} \left(\frac{dp}{dx}\right) \left[(1-\gamma)^2 \frac{h^2}{4} - z^2\right]$$

where

$$\frac{dp}{dx} \cdot (1-\gamma)h \cdot 1 = \frac{\partial \sigma}{\partial x} \cdot 1 \text{ , driving force}$$

$$\rightarrow \quad \frac{dp}{dx} = \frac{1}{(1-\gamma)h} \cdot \left(\frac{\partial \sigma}{\partial x}\right)$$

therefore $U_x = -\frac{1}{2\mu} \frac{1}{(1-\gamma)h} \left(\frac{\partial \sigma}{\partial x}\right) \left[\frac{(1-\gamma)^2 h^2}{4} - z^2\right]$

Since the net flow rate at each station and the velocity profile for the lower flow is parabolic we have:

$$\frac{1}{2} V_s \cdot \gamma h \cdot 1 = \frac{2}{3} (1-\gamma)h \cdot \frac{1}{2\mu} \frac{1}{(1-\gamma)h} \cdot$$

$$\cdot \left(\frac{\partial \sigma}{\partial x}\right) \cdot \frac{(1-\gamma)^2 h^2}{4}$$

therefore

$$\frac{1}{2} \gamma^2 = \frac{1}{3} \frac{(1-\gamma)^2}{4} \text{ or } 5\gamma^2 + 2\gamma - 1 = 0$$

$$\gamma = 0.29$$

Therefore the velocities profiles are:

Region (1): $\frac{V_x}{V_s} = 1 - \frac{Z}{0.29h}$

or $V_x = \left(\frac{\partial \sigma}{\partial T}\right) \frac{0.29h}{\mu} \left(1 - \frac{Z}{0.29h}\right) \frac{dT}{dx}$

Region (2): $U_x = -\frac{1}{2\mu} \frac{1}{0.71h} \cdot \left(\frac{\partial \sigma}{\partial T}\right)\left[\left(\frac{0.71h}{2}\right)^2 - Z^2\right] \frac{dT}{dx}$

Note: the exact solution predicts $\gamma = 1⅓$ [18].

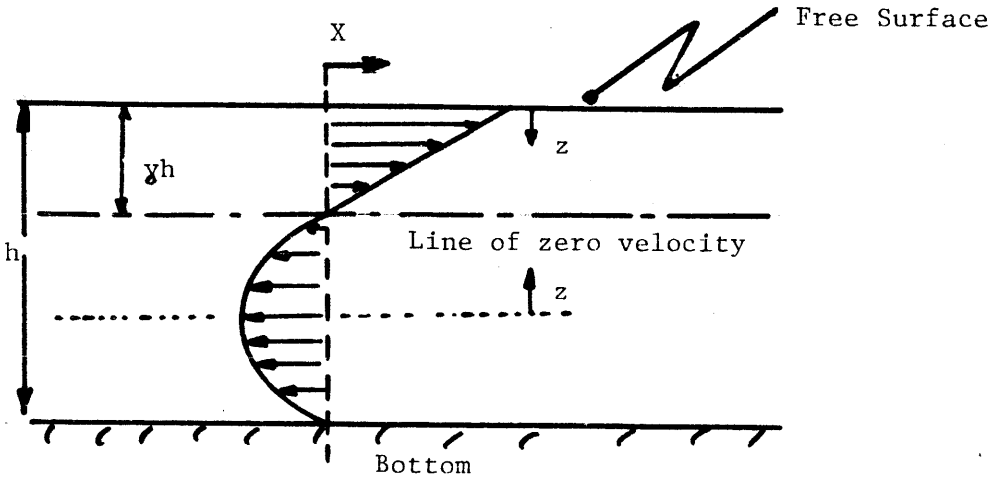

FIGURE 46 : Surface tension driven flow.

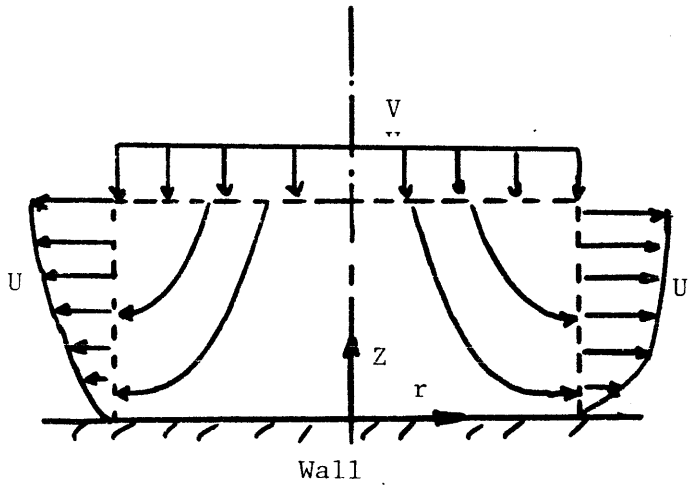

Axisymmetric stagnation Type Flow

FIGURE 47: Stagnation Flow.

APPENDIX C

STAGNATION FLOW

If U is the radial component of velocity and V is the axial component, the potential flow solution is (Figure 47):

$$U = a\,r \quad \text{and} \quad V = -2\,a\,z$$

and the constant boundary layer is found to be:

$$\delta = 1.95\,\sqrt{\nu/a}.$$

Following the symbols in Schlichting's book, p. 70-75 and values for $d\phi/d\eta$, $d^2\phi/d\eta^2$, $d\phi/d\zeta$, and $d^2\phi/d\zeta^2$ obtained from table 5.1 of the same reference, the skin friction factor is calculated as:

$$f_r = \frac{r\,\mu\,\frac{a}{\nu}\,\sqrt{a\nu}\,\phi''(0)}{\frac{1}{2}\,\rho\,U^2}$$

or substituting the expression for U from above, we get:

$$f_r = \frac{a\,r\,\sqrt{a\nu}\,\phi''(0)}{\frac{1}{2}\,a^2\,r^2}$$

or

$$f_r = \frac{2\,\phi''(0)}{\frac{a\,r\,r}{\nu}}$$

substituting the value for $\phi''(0)$, then:

$$f_r = \frac{2.624}{Re_r}$$

If V_j is the jet velocity and D_j is the jet diameter, a good approximation for the radial stream velocity is:

$$V_r = \frac{r}{D_j}\,V_j$$

From a simple balance of the shear force with the opposed the induced motion viscous forces, the surface velocity is obtained as:

$$V_{sf} = \text{contant} \cdot \mu_{gp}\,\nu_{gp}^{-0.5}\,B_j\,W\,\frac{d}{4\,\mu_m}$$

where μ_{gp}, ν_{gp} are the dynamic and kinematic viscosity of the plasma and gas stream, μ_m is the viscosity of the melt, and B_j is a parameter defined as the ratio of jet velocity over the diameter of the arc. The dimensions of the pool are specified by the pool surface radius W and the depth d.

APPENDIX D

COMPUTER CODE CONVECT

The developed computer code CONVECT is presented next. The code operates with ADINAT results as an input file. The two parameter model is considered.

```
C
C*************************************************************************
c*                  **program  CONVECT**                                 *
c*                                                                       *
c*                      developed                                        *
c*                         by                                            *
c*                  GEORGE EM KARNIADAKIS                                *
c*                                                                       *
c*                                                                       *
c*                      JUNE 1984                                        *
c*************************************************************************
c
c                                                                       .
c.... The convection heat transfer problem in the weld pool             .
c.... Two parameter model. Interface boundary: Parabola + Ellipse       .
c                                                                       .
c.....Plate dimensions : Height-D   Radius-W                            .
c.....Pool dimensions  : Depth -de  Aspect ratio-al                     .
c.....Arc characteristics : Arc current-ci Arc voltage-vd               .
c....                       Arc efficiency-eff electrode diam-ed        .
c....                       Jet velocity -vj                            .
c....                       Physical properties-vsg,rhog                .
c....Properties of molten steel :cp,tk,rho,vsk,pr,gst,tm                 .
c....Cross-conduction correction : scd                                  .
c....Parameters define the deformable mesh :vde,vwi                     .
c....Parameter  define the velocity field : cvl                         .
c.......................................................................
c
c
c
      dimension va(35),vs(35),vp(35),dd(35),conm(13),con(13)
      dimension hdv(13),alx(12),ex(12),prex(12),dan(12)
     *,etk(12),tsto(13),dt(13),adt(13),sumex(12),dte(35),vol(13)
      dimension ah(3,13),sp(13),t(13),su34(13),yir(13),yiv(13)
      dimension arr(3,13),hvf(13),hv(13),hd(13),g(13),d12(12)
      dimension qx(13),qy(13),y(13),z(13),fi(13),tg(13),ro(13)
      dimension hq23(13),hq34(13),qf(13),f(13),fh(13),ga(13)
      dimension hfl(7),he(7),hel(7),zi(7)
      DATA LI,LO,LSI,LSO/5,5,7,10/
      open(UNIT=LSI,NAME='CONVECT.INP',TYPE='old',readonly)
      read(LSI,*) al,de,rho,vsk,cp,tk,rhog,vsg,vj,ed,tm,vd,eff,
     *pr,CVL,W,D,VDE,VWI,ndc,crat,gst,sigmat,scd,ns
      write(LO,8) al,de,rho,vsk,cp,tk,rhog,vsg,vj,ed,tm,vd,eff,
     *pr,ncont,cvl,w,d,sigmat,scd,ns
 8    format(2x'al:',f5.3,2x'de:',f8.5,2x'rho:',f8.3,2x'vsk:'
     *,f8.5,/
     *2x'cp:',f8.3,2x'tk:',f8.3,2x'rhog:',f10.5,2x'vsg:',f10.5,/
     *2x'vj:',f8.3,2x'ed:',f8.5,2x'tm:',f8.3,/
     *2x'vd:',f8.3,2x'eff:',f5.3,2x'pr:',f5.3,/
     *2x'ncont:',i4,2x'cvl:',f5.3,2x'w:',f8.5,2x'd:',f8.5,/
     *2x'sigmat:',f8.5,2x,'scd:',f8.5,2x'ns:',i3)
      read(7,*) (qx(n),n=1,13),(qy(n),n=1,13),(hfl(n),n=1,7)
      pi=3.141592
c.....calculation of heat from the side
      zi(1)=0.0
      zi(3)=d-0.6*d
      zi(5)=d-0.25*d*vde
      zi(7)=d
      zi(2)=(zi(1)+zi(3))/2.
      zi(4)=(zi(3)+zi(5))/2.
      zi(6)=(zi(5)+zi(7))/2.
      do 6 n=1,7
```

```
      he(n)=2.*pi*w*hfl(n)
      call qtfg(zi,he,hel,n)
 6    continue
      hesd1=hel(3)
      hesd2=hel(5)-hel(3)
      hesd3=hel(7)-hel(5)
      hesd=hel(7)
      do 11 n=1,13
      fi(n)=0.0
      tg(n)=0.0
      ro(n)=0.0
      fh(n)=0.0
      ga(n)=0.0
   11 continue
      BEN=D-0.25*D*VDE
      DEN=D-(0.25*D*VDE+0.6*D)/2.
      tg(3)=0.2*d/(0.4*w*VWI)
      tg(5)=DEN/(0.4*w*VWI)
      tg(7)=BEN/(0.4*w*VWI)
      tg(9)=BEN/(0.25*w*VWI)
      tg(11)=BEN/(0.125*w*VWI)
      do 4015 n=1,13,2
      fi(n)=atan(tg(n))
      fi(13)=pi/2.
      if(n.eq.1) go to 4015
      fh(n)=(fi(n)+fi(n-2))/2.
4015  continue
      do 4018 n=2,12,2
4018  fi(n)=fh(n+1)
      write(lo,5050) (fi(n),n=1,13)
5050  format(13(2x,f12.7,/))
      do 4117 n=1,3
      ro(n)=de/(sin(fi(n))**2+(cos(fi(n))/al)**2)**0.5
      y(n)=ro(n)*cos(fi(n))
      z(n)=d-ro(n)*sin(fi(n))
4117  continue
      alfa=(z(3)-(d-de))/y(3)**2
      do 4118 n=4,13
      riza=(sin(fi(n))**2+4.*alfa*de*cos(fi(n))**2)**0.5
      ro(n)=(-sin(fi(n))+riza)/(2.*alfa*cos(fi(n))**2)
      y(n)=ro(n)*cos(fi(n))
      z(n)=de-alfa*y(n)**2
4118  continue
      z(1)=d-z(1)
      z(2)=d-z(2)
      z(3)=d-z(3)
C
      sp(1)=0.0
      do 13 n=1,13
      IF(n.eq.1) go to 14
      sp(n)=sp(n-1)+((z(n)-z(n-1))**2+(y(n-1)-y(n))**2)**0.5
```

```
      qr(n)=(qx(n)**2+qy(n)**2)**0.5
      f(n)=2.*pi*y(n)*qf(n)
   13 continue
      do 16 n=1,13
      yir(n)=2.*pi*y(n)
      yiv(n)=pi*y(n)**2
      call qtfg(sp,f,hd,n)
      call qtfg(sp,yir,su34,n)
      call qtfg(sp,yiv,vol,n)
   16 continue
      tqh=hd(13)
      cia=tqh/(eff*vd)
      if(ndc.eq.0) go to 61
      ci=cia*crat
      go to 62
    1 ci=cia
    2 be=vj/ed
      write(lo,1821) ci,cia
  821 format(5x'ci:',f12.3,4x'cia:',f12.3)
      sk=CVL*(ci/10**5)**2*(1.+al)/(pi*vsk*al*de)
      st1=0.035*(vsg*rhog)**0.5*be**1.5*al*de**2/vsk
      va(1)=2.*sk-0.01*st1
      vs(1)=2.*sk-0.01*st1
      vp(1)=2.*sk-0.01*st1
      st=st1
      sud=0.0
      lil=50
      if(scd.eq.0.) lil=1
      tmax=0.0
      amd12=10.

....overall loop........

      do 5000 ml=1,34
      nmot=1
      mln=ml
      if(vs(ml).lt.0.0) nmot=-1
      write(L0,9) va(ml),vs(ml),vp(ml),st
    9 format('va:',f10.5,2x'vs:',f10.5,2x'vp:',f10.5,/
     *       5x'st:',f10.5)
      the=atan(2.*abs(vs(ml))/abs(va(ml)))
   15 r=de/((sin(the))**2/al**2+(cos(the))**2)**0.5
      xi=r*(sin(the)/(abs(va(ml))/abs(vp(ml))+1./sin(the)))**0.5
      yi=xi/tan(the)
      fm=pi/2.*xi**2*rho*abs(va(ml))
      write(L0,901) xi,yi,r
  901 format(2x'xi:',f10.5,1x'yi:',f10.5,1x,'r:',f10.5)


      do 900 i=1,12
      if(nmot.eq.-1) go to 885
```

```
      dan(i)=su34(14-i)-su34(13-i)
      etk(i)=scd*tk/(0.5*(ro(14-i)+ro(13-i)))
      go to 886
885   dan(i)=su34(i+1)-su34(i)
      etk(i)=scd*tk/(0.5*(ro(i)+ro(i+1)))
886   prex(i)=1.0
900   continue
5995  ncond=0
      if(abs(vs(m1)).lt.0.001.or.tmax.gt.4000.)
     *ncond=1
      if(ncond.eq.0) go to 108
      do 6001 n=1,13
      conm(n)=2.*pi*tk*y(n)/ro(n)
      call qtfg(sp,conm,con,n)
6001  continue
      tmax=tqh/con(13)+tm
      tvar=tm
      hdvn=tqh*con(7)/con(13)
      write(lo,6002) tmax,hdvn
6002  format(2x'---conduction only---',/
     *2x'tmax:',f10.3,2x'hdvn:',f10.3)
      go to 3018
108   do 109 n=1,13
109   tsto(n)=0.0
c
c....temperature field
c

      alfa=2.*abs(vp(m1))/(de*al**0.5*pi)
      re=alfa*rho/vsk
      ht=0.76*tk*re**0.5*pr**0.4
c
      do 1000 lt=1,lil
      write(LO,1001) lt
1001  format(2x,'***loop lt=',i3,1x'starts')
      lti=lt
      vr=1.0
      vr1=1.0
      ulim=0.1
      do 1010 n=1,12
      alx(n)=1.0
      if(lt.eq.1) go to 1005
      alx(n)=alog((tmax-t(n))/(tmax-t(n+1)))
      if(alx(n).lt.0.00001) ulim=2.0
      if(alx(n).eq.0.000) alx(n)=1000.0
      do 1002 nn=1,13
1002  tsto(nn)=t(nn)
1005  if(lt.eq.1.or.alx(n).eq.1000.0) vr=0.0
      if(lt.eq.1) vr1=1.01
      if(lt.eq.1.and.scd.eq.0.0) vr1=1.0
      par1=2.*fm*cp*vr1/dan(n)
```

```
      par2=vr*etk(n)/aix(n)
      ex(n)=exp(-ht/(par1-par2))
 1010 continue
      prex(1)=ex(1)
      do 1020 n=1,11
 1020 prex(n+1)=prex(n)*ex(n+1)
      sumex(1)=(prex(1)-1.)*dan(1)/alog(ex(1))
      do 1025 n=2,12
      sumex(n)=sumex(n-1)+(prex(n)-prex(n-1))*dan(n)/alog(ex(n))
 1025 continue
      t(1)=tm+tqh/(ht*sumex(12))
      do 1030 n=1,12
      t(n+1)=tm+(t(1)-tm)*prex(n)
      d12(n)=abs(t(n+1)-t(n))
 1030 continue
      tmax=tqh/(2.*fm*cp)+t(13)
      if(tmax.gt.4000.) go to 5995
      tvar=t(13)
      if(nmot.eq.-1.and.scd.ne.0.0) tvar=t(1)
      do 1028 jj=1,13
      dt(jj)=tsto(jj)-t(jj)
 1028 adt(jj)=abs(dt(jj))
 1380 write(LO,1400) tmax,(t(n),dt(n),n=1,13)
 1400 format(10x'tmax:',f10.2/8x't',10x,'dif t'/
     *13(2x,f10.2,1x,f10.2,/))
      dtmax=max(adt(1),adt(2),adt(3),adt(4),adt(7),adt(9),adt(11))
      if(dtmax.lt.ulim) go to 1800
 1000 continue
 1800 do 3000 i=1,13
      if(nmot.lt.0) go to 3006
      hq23(i)=2.*fm*cp*(t(1)-t(i))
      hq34(i)=2.*fm*cp*(t(i)-t(13))
      hvf(i)=ht*(t(14-i)-tm)
      go to 3007
 3006 hq23(i)=2.*fm*cp*(t(14-i)-t(13))
      hq34(i)=2.*fm*cp*(t(1)-t(i))
      hvf(i)=ht*(t(i)-tm)
 3007 q(i)=2.*pi*y(i)*hvf(i)
      call qtfg(sp,g,hv,i)
 3000 continue
      hdv(1)=0.0
      do 3015 n=2,13
      hdv(n)=tqh*sumex(n-1)/sumex(12)
 3015 continue
      if(nmot.lt.0) hdvn=hdv(7)
      if(nmot.gt.0) hdvn=hdv(13)-hdv(7)
 3018 am1=m1
      dte(m1)=sigmat*tmax-tvar
      if(dte(m1).gt.1000.) dte(m1)=0.8*dte(m1)
      sud=sud+am1*dte(m1)
      dte(m1)=2.*sud/(am1*(am1+1.))
```

```
      IF(ML.EQ.1) GO TO 1036
      DD(ML)=HD(7)-hdvn
      DDD=DD(ML)-DD(ML-1)
      dd1=abs(ddd)
      IF(DD1.LT.0.8) GO TO 5001
1036  dd(1)=hd(7)-hdvn
      st2=0.125*gst*dte(ml)/(al*vsk)
      st=st1+st2
      va(ml+1)=2.*sk-0.01*st
      vs(ml+1)=2.*sk-0.01*st
      vp(ml+1)=2.*sk-0.01*st
      vpd=abs(vp(ml+1)-vp(ml))
      if(vpd.lt.0.00001) go to 5001
      write(LO,1985) ml,DDD,dte(ml)
1985  format(2x,'**********************************'/
     *5x,'ml:',i5,2x,'ddd:',f10.2,/
     *5x'dte:',f10.3)
5000  continue
5001  write(LO,5005) ddd
5005  format(2x,'**dif in q34(7):',f10.3)
      do 1040 n=1,13
      arr(1,n)=fi(n)
      arr(2,n)=qf(n)
      arr(3,n)=hvf(n)
      ah(1,n)=fi(n)
      ah(2,n)=hd(n)
      ah(3,n)=hdv(n)
      if(nmot.gt.0) ah(3,n)=hdv(13)-hdv(14-n)
1040  continue
c
      wi=al*de
      thi=the/pi*180.
c
c     print output
      open(UNIT=LSO,NAME='con.out',TYPE='new')
      write(LSO,42) (y(n),z(n),fi(n),qx(n),qy(n),qf(n),
     * n=1,13)
42    format(30x'**input information**'//
     *5x'y',10x'z',6x'fi'12x'qx',12x,'qy',12x'qf'/
     *13(1x,f8.5,1x,f8.5,1x,f8.5,1x,f14.2,1x,f14.2,
     *1x,f14.2,/))
      write(LSO,43) ((arr(i,j),i=1,3),j=1,13)
      write(LSO,43) ((ah(i,j),i=1,3),j=1,13)
43    format(1x,13(f14.4,1x,f14.4,1x,f14.4,/))
      if(nmot.gt.0)
     *write(LSO,46) (fi(n),qf(n),hvf(n),t(14-n),n=1,13)
      if(nmot.lt.0)
     *write(lso,46) (fi(n),qf(n),hvf(n),t(n).n=1,13)
46    format(30x,'**input for plotting**'//
     *5x,'fi',12x,'qf',12x,'hvf',15x 't' /
     *13(f12.4,1x,f15.4,1x,f15.4.1x,f15.4,/))
```

```
      if(nmot.gt.0)
     *write(LSO,604) (ex(13-n),prex(13-n),etk(13-n),
     *dan(13-n),n=1,12)
      if(nmot.lt.0)
     *write(lso,604) (ex(n),prex(n),etk(n),dan(n),n=1,12)
604   format(20x,'**exponential coefficients**'//
     *8x,'ex',10x,'prex',10x,'etk',10x'dan'/
     *12(2x,f12.3,1x,f12.3,1x,f12.3,1x,f12.9,/))
      write(LSO,47)
 47   format(30x'***convection in the weld puddle***',/,
     *25x'**************************************' ,///
     *5x'*the simple model of a heat exchanger is employed'/
     *5x'*motion of the melt due to e.m. and gas+plasma stream'
     *'is considered',//10x'all units are in the s.i. system',//)
      write(LSO,48) rhog,vsg,ed,vj,c1,vd,c1a,eff
 48   format(30x'* arc characteristics *',/
     *25x'**************************************',//
     *5x'plasma+gas:'2x'density=',f10.7,2x'dyn visc=',f10.7,/
     *5x'arc diam:',f8.3,3x'jet vel:',f8.3,3x'arc current:',f8.3,
     *2x'arc voltage:',f8.3,/20x'average current value:',f10.3,/
     *20x'effic(heat input):',f5.4,/)
      write(LSO,49) rho,vsk,cp,tk,pr
 49   format(30x'*physical properties of the molten metal*'/
     *30x'**************************************',/
     *3x'density:',f8.3,3x'dyn visc:',f8.3,3x'spec heat:',f8.3,/
     *3x'ther conduct:',f8.3,3x'prandl no.:',f8.3,/)
      write(LSO,50) th1,al,de,w1,x1,y1,fM
 50   format(30x'*characteristics of  the weld puddle*',/
     *30x'**************************************'//
     *5x'angle of equilibrium(deg):',f8.3,/
     *5x'puddle width-depth ratio:',f10.5,
     *5x'depth:',f10.5,5x'width:',f10.5,/
     *5x'x1:',f10.7,5x,'y1:',f10.7,2x,'mass flow rate:'
     *,f10.7)
      write(LSO,55) (vs(i),va(i),vp(i),dte(i),i=1,34),
     *tmax,t(1),t(2),t(12),t(13),ht,sk,st
 55   format(30x'velocity field:'/
     *30x'**************************************'//
     *5x'surf vel:',5x'axis vel:'5x'per vel:'7x'dte'/
     *34(2x,f10.5,2x,f10.5,2x,f10.5,2x,f10.3,/)//
     *30x'temperature field:'/
     *25x'**************************************'//
     *2x'max temp:',f10.3,2x't2:',f10.3,2X't:',f10.3,2x't4:',f10.3,
     *2x't5:',f10.3/3x'heat trans coef',f10.2/2x'contribut in velocity
     *due to  e.m. force: sk=',f10.5,2x'plasma moment: st=',f10.5//)
      write(LSO,60)(hq23(n),hq34(n),hv(n),su34(n),vol(n),n=1,13),tqh
 60   format(8x'hq23',13x,'hq34',12x,'hv'10x,'su34'10x'volume'/
     *13(1x,f14.3,2x,f14.3,2x,f14.3,f14.8,f14.8,/)
     */15x,'total heat',f10.3//)
      write(lso,56) hesd1,hesd2,hesd3,hesd
 56   format(10x'*****heat from the cold side******'/
```

```
      WRITE(LO,159) VA(mln),VS(mln),VP(mln)    114
159   FORMAT(2X,'VA:',F10.5,2X,'VS:',F10.5,2X,'VP:',F10.5)
 150  stop
      end
      subroutine qtfg(x,y,z,ndim)
      dimension x(1),y(1),z(1)
      sum2=0.0
      if(ndim-1) 4,3,1
c     integration loop
1     do 2 i=2,ndim
      sum1=sum2
      sum2=sum2+0.5*(x(i)-x(i-1))*(y(i)+y(i-1))
2     z(i-1)=sum1
3     z(ndim)=sum2
4     return
      end
```